Analysis of Extreme Precipitation Events in Regional Climate Simulations for the Alpine Region

Master's Thesis

Faculty of Science

University of Bern

presented by

Jan Rajczak

2011

Supervisor:

Prof. Dr. Christoph Schär
Institute for Atmospheric and Climate Science, Swiss Federal Institute of Technology, ETH Zürich

Co-Supervisor:

PD Dr. Christoph C. Raible
Climate and Environmental Physics Department, University of Bern
and Oeschger Centre for Climate Change Research

Advisor:

Dr. Pardeep Pall
Institute for Atmospheric and Climate Science, Swiss Federal Institute of Technology, ETH Zürich

ABSTRACT

Based on 10 transient regional climate model simulations from the ENSEMBLES project, this study investigates projected changes in 21st century precipitation extreme and climatological diagnostics for the Alpine and central European region. Two scenario periods in the mid and late 21st century, namely 2021-2050 and 2070-2099, are compared to conditions in 1961-1990. Both basic climatological precipitation indices and precipitation extreme indices for each time slice under consideration are estimated, applying techniques of extreme value theory in order to estimate return values and periods for extreme events with recurrences ranging from 2 to 100 years. The analyses are carried out on seasonal levels to appropriately capture seasonal change patterns. Special attention is devoted to the assessment of inter-model variability in the projections. An additional study addresses future changes in heavy rainfall events on a more local scale for Switzerland only.

The results imply that climate change will likely have a serious effect on precipitation and precipitation extremes in the 21st century across central Europe and in the Alps. According to the projections, there will be a marked increase in the intensity and frequency of heavy rainfall events in the northern Alpine region in the fall and south of the Alps in the winter. An increase in extremes and the strength of single precipitation events is, however, projected across all seasons. At the same time, the simulations suggest substantial reductions in precipitation frequency and the mean in the summer and spring months. Taken together, the simulated changes in precipitation show a potential for severe climatic events, as expressed by an increased risk of heavy rainfalls and droughts. Thereby one has to keep in mind that the performance of ENSEMBLES RCMs in simulating present day conditions is quite good. The results furthermore imply that changes in basic climatological and intense diagnostics are governed by different physical and dynamical considerations on a disproportionate scale. The exact processes that cause the projected changes remain an open question to which this study tries to encourage. Hereby, circulation and weather-type changes as well as an increase in the warming airs moisture uptake capacity should be taken into account in future research questions.

In addition, this study reveals that individual RCM change projections are affected by inter-model spread. In general but mainly in winter and fall, the cluster of RCM projections depend on the driving GCMs, which therefore highly contribute to the over-all spread across model projections. In summer, the general spread between the whole set of models is larger, to a certain degree independently of the driving GCMs. Therefore individual model parameterizations in summer seem to be the main driver for the total range of inter-model spread. A comparison of inter-model spread for single diagnostics reveals the smallest spread and for this reason most certainty for projections of intense precipitation diagnostics, namely intensity and the 90%-quantile. The integrating measure of mean precipitation and diagnostics obtained through extreme value modelling show the largest inter-model variability and uncertainty within individual projections. Nevertheless, the models are compatible in the change-structure across all seasons.

Contents

List of Figures

List of Appendix Figures

List of Tables

1 Introduction

1.1 Motivation and Introduction

There is increasing interest in extreme weather and climate phenomena, such as extreme temperature, storm and heavy precipitation events, due to their potential to cause severe societal, economic and environmental impact [*Diaz and Murnane*, 2008; *Solomon et al.*, 2007]. In particular, there is increasing interest in learning more about the frequency and intensity of extreme events that occur as a result of climate change, especially, since there have been a number of recent extreme events that have caused loss of lives and serious economic damages to private property and infrastructure. Single extreme events and increased climate variability are believed to have a greater impact than long-term changes in the mean of climatic variables [*Fischer and Schar*, 2009; *Katz and Brown*, 1992; *Schar et al.*, 2004]. Special interest in terms of climatic extremes is thereby related to hydrological extremes like droughts, due to lack of precipitation, and heavy rainfall events [*Nott*, 2006]. As the latter are associated with floods, they often imply severe damage to infrastructure and generate very large economic losses. Examples of hydrologic extreme events are found regularly in instances around the world. With a focus on the Alpine region and on Switzerland in particular, one can designate the August 2005 flood as an example for an extreme precipitation event causing severe impact and damage [*MeteoSchweiz*, 2006].
Considering extreme precipitation events, the most recent report of the Intergovernmental Panel on Climate Change (IPCC) suggests that the hydrologic cycle will intensify as the climate warms and that extremes are likely to occur more frequently and become more intense [*Solomon et al.*, 2007]. Global changes in the character of precipitation and precipitation extremes have been observed in the past decades [*Alexander et al.*, 2006; *Frich et al.*, 2002; *Klein Tank and Konnen*, 2003; *Min et al.*, 2011]. The most prominently observed changes in precipitation are an increase in the mean in the tropics, mid- and high-latitudes and a decrease in the subtropics. Regarding extreme precipitation, a widespread global increase, independently of the direction and magnitude of changes in the mean, is found. In this regard, [*Alexander et al.*, 2006] point out that the fraction of heavy precipitation contributing to the total amount of precipitation has increased within the last decades. This means that each single precipitation event has become heavier. Global climate simulations reveal a continuation of the observed trend in the course of the 21st century [*Kharin and Zwiers*, 2000; *Kharin et al.*, 2007; *Solomon et al.*, 2007].
In summary, with a focus on intense precipitation, instrumental observations and projections show that changes in mean and extreme precipitation diagnostics do not scale proportionately and that in some areas and seasons, even reverse trends are to be found.
Associated with ongoing climate change, global temperatures have risen and will continue to rise, most likely due to anthropogenic emissions of greenhouse gases (GHG) that cause radiative forcing in the climate system [*Solomon et al.*, 2007]. For precipitation and its extremes, a trend is - as mentioned before - detectable but the direct link to global warming, anthropogenic activities and radiative forcing is not yet fully understood. Despite these uncertainties, it is assumed that global warming causes the hydrologic cycle to intensify. In this motive, several studies have examined the hydrological response to increasing temperature [*Allen and Ingram*, 2002; *Haerter et al.*, 2010; *Held and Soden*, 2006; *Liu et al.*,

2009; *O'Gorman and Schneider*, 2009; *Pall et al.*, 2007]. As these theoretical studies show, and as instrumental observations from recent decades [*Alexander et al.*, 2006] and future projections [*Kharin et al.*, 2007] consistently confirm, one can assume that changes in the mean and extreme precipitation are highly complex and behave disproportionately as the climate warms. This implies that changes in the mean and in extremes are governed by different physical and dynamical considerations within the atmospheric and climate system. While global mean precipitation responds with an intensification of ~2% per Kelvin warming, increases in precipitation extremes are approximately related to the moisture uptake capacity of the atmosphere, which increases, according to the Clausius-Clapeyron relation (in the following CC), by a factor of 7% per Kelvin warming [*Frei et al.*, 1998; *Kharin and Zwiers*, 2005].

Simply expressed, atmospheric processes governing precipitation changes can be distinguished into a thermodynamical and dynamical contribution [*Emori and Brown*, 2005]. Thermodynamic processes relate to changes in the moisture content of the air and its release, while dynamic processes relate to changes in the atmospheric circulation and the tropospheric energy budget. The latter is assumed to govern changes in the mean. This implies that changes in the mean are constrained by the tropospheric energy budget, where loss and gain of energy through several complex processes at the surface, in the troposphere and at its top play an important role [*Allen and Ingram*, 2002]. Experiments [*Pall et al.*, 2007] show that scaling extremes to the air`s moisture uptake capacity (CC) at given temperature increases is an approximately reliable estimate for changes in precipitation extremes. However, it has also been shown that the temporal scale used regarded to investigate this scaling, highly governs the response of extreme precipitation to temperature increases [*Haerter et al.*, 2010; *Lenderink and Van Meijgaard*, 2008].

In regard to human-induced climate change, recently published studies are of special interest and worth noting, as they show that the severity of recent heavy rainfall events can to a certain degree be attributed to anthropogenic activities [*Min et al.*, 2011; *Pall et al.*, 2011].

Nevertheless, changes in the character of precipitation and of climatic variables in general have to be considered on a more regional scale when trying to assess possible future impacts of climate change on appropriate spatial scales. Recent studies of observed and future changes in precipitation characteristics for Europe find coincident change patterns [*Beniston et al.*, 2007; *Frei and Schmidli*, 2006; *Kendon et al.*, 2008; *Klein Tank and Konnen*, 2003; *Kundzewicz et al.*, 2006]. The global trend showing disproportionate change between precipitation indices is thereby coincidently confirmed on a European scale. Also, an intensification of precipitation is found. The studies furthermore reveal that central Europe, and particularly the Alps, lie within a transition zone between a general moistening in the northeastern and a drying in the southwestern parts of Europe. The position of this transition zone highly depends on the season. Regions afflicted by a decrease in precipitation spread out to the north in summer and advance backward across the European continent in winter.

Assessing climate risks and future impacts on an even more regional scale within Europe requires expert knowledge in order designate regions in which heavy rainfall and its impacts occur more strikingly than in others. Affected regions are inevitably more vulnerable towards extreme precipitation events in a changing climate - in particular when located in densely populated regions, where heavy rainfall events can cause severe impact. The European Alps, as a mountainous region situated in densely populated central Europe, clearly present a region that is highly vulnerable towards extreme precipitation and its effects [*Beniston*, 2003; *Frei and Schmidli*, 2006]. As a consequence, many studies have investigated precipitation extremes and associated impacts in the Alpine (and European) region in order to improve the understanding of relevant processes and assess possible future climatic conditions and their consequences.

For instance, a study on instrumental records has shown that precipitation events in the Alpine region, particularly in Switzerland, became more intense during the 20th century [*Schmidli and Frei*, 2005]. Based on future projections for the 21st century, this trend is likely to continue [*Frei et al*., 2006].

The intention of this study is to complement the series of studies on Alpine and European climate change and evaluate projected changes in precipitation extreme and basic descriptive diagnostics in the Alpine and the surrounding region in the 21st century. This study relies on simulations of an ensemble of 10 transient recent regional climate models (RCMs) from the EU-ENSEMBLES project [*van der Linden and Mitchell*, 2009] featuring a horizontal grid-resolution of 25km.

As the name infers, RCMs are climate models that run with an increased grid-resolution and therefore allow an examination of climate change from a regional point of view. Due to their high computational demand, they are commonly run over limited areas (e.g. Europe). A RCM is thereby embedded into a globally running General Circulation Model (GCM) by application of dynamical downscaling techniques [*Giorgi and Mearns*, 1999]. The GCM delivers driving boundary conditions as well as possible climate forcing, such as for example an emission scenario to account for human-induced climate change.

Making use of RCMs as a tool for the assessment of climate change and possible impacts on regional scale is believed to be very promising [*Giorgi*, 2008]. Compared to GCMs, nested RCMs are able to resolve atmospheric processes on local and regional scales in much more detail. Processes responsible for meteorological extremes operate on small spatial and short temporal scales. Such processes are yet unresolved by current GCMs, due to their insufficient grid resolution and therefore very generalized physical parameterization of sub-grid processes. The complex topography of the Alps enhances the importance of small-scale processes in model simulations. It has been proved that PRUDENCE RCMs, with a horizontal grid spacing of 50km, are able to reasonably reproduce meso-scale weather-systems and the spatiotemporal character of precipitation in the Alpine region [*Frei and Schar*, 1998; *Frei et al*., 2006; *Frei et al*., 2003]. Studies have also proved that ENSEMBLES RCMs, as used in this study, are able to well capture the Alpine precipitation climate character for present-day climatic conditions [*Arnold*, 2009; *Arnold et al*., 2011].

There is an added value to considering several RCM simulations to assess information about future climatic conditions; namely, one can draw conclusions about uncertainty in future climate projections. Model-uncertainty arises from different model formulations and physical parameterizations within the individual RCM setups. Especially on decadal scales, this can present a large source of uncertainty [*Hawkins and Sutton*, 2009]. In comparison to continuous variables like temperature and pressure, precipitation is highly sensitive to different parameterization-schemes as the occurrence and strength of precipitation is governed by several parameters including the inter-relation of different meteorological quantities and the underlying topography and surface properties [*Buonomo et al*., 2007]. Uncertainty in terms of different model-formulations can be estimated by taking several different RCM simulations into account. These are then forced by the same driving GCM to deliver equal boundary conditions to each RCM of consideration [*Frei et al*., 2003]. Differences in the RCM projections are then attributable to their different formulations.

Other uncertainties related to climate simulations arise from the internal variability of the climate system (e.g. inter-annual variability) and scenario uncertainty, of which the latter steadily increases with runtime and becomes the main source of uncertainty at timescales of about ~100 years [*Hawkins and Sutton*, 2009].The present investigation examines the IPCC A1B emission scenario and addresses uncertainties associated with inter-annual variability by applying resampling methods.

1.1.1 Objectives and research question

This study investigates 10 transient regional climate simulations from the EU-ENSEMBLES project and examines projected climate change signals for the 21st century with respect to present-day climatic conditions. The focus of this study lies on projections of extreme precipitation events and basic precipitation diagnostics in the Alpine and its surrounding region. The main objectives of this analysis can thereby be separated into two relevant tasks:

1. Assessment of changes
The presented study elaborates on how climate, in terms of precipitation extremes and the general character of precipitation, will change in the course of the 21st century. The inclusion of 10 different model simulations raises the potential of certainty of the conclusions that are to be drawn.

2. Assessment of inter-model differences
This study also addresses potential uncertainties through a detailed comparison of the individual model-projections. This comprises special attention to the inter-relation and comparison of RCMs driven by the same GCM, but also to the general variability between the whole set of models examined. Furthermore, special attention is devoted to the seasonal dependence of inter-model variability, which is most likely to occur because of different processes composing precipitation and its extremes in the course of the year. For instance, summer precipitation events operate on small spatial and temporal scales and are therefore hard to capture in RCMs, especially, in comparison to large-scale and persisting precipitation events in winter and fall.

In general, this study incorporates several analysis steps that have been undertaken in a previous study by *Frei et al. (2006),* which have applied similar analysis steps to older and coarser RCM simulations for the entire European and Alpine region.

1.1.2 Structure of this thesis

A short geographical and climatological description of the Alpine region supplements this introduction.
Chapter two describes the model data and methods used. The section on methods also includes theoretical explanations on the techniques of extreme value modeling. The individual adoption of extreme value analysis in the framework of this study is also delineated here.
Chapter three is devoted to the presentation of results. The results section is subdivided into three parts. The first part presents results for short-term climate change, meaning the comparison of conditions in the period 2021-2050 with respect to the reference period of 1961-1990. In the second part, the viewpoint is extended to the period 2070-2099, describing long-term changes in the late 21st century. A third part of the results section presents a case study in which simulated return values for heavy rainfall events in three Swiss sub-domains are regarded for present-day, mid- and late-21st century conditions.
Chapter four summarizes, draws conclusions and discusses the results obtained in this study.
This thesis comprises several figures and tables. In additional to the presented information within the text and main part of the thesis, a comprehensive set of figures is presented in the appendix, emphasizing the individual model projections.

1.2 The Alps and their Precipitation Climate

The Alps form the major topographic feature in central Europe. Made up of an arc-shaped mountain range, the Alps have a length of about 800km in zonal direction, reaching from the French Mediterranean coast to eastern Austria. Countries with a proportion of the Alpine range are from west to east: France, Switzerland, Italy, Liechtenstein, Austria, Germany and Slovenia. During their course, the Alps slightly vary in width by approximately 200km. The mean crest height is about 2500m above sea level, whereas highest peaks in the western Alps often exceed 4000m in altitude. A topographical map, showing the mountain belt and its adjacent forelands in topographical detail is given in Figure 1-1. As illustrated, several valleys and rivers run through the Alps, mainly from north to south or vice versa. A small number of major rivers (e.g. Rhone and Inn) flow parallel to the main crest forming distinct valleys that subdivide the Alps into different massifs and characteristic regions. This alpine dissection also finds its imprint in the spatial distribution of climatological variables.

Figure 1-1: Schematic topography of the Alpine Region (Source: maps-for-free.com).

On a large scale, the Alps are of prominent importance to central Europe. Being the source-region of four main European rivers (namely: Danube, Po, Rhine and Rhone), they supply water to large areas of Europe and therefore constitute an important component of the central European hydrological cycle. This fact is of special interest as future conditions the Alpine precipitation climate and climatic / hydrologic change imply a potential for large-scale socio-economic impact.

Climate across the Alps is not only highly variable as a result of its complex topography. The large spatial variability of climate in the Alpine Region is also generated from the incorporation of a sharp boundary separating temperate climate in the north from the Mediterranean climate in the south. In addition, the Alps experience both continental and maritime influences. As a large mountain range, the Alps also can highly impair atmospheric and climatic processes. Such processes include the modification and blocking of atmospheric flow, air masses and meso-scale weather-systems and the initiation of thermodynamic processes associated with the ascent and descent of air masses. Thermodynamic processes enhance relevant topographic precipitation mechanisms like orographic precipitation, rain-shadowing and convection [*Barry*, 2008; *Frei and Schar*, 1998; *Whiteman*, 2000].

Altogether, these processes have a large effect on Alpine precipitation and thus lead to a spatially averaged annual precipitation amount that is twice as large as in surrounding flatland

areas. On a small scale, however, the precipitation climate found in the Alps is characterized by a very pronounced spatial and seasonal variability. Annual mean values of precipitation within the Alps vary from around 500mm/year in eastern foreland areas and shielded inner-alpine valleys up to 4000mm/year in the Swiss Jungfrau region[*Frei and Schar*, 1998; *Frei and Schmidli*, 2006].

Very good and detailed summaries on the precipitation climate of the Alps are given in [*Frei and Schar*, 1998; *Frei and Schmidli*, 2006]. Referring to these two references, the most important characteristics are discussed in the following. A detailed spatial representation of seasonal precipitation climatologies for several precipitation diagnostics, based on [*Frei and Schar*, 1998], is also presented in Figure 1-2. The depicted diagnostics are, wet day frequency, the mean, mean wet day intensity, the 90%-quantile of wet days and the 5-year return value of 1-day precipitation events (an overview and definition of the indices shown is also given in Table 2.2-2, as these were also regarded in the analyses). The quantitative visualizations serve here as the main reference for the Alpine precipitation climatology.

As illustrated, the mean is characterized by a pronounced annual cycle, which differs in its amplitude and timing depending on the location within the Alps and across the Alpine region. Throughout all seasons, most pronounced in summer and winter, a “rim-type” precipitation anomaly is visible. Highest annual precipitation amounts are observed across the northern Alpine rim and at two pronounced wet-anomalies on the Alpine Southside situated in the Ticino and the Julian Alps. Inner-alpine areas tend to be dry due to rain shadowing. From a seasonal point of view, one can summarize that the northwestern rim and foreland experience wet conditions in winter. In summer, convection is enhanced and highest values are observed over central and eastern Alpine regions along the main Alpine crest. The two transition seasons generate very wet conditions on the Alpine Southside, distinctly pronounced over the Ticino and the Julian Alps. These two southern Alpine hotspots are not only seen in the mean. Regarding extreme indices (int, q90 and the 5-year return value) one sees the most extreme values over these two distinct southern Alpine regions. Heavy rainfall at these two locations is commonly generated by advection of moist Mediterranean air masses that converge and finally get lifted and channelized by the Alpine topography.

Taking all presented diagnostics into account (Figure 1-2) one recognizes the imprint of the climatologic transition zone across the Alpine mountain range by a contrasting character of precipitation between North- and Southside. Precipitation is more frequent in the north, whereas it is less frequent in the south. However, precipitation totals and intensity are larger in the south, implying that single precipitation events are much stronger in intensity, as can be clearly seen regarding int, q90 and the 5-yr return value. Frequent but comparatively weak precipitation events dominate the climate in the northern Alpine region, where large-scale and long-lived precipitation events are a major component of the precipitation climatology. As presented in [*Frei and Schmidli*, 2006] this finds its imprint in more frequent droughts in the south and longer durations of consecutive wet days in the north.

Also, a distinct increase of continental character to the east of the northern Alpine region is visible. Continentality is reflected by comparatively dry winter conditions in the northeast and remarkable, convection-induced precipitation maxima in summer. In the Alpine northwest, precipitation is more balanced across the year, showing wetter winter- and fall-conditions, mostly due to synoptic disturbances that regularly approach from the Atlantic region.

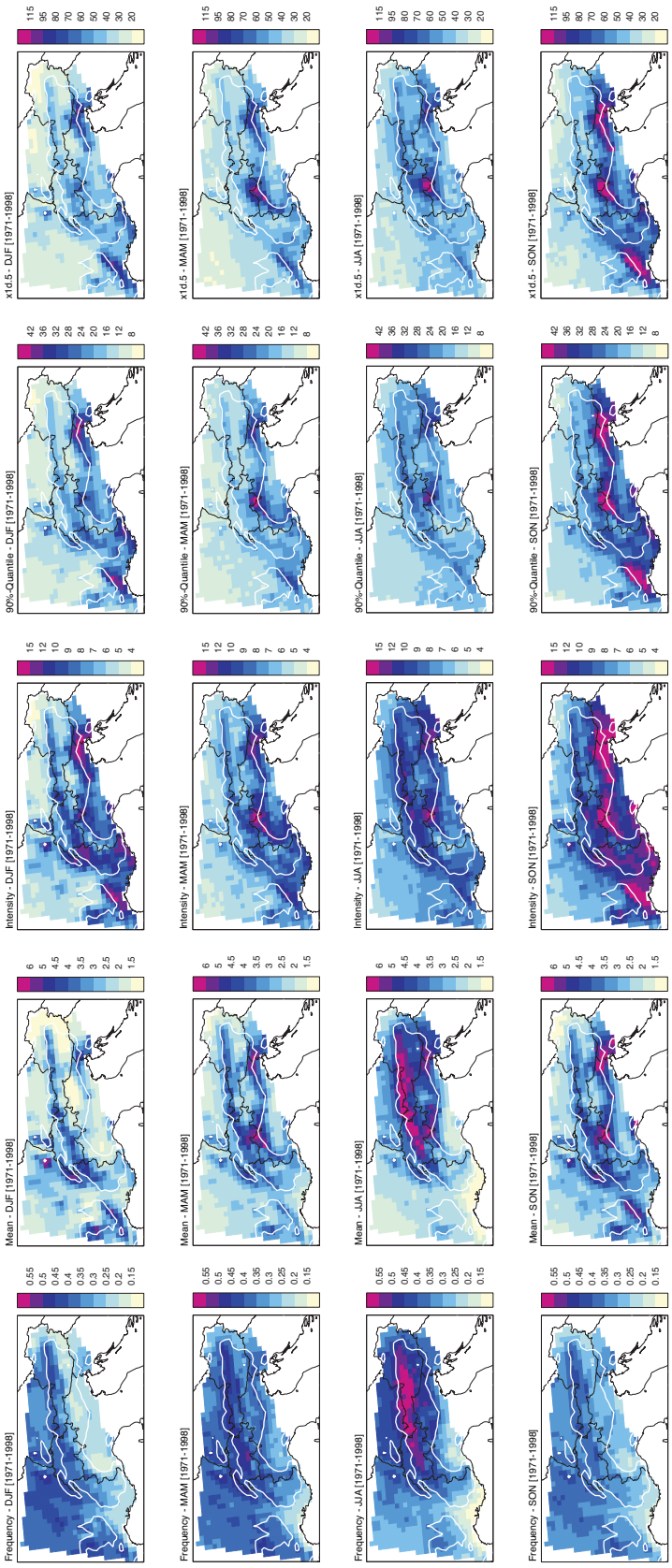

Figure 1-2: Seasonal climatology (period 1971-1998) for precipitation frequency (first, resp. left column), mean precip. (second column), precip. intensity (third column), the 90%-quantile of precip. during wet days (fourth column) and the 5-year return value of 1-day precip. events (fifth, right column). Based on the Frei and Schär (1998) gridded (observational) precip. dataset for the period 1971-1998 (Courtesy: Arnold, J.).

2 Data and Methods

2.1 Data

2.1.1 ENSEMBLES RCM Data

In this study, a set of 10 transient Regional Climate Model (RCM) simulations, stemming from the EU-ENSEMBLES project [*van der Linden and Mitchell*, 2009], is analyzed. A detailed overview of the RCMs contributing to this study is given in Table 2.1-1. As is listed in Table 2.1-1, the 10 RCMs are nested into three different atmosphere-ocean general circulation models (GCMs) by application of dynamical downscaling techniques. Five models use the ECHAM5 GCM [*Roeckner et al.*, 1996]; four, the HadCM3*Q0* GCM [*Gordon et al.*, 2000]; and one single model, the Arpege GCM [*Deque et al.*, 1994] to provide driving boundary conditions. This division allows for an examination of the question of whether model projections cluster depending on their driving GCM and therefore contributes to the understanding of model uncertainty and inter-model variability in future climate projections [*Frei et al.*, 2003; *Giorgi*, 2008; *Hawkins and Sutton*, 2009]. All model chains are forced by the IPCC SRES A1B emission scenario to account for anthropogenic emissions of GHG and associated climate change. Scenario A1B supposes global population growth peaking in the mid 21st century, extensive globalization, rapid economic growth and fast extension of new and efficient technologies. The amelioration B stands for equally weighted use of different energy sources [*Nakicenovic and Swart*, 2000]. Moreover, each RCM of consideration operates with a horizontal grid resolution of ~25km (0,22°), covering the entire European continent. The majority of models consistently operate on the same (ENSEMBLES-) grid, which is presented by a rotated latitude-longitude grid ideally matching the entire European continent. Models, running on different grids are linearly interpolated to the ENSEMBLES-grid to preserve consistency across applied analysis techniques (RCMs affected are: ICTP-RegCM, VMGO-RRCM and CNRM-RM, see also Table 2.1-1). Each ENSEMBLES RCM-integration provides an output with several meteorological parameters in daily resolution spanning from the 1950s mostly to the end of the 21st century (see Table 2.1-1). As this study focuses on projected changes in precipitation indices and extremes, only 24h-precipitation totals are used to perform the analyses. The amount of precipitation in each RCM-output is thereby given as precipitation flux (kg m^2 s^{-1}), in a preprocessing step it is converted to mm per day.

2.1.2 Observational Data

An additional case study presents present-day and future return values including associated uncertainties for three Swiss regions (see chapter 3.3). An observational reference provides a direct comparison to projected and modeled return values for present-day conditions. It is based on a gridded precipitation dataset [*Frei and Schar*, 1998] (here, also referred to as FS1998), which is made up from more than 6000 operational observations from rain gauges across the Alpine region and spans the complete period from 1971 to 1998 in daily resolution. The station data has been spatially interpolated and therefore provides a homogenous gridded dataset beneficial for reanalysis and model evaluation studies. Further details concerning the dataset can be looked up in [*Frei and Schar*, 1998]. FS1998 is also used to present the Alpine

climatology shown in Figure 1-2 and was also used to evaluate the ENSEMBLE-RCMs performance in regard of simulating extreme precipitation and related diagnostics in the Alpine region (see section 2.1.3).

Table 2.1-1: Regional Climate Models (RCMs) used in this study.

IPCC SRES	GCM	RCM	Institution	Abbrev-iation	Period	Grid / Resolution	Reference
A1B	ECHAM5	HIRHAM5	DMI –Danish Meteorological Institute	DMI – HIRHAM	1950-2099 Investigation: SCEN1 & SCEN2	Europe 0.22°(~25km) rotated pole regular lat/lon	*[Christensen, 2007]*
		RACMO	KNMI – Royal Netherlands Meteorological Institute	KNMI – RACMO	1950-2100 Investigation: SCEN1 & SCEN2	Europe 0.22°(~25km) rotated pole regular lat/lon	*[Van Meijgaard, 2008]*
		REMO	MPI – Max Planck Institute for Meteorology, Germany	MPI – REMO	1950-2100 Investigation: SCEN1 & SCEN2	Europe 0.22°(~25km) rotated pole regular lat/lon	*[Jacob et al., 2007]*
		RCA	SMHI – Swedish Meteorological and Hydrological Institute	SMHI – RCA	1950-2100 Investigation: SCEN1	Europe 0.22°(~25km) rotated pole regular lat/lon	*[Kjellström, 2005]*
		RegCM	ICTP – International Center for Theoretical Physics, Italy	ICTP – RegCM	1950-2100 Investigation: SCEN1	Europe 0.22°(~25km) rotated pole lambert projection	*[Pal et al., 2007]*
	HadCM3Q0	CLM	ETHZ – Swiss Federal Institute of Technology	ETHZ – CLM	1950-2099 Investigation: SCEN1 & SCEN2	Europe 0.22°(~25km) rotated pole regular lat/lon	*[Böhm, 2006]*
		HadRM	HC – Met Office – Hadley Centre, United Kingdom	HC – HadRM	1950-2100 Investigation: SCEN1 & SCEN2	Europe 0.22°(~25km) rotated pole regular lat/lon	*[Collins et al., 2011]*
		HIRHAM	METNO – Norwegian Meteorological Institute	METNO – HIRHAM	1950-2050 Investigation: SCEN1	Europe 0.22°(~25km) rotated pole regular lat/lon	*[Haugen and Haakenstrand, 2006]*
		RRCM	VMGO – Voeikof Main Geophysical Observatory, Russia	VMGO – RRCM	1950-2050 Investigation: SCEN1	Europe 0.22°(~25km) rotated pole lambert projection	*[Shkolnik et al., 2008]*
	Arpege	RM5.1	CNRM – National Center of Meteorological Research, France	CNRM – RM	1950-2100 Investigation: SCEN1	Europe 0.22°(~25km) rotated pole lambert projection	*[Radu et al., 2008]*

2.1.3 Performance of ENSEMBLES-RCMs

This section addresses the performance and quality of ENSEMBLES-RCMs in simulating extreme precipitation and related diagnostics in the Alpine region. It has already been shown that the RCMs from the PRUDENCE project capture and simulate reasonably well precipitation and its extremes in the Alpine region [*Frei et al.*, 2006; *Frei et al.*, 2003]. In a prevailing study, focusing on ENSEMBLES RCMs and considering the same basic and extreme precipitation diagnostic as used in this study, good performance also has been shown [*Arnold*, 2009; *Arnold et al.*, 2011]. The evaluation was performed against FS1998 as observational reference (see section 2.1.3) and RCMs were thereby forced by ERA40-reanalysis data. Prominent findings of importance for statements made in this study, can be summarized as follows. Figure 2-1 and 2-2 show the performance of 15 ENSEMBLES RCMs

(of these, 9 of the 10 that are used in this study) in simulating 5-year return values for 1-day events on seasonal level in the Northern and Southern Alpine region in the period 1971-1998. The Southern region roughly corresponds to the Southern region used in this study (see section 2.2.3). The Northern region roughly corresponds to the two Northern regions used in aggregation. For the Northern Alps, a good reproduction of return values is obvious. Inter-model spread is clearly larger in the Southern Alps, where the performance of models is weaker when compared with the Northern Alpine performance. In the Southern Alps many models considerably under-estimate precipitation extremes (except in winter, where many models over-estimate return values). However, the general performance of ENSEMBLES RCMs in simulating extreme precipitation is good. Regarding other important diagnostics, for instance, precipitation intensity and frequency (illustrated in the Appendix-Figures A 1 to A 4), some slight drawbacks are worth noting. RCMs show the tendency to considerably over-estimate frequency and hence under-estimate intensity at the same time.

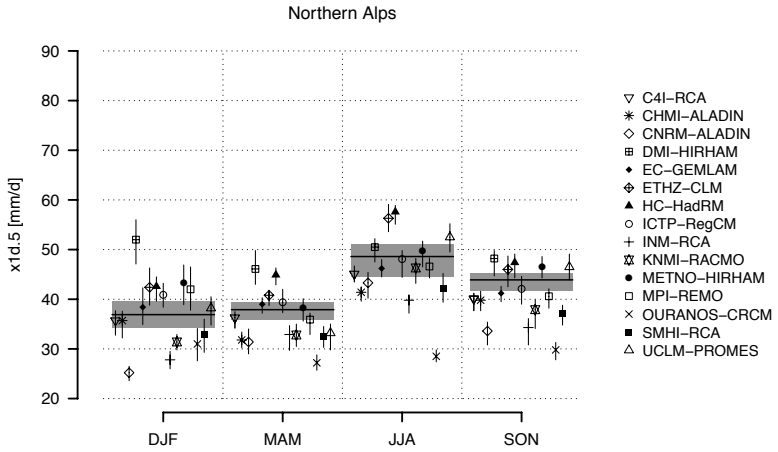

Figure 2-1: Domain-mean values and 90% confidence intervals for the 5-year return value of 1-day precipitation events on seasonal level in period 1971-1998 in the Northern Alpine region as simulated by 15 EU-ENSEMBLES RCMs (depicted by symbols and lines) and as observed, based on the FS1998-dataset (depicted as grey shaded area). Source: Arnold et al (2011, in prep.)

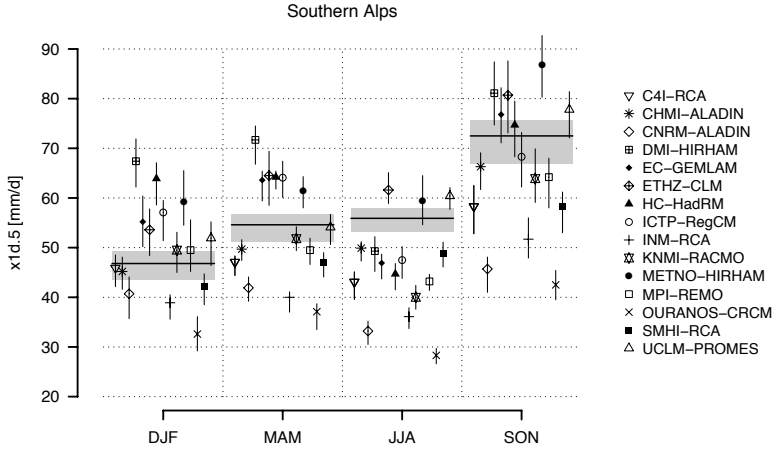

Figure 2-2: Domain-mean values and 90% confidence intervals for the 5-year return value of 1-day precipitation events on seasonal level in period 1971-1998 in the Southern Alpine region as simulated by 15 EU-ENSEMBLES RCMs (depicted by symbols and lines) and as observed, based on the FS1998-dataset (depicted as grey shaded area). Source: Arnold et al (2011, in prep.)

2.2 Methods

The aim of this study is to analyze 21st century projections of precipitation indices and extremes with respect to present-day climatic conditions as simulated by a set of 10 RCMs for the Alpine and adjacent central European region. Associated with climate change and the demand for more detailed knowledge about possible future climatic conditions and their impact, analyses on future extremes have become popular and suggestions on how to investigate changes in weather and climate extremes have been proposed [*Klein Tank and Zwiers*, 2009].

There are several methods to statistically define meteorological / climatological extremes, for instance by taking into account upper quantiles / percentiles of the frequency distribution, by exceeding critical thresholds or by modeling of rare events applying techniques of extreme value theory. This study uses basic climatological diagnostics, including the 90%-quantile, and extreme value modeling to characterize extremes and to additionally describe the precipitation climate. From a methodological point of view, this study is in strong accordance to the study conducted by [*Frei et al.*, 2006].

The investigation refers to 30-year climatic norm-periods on a seasonal scale, using the period 1961-1990 as the control period representing present-day climatic conditions (CTRL). Two future scenario time slices are analyzed comparatively to CTRL in order to assess change signals. Namely, these periods are the scenario period 2021-2050 (scenario 1, SCEN/1) taking ten RCMs into account, and secondly period 2070-2099 (scenario 2, SCEN/2) basing on a reduced subset of 5 RCMs (for an overview see labeled RCMs in Table 2.1-1 and time-slices in Table 2.2-1).

Table 2.2-1: Time slices investigated in this study.

Time Slice			**Period**	**Number of RCMs**
Abbreviation	*Name*	*Climatic condition*	*Time-slice*	**analyzed**
CTRL	Control	Present-day	1961-1990	10*
SCEN 1	Scenario 1	Mid-21st century	2021-2050	10*
SCEN 2	Scenario 2	Late-21st century	2070-2099	5*

* RCMs contributing to the investigation of each time slice are denoted in Table 2.1-1.

Table 2.2-2: Diagnostics examined in this study (in accordance to Frei et al. (2006).

Abbreviation	**Definition**	**Unit**
mea	climatological mean precipitation.	mm/d
fre	wet day[a] frequency, days with precipitation ≥ 1mm.	fraction
int	wet day[a] intensity, mean precipitation on days with precipitation ≥ 1mm.	mm/d
q90	empirical 90% quantile of precipitation during wet days[a].	mm/d
x1d.TT[b]	return value of 1-day precipitation intensity with a return period of TT.	mm/d
x5d.TT[b]	return value of 5-day precipitation intensity with a return period of TT.	mm/d

[a] a wet day is a day with precipitation ≥ 1mm.
[b] return period: 2, 5, 10, 20, 50, 100 years.

Two types of measures are thereby considered on a grid-point scale (Table 2.2-2). Firstly, basic descriptive indices representing the frequency distribution, precipitation character and moderate extremes are regarded. Secondly, extreme value analysis is applied to characterize events of very rare nature. In this study, rare precipitation events with return periods between

2 and 100 years are studied by adopting the block-maximum technique (BM) of extreme value theory.
Concerning heavy rainfall events, one should note that from a seasonal point of view, the character and synoptic origin of extreme rainfall in the Alpine region substantially differs. Being of convective nature and thus short-lived in summer, extremes in winter mostly evolve from large-scale synoptic disturbances causing long-lived multi-day precipitation periods. As a consequence, the analyses focus on 1-day extreme events in summer, spring and fall. Five-day extremes are considered in winter. A series representing 5-day rainfall events is obtained by applying a 5-day moving average window to a set of daily winter-precipitation data. All investigations are performed seasonally, which allows capturing possible seasonal changes and variations in a future climate. Seasons are thereby distinguished according to the commonly used climatic separation as follows: Winter, DJF; spring, MAM; summer, JJA and fall, SON.
To additionally assess simulated changes and inter-model differences on a regional level in more detail, three Alpine sub-regions are defined representing different climatic regimes within the Alpine region. For these three sub-regions, domain-mean changes between control and scenario time slices are investigated for all regarded diagnostics. This additionally includes the calculation of uncertainties to account for inter-annual variability and assess significances in simulated change signals. Uncertainty is thereby expressed by confidence intervals, which are estimated by applying bootstrapping techniques.
A further analysis, includes a detailed investigation of absolute return values and periods across three Swiss sub-domains, focusing on the three regarded time slices using a multi-model ensemble of 5 RCMs and observational records for the period 1971-1998 [*Frei and Schar*, 1998]. Methodological steps behind this additional study are further explained in section 3.3.1.

2.2.1 Descriptive Indices

Several descriptive / empirical measures are considered in this study with the aim to describe the character and process of precipitation, as well as moderate extremes. In general terms, one can summarize these measures as **climatological indices**. A set of different indices is thereby adequate to examine changes in precipitation more accurately, as the mean itself does not comprehensively explain the entire character of precipitation. Nevertheless, the mean integrates most descriptive measures and therefore states a fundamental diagnostic.
Considered descriptive measures are: mean precipitation (mea), wet day frequency (fre), wet day intensity (int) and the 90%-quantile of the precipitation intensity distribution on wet days (q90). All indices are also listed and further explained in Table 2.2-2. In the analyses, a wet day is defined as a day on which the 24h-precipitation amount is larger or equal to 1mm. Earlier studies have shown that the exact definition of this threshold did not affect the latter results to a large degree [*Frei et al.*, 2006].
Mean, intensity and frequency allow the description of the precipitations character and basic climatology at a given location. Changes in mean, frequency and intensity together also allow an explanation and interpretation of changes in precipitation extremes and the precipitation climatology in general. Moreover, the 90%-quantile is a basic measure for moderate rainfall extremes. In the Alpine region q90 roughly corresponds to a return period of 2 to 3 years. Intensity and q90 are furthermore independent of precipitation frequency. Regarding extremes, one should keep in mind that a consistent change signal and pattern for moderate extremes (q90) might be clearer to detect than for events of very rare occurrence obtained by extreme value modeling [*Frei and Schar*, 2001]. Such changes in q90 can be assumed to be a reliable estimate for future changes in extreme precipitation events.

All descriptive measures are based on series of 24h-precipitation totals, seasonally separated and obtained for each grid-point. Sub-regional values are calculated by averaging over all grid-points contained in the region of interest. Change signals depict the ratio between scenario and control integration.

2.2.2 Extreme Value Modeling

For heavy rainfall events with a very rare frequency of occurrence, empirical indices derived from the frequency distribution are not a useful measure, because values of interest lie in the far tail of the frequency /probability distribution or even exceed the highest value of the underlying 30-year dataset. Therefore, heavy rainfall event, must be modeled, by applying techniques of extreme value theory [*Coles*, 2001; *Klein Tank and Zwiers*, 2009]. These are commonly applied techniques in climate research, especially in regional impact studies [*Fowler et al*., 2007; *Frei et al*., 2006; *Hanel and Buishand*, 2011]. The modeling approach associated with extreme value analysis is basically is an extrapolation to the very far tails of the frequency /probability distribution. Being a special field in statistics, the subject of extreme value analysis is of a complex nature. There are different approaches to modeling extreme events. Two main approaches are mostly considered when modeling extremes associated with return periods and return values. These two approaches are namely, the peak-over-threshold (POT) and the block-maxima (BM) approach. The latter is applied in this study. Consequently, POT will not be discussed here in further detail. A detailed disquisition on POT and also BM is, however, given in [*Coles*, 2001]. The two approaches differ distinctly for example, in the way original underlying data is incorporated into the modeling of extreme events. Further differences are of a distributional character. In general, the advantage of block-maximum over POT is that it is more more accurate as only a few major assumptions have to be made a priori.

As already stated, the present investigation uses the **block-maxima method** to estimate return values and return periods of heavy rainfall events. In order to apply the block-maxima method, one has to divide the original dataset into several blocks of equal size: for example, by separating data in daily resolution into blocks by means of months, seasons or years. For each of these blocks the, greatest value is then extracted leading to a data-series containing only the most extreme values from each block (block maxima) in the time slice of consideration. The length of the resulting series of block maxima is equal to the number of blocks defined in advance. In the study presented, the original data is given by seasonally separated 30-year long time-series of daily precipitation amounts. Here, a block is defined as a season within each one of the 30 single years. This leads to a set of 30 (respectively 29 in DJF) maxima used in further analysis steps. The extraction of seasonal maxima is performed for each grid-cell separately: so too is also the estimation of return values and periods. In order to avoid unreliable estimates, dry grid boxes are excluded from extreme value analysis [*Frei et al*., 2006]. A grid-box is thereby assigned as being too dry and consequently excluded from the analysis if its seasonal wet day frequency in one of the considered time-slices is smaller than 0.02 (2%).

Following the "extremal types theorem" the distribution of a series of block maxima is distributed according to one of three asymptotic limit distributions. These namely are the Frechet-, Gumbel- or Weibull-distribution [*Kotz and Nadarajah*, 2001]. These three distributions can be generalized and combined to a so-called **General Extreme Value distribution (GEV)** [*Coles*, 2001; *Kharin and Zwiers*, 2005; *Klein Tank and Zwiers*, 2009]. The convergence of maxima towards a GEV (resp. one of the three limit distributions) is independent of the underlying datasets distribution under the assumption that the data is indeed independent and identically distributed. A GEV is characterized by three parameters

that have to be estimated in order to fit a GEV. These are: the location parameter (μ), the scale parameter (σ) and the shape parameter (ξ). The latter is the most important as it governs the tail and shape of the GEV and therefore largely influences estimated return periods and values. A shape parameter smaller than 0 depicts a heavy-tailed Fréchet-distribution: ξ=0 presents the light tailed Gumbel-distribution and a shape parameter greater than 0 the short-tailed Weibull case. The GEVs cumulative distribution function (CDF) is given by:

$$GEV(x) = \exp\left\{-\left[1+\xi\left(\frac{x-\mu}{\sigma}\right)\right]^{-1/\xi}\right\}$$

$$\text{where:} \qquad 1+\xi\left(\frac{x-\mu}{\sigma}\right) > 0$$

Here, a GEV distribution is fitted to series of 30 seasonal maxima (29 for winter analyses) at each grid-point using a **maximum-likelihood** procedure (MLE) in order to estimate the three GEV-parameters [*Coles*, 2001; *Hosking*, 1985].
Several methods in estimating parameters exist. In this context, it is worth noting that L-moments (LM) is usually a more robust estimation procedure when analyzing data with small sample sizes, as is the case in the study presented [*Katz et al.*, 2002; *Kharin and Zwiers*, 2005]. In the presented analyses, however, MLE is applied for the purpose of achieving consistency with [*Frei et al.*, 2006]. For this reason, and as also has been undertaken by [*Frei et al.*, 2006], a Bayesian **geophysical prior** distribution for the **shape parameter** is implemented to modify the MLE-procedure in order to avoid unrealistic estimates. The Bayesian prior distribution is characterized by a mean of -0.1 and variance of 0.122^2. It was proposed in [*Martins and Stedinger*, 2000] for the application of MLE to small sample sizes in geophysical applications (see also [*Frei et al.*, 2006] for proof of enhanced skill when applying to similar data as given in this study). The implementation of the prior distribution is thereby assumed to even enhance the skill of MLE compared to LM when analyzing geophysical data with small sample sizes [*Martins and Stedinger*, 2000].
Moreover, the climate in each 30-year periods regarded is considered as being stationary. In terms of parameter-estimation, time slices of longer extent should include a time-dependent estimation of parameters, in order to account for trends and variability [*Kharin and Zwiers*, 2005; *Klein Tank and Zwiers*, 2009]. As this study deals with commonly used 30-year long climatic norm periods such an implementation is not necessary.
Finally, having extracted the seasonal (block) maxima of a given time-slice and having then estimated the three parameters characterizing the fitted GEV distribution (at each grid-point) using MLE, one is now able to calculate return values and periods. Therefore one uses the inversion of the GEVs CDF, also known as the quantile function, which is given by:

$$x_p = \begin{cases} \mu - \frac{\sigma}{\xi}\left[1-\{-\log(1-p)\}^{-\xi}\right] & ,for \quad \xi \neq 0 \\ \mu - \sigma\, log\,\{-\log(1-p)\} & ,for \quad \xi = 0 \end{cases}$$

The p-year return value is given by x_p, being the daily precipitation rate exceeded once in a return period of p years. In other words, x_p refers to the threshold exceeded in any year of interest (within the considered time-slice) with a probability of 1/p. Return values, in the present analysis, are calculated for events with return periods of 2, 5, 10, 20, 50 and 100 years (see also Table 2.2-2). In general, the uncertainty afflicted with estimated return periods / values considerably increases for return periods twice as large as the underlying datasets

length [*Klein Tank and Zwiers*, 2009], such that the 100-year return value should be treated carefully.

2.2.3 Alpine Sub-regions

In addition to the spatial analysis on grid-point scale, three sub-regions covering the Alpine mountain range and parts of the adjacent foreland-belt are defined with the purpose of evaluating and characterizing regional changes more accurately. The regions defined are depicted in Figure 2-3. Their definition is made up according to climatological characteristics as described in the following.

North- and Southside are separated with respect to previous studies on extreme precipitation in the Alps [*Arnold*, 2009; *Frei et al*., 2006]. The Alpine main-crest serves as the divide between the Northern and Southern Alpine region as it also separates two distinct climatic regimes. These regimes are particularly reflected in terms of precipitation and the character of its extremes (section 1.2, [*Frei and Schar*, 1998; *Frei and Schmidli*, 2006]).

Divergent to previous studies, the region north of the main crest is separated into a Northwestern (NW) and Northeastern (NE) part. This subdivision can be explained by an increase of continental influence to the northeast and vice versa an increasing maritime influence to the west of the northern Alpine region. Regarding the annual cycle of precipitation, this is expressed by a pronounced summertime maxima in the Northeast and more or less annually balanced precipitation - locally peaking in fall and winter - in the Northwestern Alpine region (section 1.2 and Figure 1-2). Interestingly, the patterns also appear in the modes of a principal component analysis (PCA) applied to a reanalysis-dataset of daily precipitation [*Schmidli et al*., 2001]. The divide between the two northern Alpine regimes is roughly situated across the Arlberg pass in westernmost Austria [*Frei and Schar*, 1998]. As a result of this, the Arlberg region/pass serves as the separator between the two northern regions in this study.

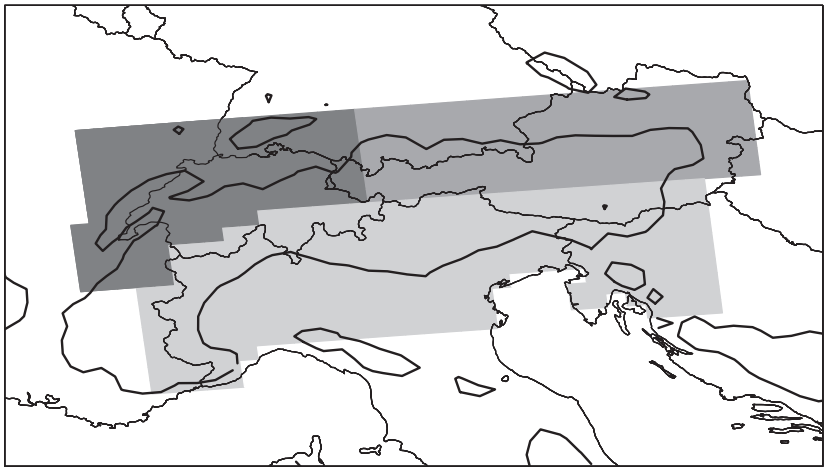

Figure 2-3: Alpine sub-regions used in this study. Gray shaded areas depict the sub-regions. Thin black lines denote the 700m a.s.l. isoline as represented by the ENSEMBLES-E-Obs topography. Bold lines indicate country borders and coastlines.

2.2.4 Confidence Intervals and Significances

In the interest of uncertainties and significances one can gain valuable information by using resampling methods to estimate confidence intervals [*Wilks*, 2006]. Here, a non-parametric bootstrapping approach is applied to determine 90%-confidence intervals for the estimates of

domain mean changes in descriptive indices and return values on seasonal level [*Frei et al.*, 2006]. Similar procedures have already been commonly applied in other studies focusing on changes in return values and their uncertainties [*Fowler et al.*, 2007; *Kharin and Zwiers*, 2005]. In change-studies, it is necessary to account for uncertainties in projections: especially as inter-annual variability is a crucial factor raising uncertainties.

In this study, change is expressed as the ratio between the average values of scenario and control simulations. According to the approach conducted by *Frei et al. (2006),* bootstrap samples are generated by resampling of years (extremes) /days (empirical diagnostics) at each grid-box. For the purpose of preserving the spatial correlation of precipitation fields, resampling at each sub-regions grid-box is performed for the same years /days. All in all, 50 bootstrap samples are generated for each scenario and control time-slice, representing 50 domain-mean values for a considered time-slice. A sub-regional bootstrap sample is thereby constructed by averaging the results obtained from all grid-boxes within a sub-region. The ratio (change) is then finally calculated by resampling between the 50 pairs of generated scenario and control bootstrap samples leading to 50 change estimates. This results in a frequency distribution containing 50 samples, from which the 5%- and 95%-percentiles are obtained to present the lower (q5) and upper bound (q95) of the confidence interval. From the information given by the confidence intervals range one can conclude whether changes are significant or not. If the value 1.0 - which represents no change - does not lie in the range limited by the upper and lower bound, one can infer that the projected change is significant with respect to conditions in the reference period (CTRL). In addition, resampling indicates the best estimate, being the median of the generated frequency distribution and therefore the most probable change signal between scenario- and control-integration.

3 Results

This chapter presents the results obtained throughout this study. The results section is subdivided into three sub-sections. The first part focuses on short-term changes for the mid-21st century. The second part extends the time-horizon and presents changes obtained from late-21st century simulations. The two first parts generally follow a similar structure. First, the spatial distribution of change is presented with the focus on central Europe / the Alpine region. Then a more detailed disquisition of individual model-projections, considering all investigated measures on sub-regional level is shown. The first part includes a more detailed inter-model assessment and an examination of individually projected spatial patterns. The third part is devoted to a case study in which absolute return values for three different inner-Swiss domains are estimated by a multi-model ensemble for present-day, mid-21st- and late-21st -century conditions. It infers how heavy rainfall events will change in future climatic conditions in terms of absolute values.

3.1 Short-Term Change

Results obtained for the analysis on short-term climate change are presented in this first part. Short term refers to changes as simulated for period 2021-2050 (SCEN1, also referred to as mid-21st century) with respect to the baseline period 1961-1990 (CTRL, also referred to as present-day conditions). The analysis of mid-21st century changes is most extensive, considering 10 regional climate models (Table 2.1-1). Results presented for mid-21st century changes are most extensive and take into consideration detailed illustrations of inter-model variability.

3.1.1 Spatial Distribution of Change

The spatial distribution of simulated change on seasonal level for all studied diagnostics from an ensemble of 10 RCM simulations is presented in Figures 3.1-1 to 3.1-3. The change signal shown refers to the ratio between period 2021-2050 (SCEN1) with respect to conditions in period 1961-1990 (CTRL). Changes between both time-slices are calculated for each RCM individually. To finally summarize the 10 RCMs individual results, the ensemble-median at each grid-box is chosen to be an appropriate measure in order to cancel out extreme outliers and summarize the results. Beyond that, grid-cells showing agreement in the sign of change are stippled, which means that 8 out of 10 (80%) models agree in the sign of simulated change. Blue (red) stippling denotes agreement in increase (decrease).
In order to capture distinct and systematic change patterns around the Alpine mountain range and region, the maps focus on central Europe, presented by the area between 42°N in the south, 52°N in the north, 0° in the west and 20°E in the east. The Alps form the major feature located in the center of the domain. Mountainous regions are designated by 700m-isolines, which explicitly outlines the arc-shape of the Alpine mountain range in the center of each plot.

Changes in precipitation **frequency** (fre) are shown in the left column of Figure 3-1. For fre one generally sees quite smooth change patterns in fall and winter with regions of model

agreement in an increase north and a decrease south of the Alps. Besides that, great areas across France (in fall) and east of the Alps (in winter) show no change in the occurrence of precipitation, marking the transition-zone in simulated change signals. In summer and spring, the models coincide, showing widespread decreases in frequency with greatest magnitudes towards the Mediterranean. The Alpine mountain belt (roughly denoted by the 700m-isoline), especially in winter and fall, depicts a region of sharp contrasts narrowed at the main-crest.

Very similar change patterns show up for the **mean** (mea), which is depicted in the right column of Figure 3-1. However, compared to fre, increases of mea north of the Alps in fall and winter are larger in magnitude and also regions of model agreement are of a greater extent. Especially in fall, the main crest of the Alps divides the southern and northern Alpine regime considerably sharp, showing an increase to the north and a decrease to the south of it. On the other hand, the extent of regions showing model agreement concerning a decrease of the mean in spring and summer are smaller than the ones for frequency and, above all, only defined in southwestern parts of central Europe (the Mediterranean proportion of the Alps).

For **intensity** (int), shown in the left column of Figure 3-2, remarkably different (and independent) patterns appear compared to the projection of changes for the mean and frequency. In winter, widespread model agreement is found for slight increases north of 45°N (containing most parts of the Alps), however, within the Alps and its northern foreland-belt, models do not agree in sign. In fall, the entire region north of 45°N does also experiences a slight increase in intensity. Contrary to winter, model agreement in an increase is now seen from the inner-alpine region (main-crest) northwards on. In spring and summer, the magnitude of change is weak and the patterns are quite smooth. Areas of model agreement are then very spotty in distribution. Solely in summer, does one see a leaning towards a decrease in intensity in the southwest and an increase towards the northeast: this is very distinctly pronounced over the northeastern Alpine foreland.

Regarding the **90%-quantile** (q90) shown in the right column of Figure 3-2, one recognizes patterns that are highly correlated to the change patterns shown for intensity. Nevertheless, the distribution of changes in q90 appears spottier and locally stronger in magnitude (e.g. the increases along the northern Alpine rim in fall).

Figure 3-3 depicts projected changes in the 5-year return values for **1- and 5-day precipitation extremes** (x1d.5 and x5d.d). The spatial patterns emerging for both diagnostics are very similar, whereas x5d.5 shows a smoother character in terms of magnitudes and patterns. Furthermore, both distributions are similar to the spatial distribution of changes seen for int and q90: from which the latter depicts moderate extremes with small return values [~2 years].
Nevertheless, x1d.5 and x5d.5 show a very spotty behavior. Most distinct changes occur in fall, where one sees strong increases across great areas, especially on the northern side of the Alps. The same is visible - in alleviated character - in winter. In winter, however, one sees widespread decreases in multi-day precipitation episodes (x5d.5) across the eastern inner- and outer-Alpine regions. The most remarkable change patterns simulated over the Alps in spring and summer are represented by an elongated zone of decreases along the western Alpine main crest in spring and a widespread area of increasing summertime extremes over the northeastern Alpine foreland.

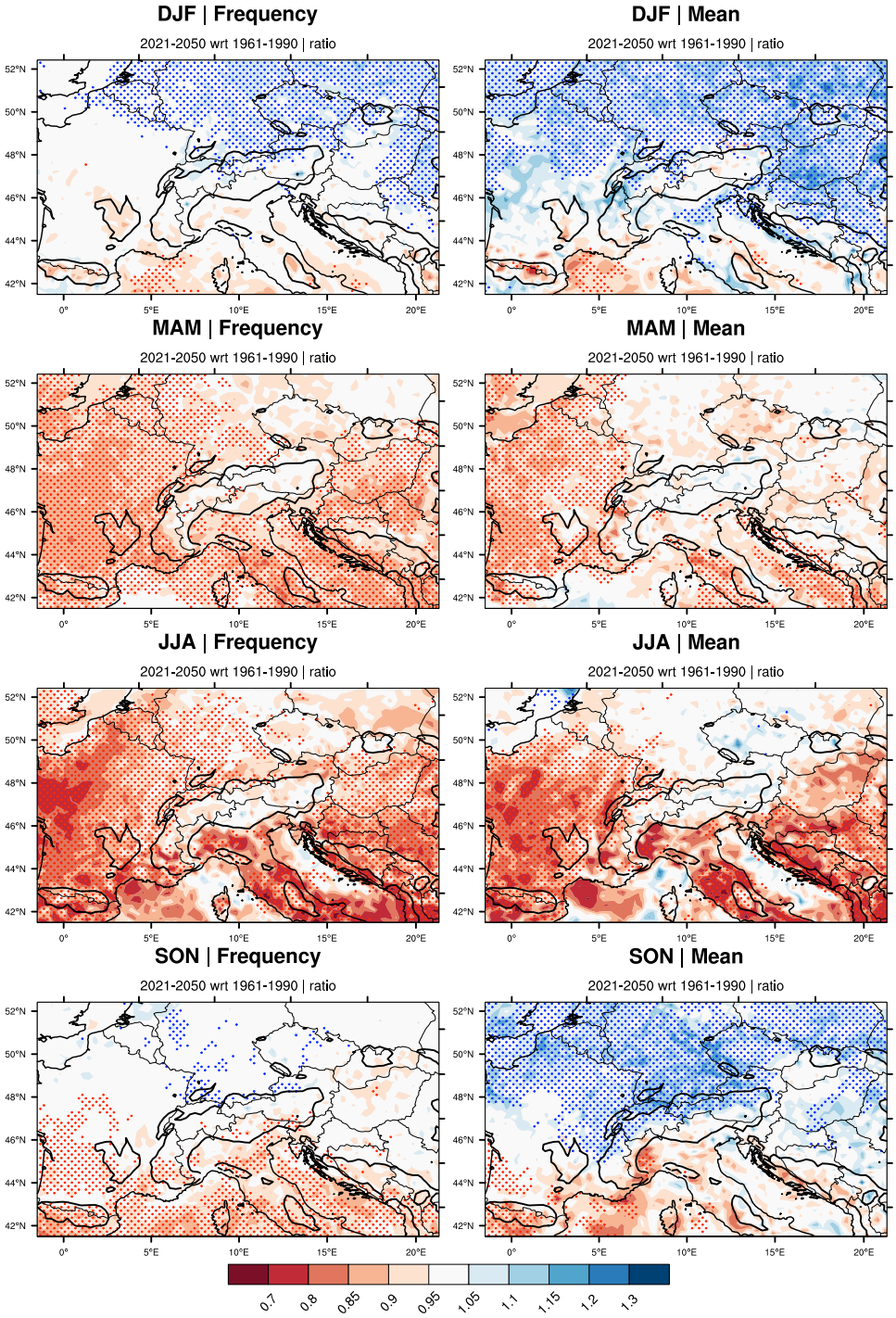

Figure 3-1: Projected change (ratio SCEN/CTRL) in precipitation frequency (left column) and the mean (right column) as simulated by a multi-model ensemble of 10 RCMs on seasonal level. Depicted is the ensemble-median change signal for period SCEN1 (2021-2050) wrt CTRL (1961-1990). Stippling denotes model agreement (80%) in increases (blue) and decreases (red). Thick lines illustrate the 700m a.s.l.-isoline as represented by the ENSEMBLES E-OBS topography.

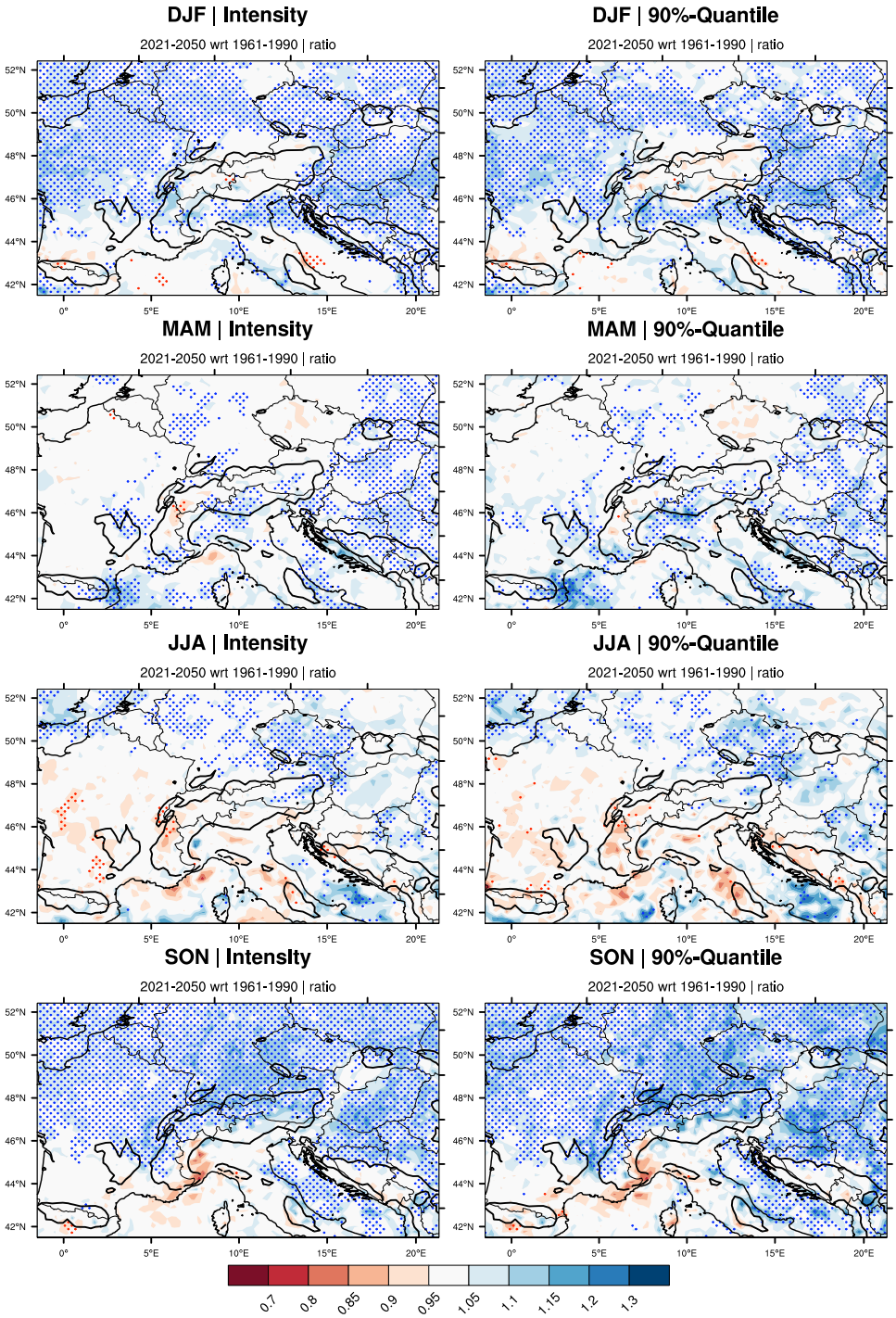

Figure 3-2: Projected change (ratio SCEN/CTRL) in precipitation intensity (left column) and the 90% quantile (right column) as simulated by a multi-model ensemble of 10 RCMs on seasonal level. Depicted is the ensemble-median change signal for period SCEN1 (2021-2050) wrt CTRL (1961-1990). Stippling denotes model agreement (80%) in increases (blue) and decreases (red). Thick lines illustrate the 700m a.s.l.-isoline as represented by the ENSEMBLES E-OBS topography.

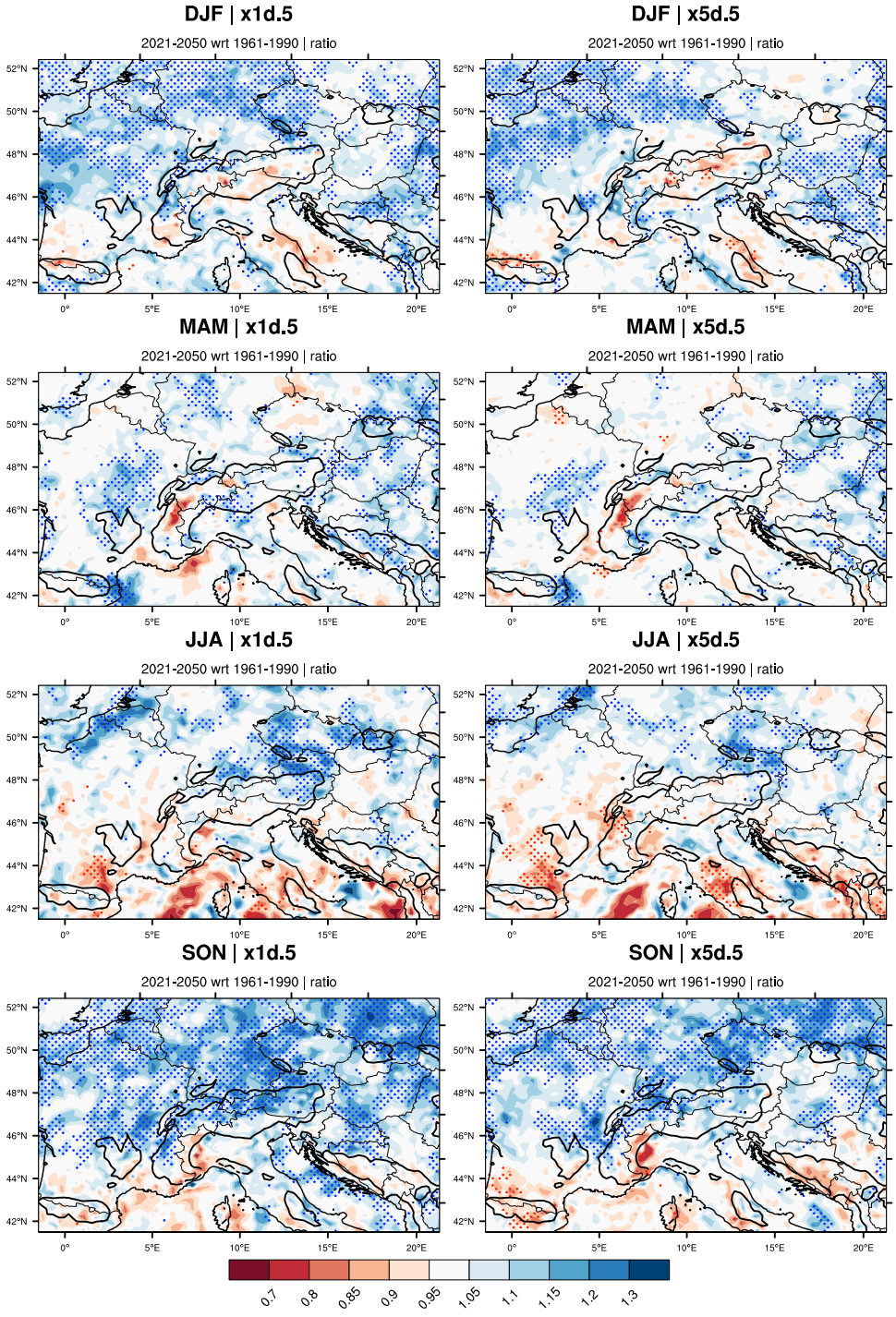

Figure 3-3: Projected change (ratio SCEN/CTRL) in the five-year return value for 1-day (left column) and 5-day (right column) precipitation events as simulated by a multi-model ensemble of 10 RCMs on seasonal level. Depicted is the ensemble-median change signal for period SCEN1 (2021-2050) wrt CTRL (1961-1990). Stippling denotes model agreement (80%) in increases (blue) and decreases (red). Thick lines illustrate the 700m a.s.l.-isoline as represented by the ENSEMBLES E-OBS topography.

3.1.1.1 Inter-model Variability

Considering the spatial distribution of projected change patterns, one should note the high inter-model variability concerning the individual spatial distributions and magnitudes of simulated changes in extremes (and also basic diagnostics). Inter-model variability is not deducible in plots showing the ensemble-median signal, as described earlier. At the most, however, spatial variability is shown by means of the very patchy distribution of areas with model-agreement and the very variable magnitude of median change-signals for intense diagnostics.

To illustrate this problem, Figure 3-4 is presented. It depicts each RCMs individually simulated spatial distribution of change for the **5-year return value of 1-day rainfall events** in **fall**. As one can clearly see, there is no consistent and robust pattern found throughout all RCM projections. In fact, models simulate very variable change patterns and magnitudes. However, to a certain degree, patterns relate to each other when considering RCMs driven by the same GCM. Two distinct examples for characteristics shown concordantly throughout GCM-groups are: the increases across the northwestern Alpine region by HadCM3Q0 models and the projected increases by most ECHAM5 models over the northeastern Alpine foreland.
In terms of **empirical diagnostics**, inter-model variability in the spatial distribution of change is weaker and emerging change-patterns show more similarity. However, this similarity also strongly depends on the driving GCM. As an example for this behavior, the individually simulated distributions of change for **intensity** in **fall** are presented in Figure 3-5. Intensity in fall is considered as its change behavior is strongly related to changes in extremes. Projected changes in intensity reproduce patterns shown for extremes in a smoothed character and therefore provide an applicative visual example for GCM-dependence. Considering the results for int, one also sees the systematic increases along the northwestern Alpine region, consistently simulated by the set of HadCM3Q0 driven RCMs. A feature reproduced by all ECHAM5-RCMs is strong decreases in northeastern Italy (lee-side of the Alpine arc) and also increases in precipitation intensity over the northeastern Alpine foreland. The single model CNRM-RM, driven by the Arpege GCM, deviates most from the whole set of RCMs, supporting the GCM-grouping hypothesis.
From these examples, one can conclude that inter-model differences in the projection of future heavy precipitation events do not primarily depend on the individual RCM parameterizations. Inter-model differences are, to a large degree governed by the driving conditions delivered by the GCMs in which the individual RCMs are nested.

A more **comprehensive overview** on this topic is given in a set of appendix-figures (Figures A 5 to A 17) showing inter-model variability on seasonal scale for several diagnostics. At large, these figures support GCM-grouping of the spatial change distributions obtained from individual RCM-projections. Figures A5 to A8 show the patterns for q90, which are highly variable across all models. Spatial variability is thereby largest for summer-projections. Frequency is shown in Figures A9 to A12. For fre, showing smooth patterns, GCM-arrangement is very pronounced. However, VMGO-RRCM obviously suffers systematic changes over mountainous terrain and thus deviates outstandingly from other HadCM-RCM projections. Furthermore, individual projections of changes in the mean are shown in Figures A13 to A17. Likewise, smooth GCM-dependent patterns show up for mea.
All shown diagnostics have a seasonal dependence in the GCM-arrangement in common. Remarkable similarities between models driven by the same GCM are thereby seen in winter and fall. In spring and especially summer, the arrangement is slightly alleviated but obvious.

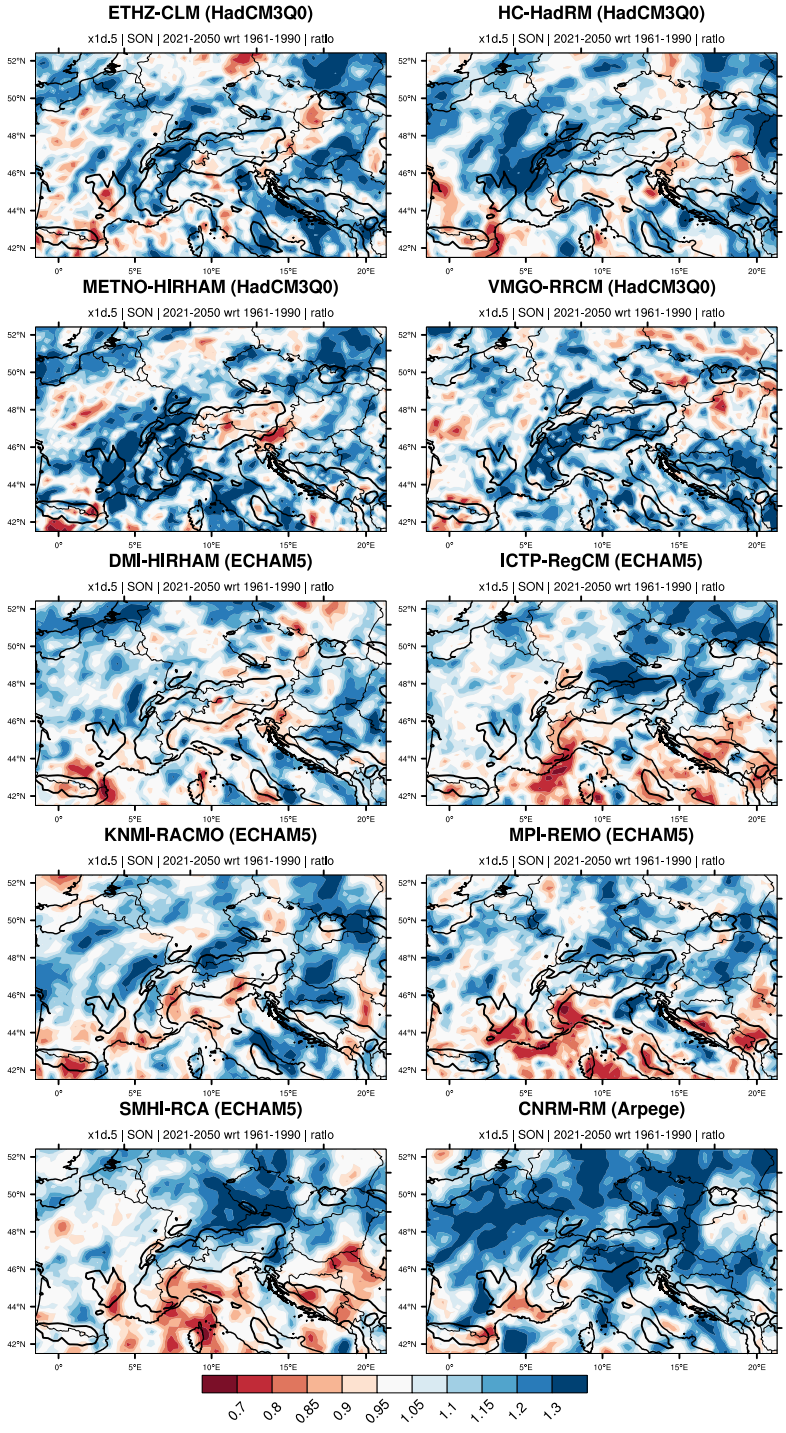

Figure 3-4: Change (ratio SCEN/CTRL) in the five-year return value for 1-day precipitation events in fall as simulated by 10 RCMs for period SCEN1 (2021-2050) wrt CTRL (1961-1990. Thick lines illustrate the 700m a.s.l.-isoline as represented by the ENSEMBLES E-OBS topography.

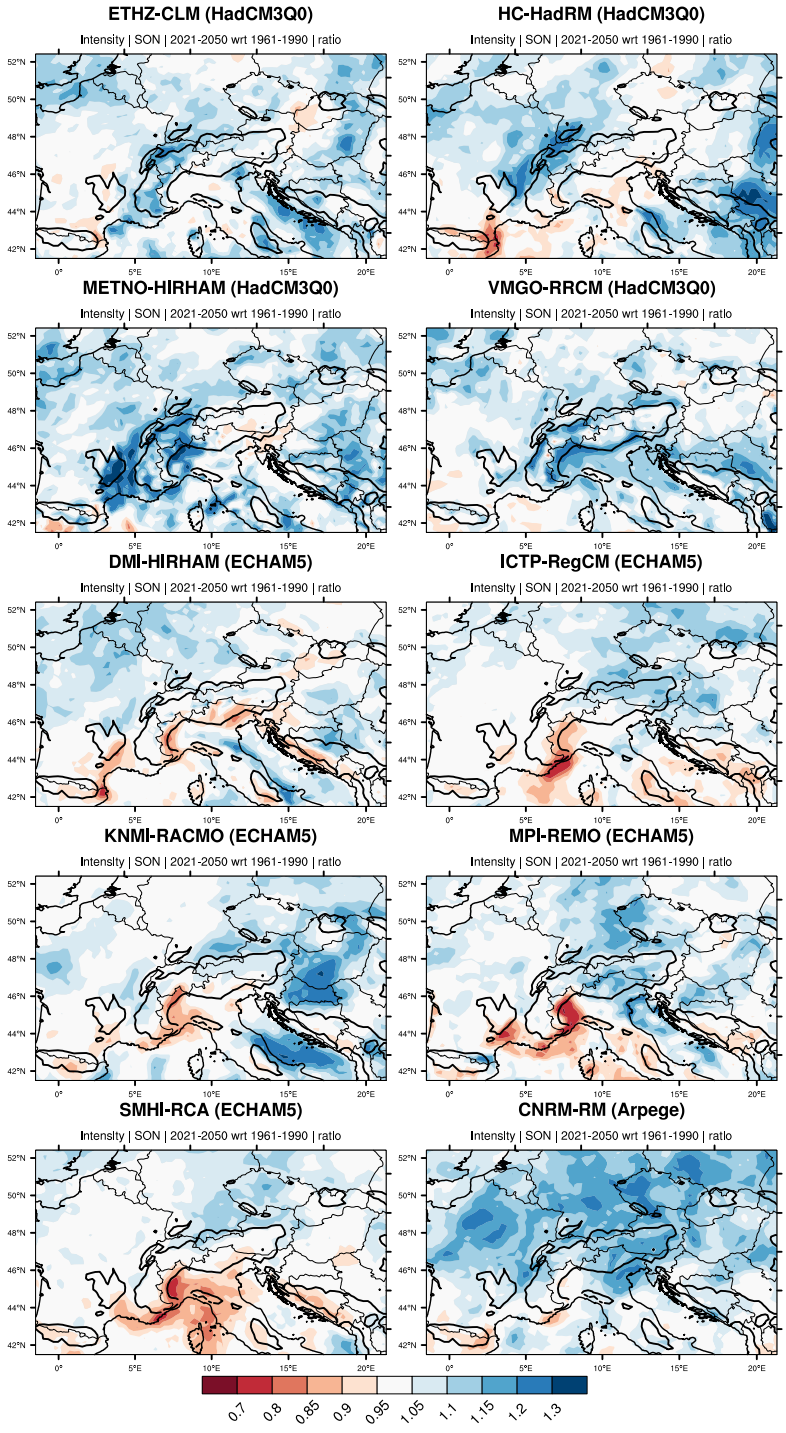

Figure 3-5: Change (ratio SCEN/CTRL) in precipitation intensity in fall as simulated by 10 RCMs for period SCEN1 (2021-2050) wrt CTRL (1961-1990. Thick lines illustrate the 700m a.s.l.-isoline as represented by the ENSEMBLES E-OBS topography.

3.1.2 Summarized Change in Domain-mean Diagnostic

The large-scale spatial distribution of change with its distinct patterns and versatile magnitudes of change for the diagnostics examined reveal a high spatial - but systematic - variability across the central European continent and Alpine region (Figures 3.1-1 to 3.1-3). This spatial variability is reflected in different and characteristic change signals and inter-diagnostic structures in the three sub-regions of closer interest (Figure 2-3). The seasonal change signals in sub-regional mean values for the diagnostics examined, as simulated by 10 RCMs, are summarized in boxplots. The figures show changes for period 2021-2050 (SCEN1) with respect to conditions in period 1961-1990 (CTRL). Figure 3-6 presents the seasonal change structure for climatological diagnostics. Figure 3-7 depicts the seasonal change in extreme 1- and 5-day rainfall events associated with return periods between 2 and 100 years.

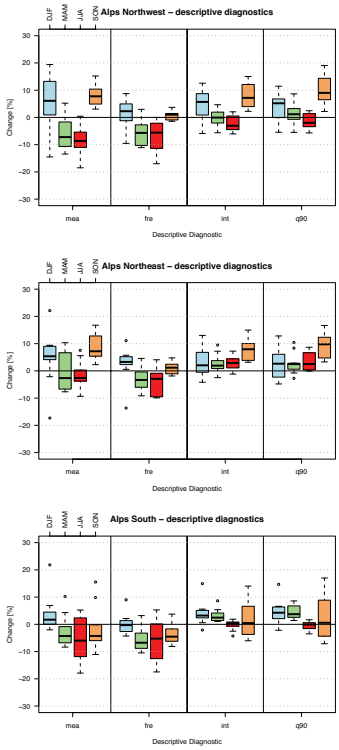

Figure 3-6: Boxplots summarizing seasonal change signals in empirical diagnostics, as simulated by 10 RCMs on sub-regional level for period 2021-2050 (SCEN1) wrt 1961-1990 (CTRL).

Descriptive Measures

Regarding the change structure of empirical measures in **NW,** one can clearly emphasize a seasonal dependency in the magnitude and sign of change. Model agreement in the sign of change can thereby be seen in a decrease of frequency (fre) and mean (mea) in summer and spring. On the other hand a majority of RCMs simulate an increase of the mean and frequency in winter. In fall, models agree in an increase of the mean while fre does not remarkably change. This implies that intensity and the 90%-quantile (q90) increase to compensate for the loss caused by the decrease in fre. As in fall, a majority of models also simulate increases in int and q90 in winter. In summer and spring, int and q90 reveal no clear change-signal,

whereas there is a leaning of models to simulate slight decreases in moderate extremes (q90 and int) in summer.

In **NE** the structure is generally similar to NW, however, the seasonal cycle of the change signals is damped in its amplitude. Moreover, it should be mentioned that, anomalous to NW, some models simulate an increase in the mean for spring and that int and q90 in spring and especially summer tend to show slightly increasing signals.

All in all, most striking changes in NE and NW are simulated to occur in fall with an increase in precipitation intensity and a positive shift of the 90%-percentile (q90) towards higher values. Also, decreases in the total amount and frequency of summer-time precipitation are a robust feature across the majority models.

In **S**, there is no evident seasonal cycle in the change structure. Most striking changes take place in summertime with a majority of RCMs simulating decreases in the mean and frequency. In weakened character, these decreases can also be seen in spring and fall. Furthermore, projections of mean precipitation in winter mainly lean towards an increase, while frequency is simulated to not change. To account for the increase in mean, intensity and q90 are by a majority models simulated to increase in winter. Increases - of similar magnitude - in int and q90 are seen in spring. For summer, models largely agree in that there is no change at all as relating to moderate extreme diagnostics. In fall, inter-model spread for the two diagnostics (int & q90) is large. The ensemble-median, however, balances out to project a stable signal.

Precipitation Extremes

Changes found in heavy rainfall events are similar to the changes simulated for the 90%-quantile and intensity. This inter-relation is also visible in the spatial distribution of change as presented before (Figure 3-2). Nevertheless, the most distinct features seen for extremes are described on a sub-regional level in the following and also in 3.1.3.

In the **NW** subdomain changes in extremes experience a seasonal cycle / variation, with most remarkable changes (increases) in winter and fall and quite stable (1-day events) / slightly decreasing (5-day events) signals in spring and summer. Inter-model spread, reflected by a large interquartile-range (box), is thereby greater for 5-day precipitation events. Moreover, some models simulate decreasing signals for extreme multi-day precipitation events in winter. Decreases in the strength of long-term precipitation periods are also simulated by a majority of models in spring and summer. This signal is oppositional to the signals projected for short-lived precipitation events in summer and spring, which by a majority of models are simulated to slightly increase in intensity.

For the **NE** sub-region changes in extremes are simulated without a seasonal cycle. Increases in 1-day extreme events are simulated by nearly all RCMs throughout all seasons, changes are thereby most prominent and very distinct in fall. However, inter-model spread (width of box) in fall projections is large. Changes in multi-day precipitation extremes are more complex and weaker. In winter there is an obvious leaning for small return periods towards decreases in return values. For large return periods, this signal becomes even more pronounced, such that most models simulate a decrease in return values for multi-day events with return periods of 100 years. This decrease states the complete opposite to the change simulated for short-lived events in winter.

In **S** there is no dominant seasonal pattern in the change signal for heavy rainfall events. Model spread and median-changes are generally not as strong in magnitude as in NW and NE. In all seasons, except summer, most models tend to simulate slight increases in return values. In summer, models tend to simulate stable to slight decreasing change signals. Also, multi-day precipitation extremes rather show a leaning towards decreases.

Summarizing the results for heavy rainfall events, they imply that extremes are likely to become more severe in future climatic conditions across all sub-regions. Most serious signals and magnitudes of change are seen in the two Northern Alpine regions. Slight differences can be drawn in the magnitude of intensification in between seasons. From a seasonal point of view, heavy precipitation events in winter and fall are simulated to increase most. Worth noting is the tendency of multi-day precipitation extremes to change less or rather become weaker in severity in comparison to one-day extremes that clearly become stronger in the majority of simulations. In some seasons, the projected signs are even oppositional (e.g. in summer-time for a return period 100 years in NW, or winter-projections in NE).

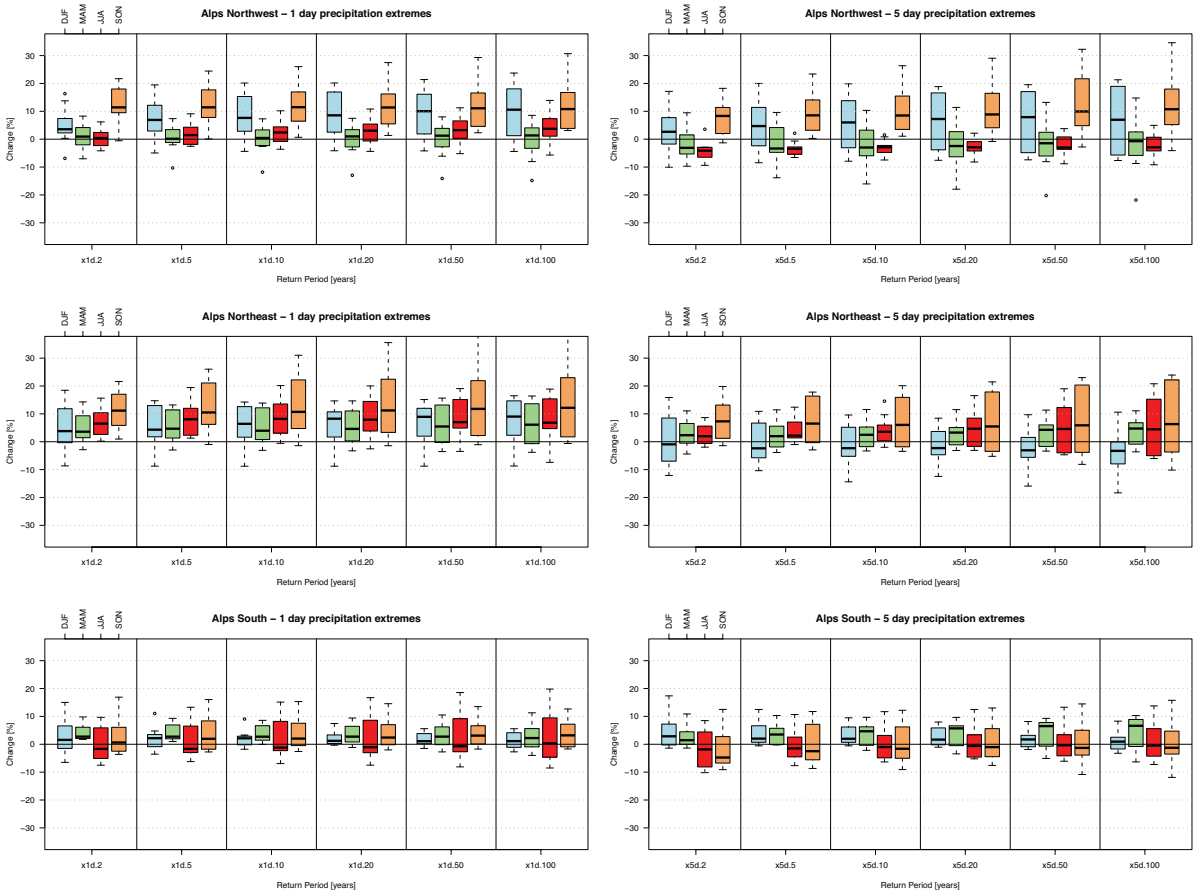

Figure 3-7: Boxplots summarizing seasonal change signals for 1-day (left) and 5-day (right) precipitation extremes with return periods between 2 and 100 years, as simulated by 10 RCMs on sub-regional level for period 2021-2050 (SCEN1) wrt 1961-1990 (CTRL).

3.1.3 Simulated Change Structure across RCMs

This paragraph presents the seasonal change structure for domain mean values across empirical and extreme diagnostics as individually simulated by 10 RCMs (Table 2.1-1) in three Alpine sub-regions (Figure 2-3). In terms of extremes, projected changes for events with return periods of 5, 10 and 50 years are considered. Moreover, associated confidence intervals are presented. These give inference about significance and uncertainty in simulated change signals. Mid-21st century conditions (2021-2050, SCEN1) are thereby compared to present-day conditions (1961-1990, CTRL).
As can be derived from the spatial distribution of change in the presented maps (Figures 3.1-1 to 3.1-2) and also from the summarizing boxplots (Figures 3.1-6 and 3.1-7), the magnitude and sign of change signals are spatially and seasonally highly variable. In additional to the results presented earlier, this section points out inter-model differences in simulating future climatic conditions on sub-regional level, as each projection of each model is presented separately. A brief summary on what is depicted in the figures and tables is given in the following.

Winter
In winter (Figure 3-8 and Table 3.1-1), inter-model variability is large. Coherent and robust change signals are thereby only seen among RCMs with same driving GCMs, especially in NE and NW. The high dispersion of model-projections reveals large uncertainties for winter-projections.
Generally, most models are certain about only weak changes in frequency, however, the CNRM-RM and VMGO-RRCM models do highly deviate from other model projections across all regions. Moreover, CNRM-RM shows large uncertainties, reflected by broad confidence intervals. Mean precipitation is mostly simulated to slightly increase in NE and NW, while projections lean towards decreases in S. Regarding int, q90 and extreme diagnostics one sees a very distinct GCM-arrangement in NW. ECHAM5-driven RCMs mostly simulate significant increases between 10% and 15% accompanied by significant increases in int and q90, while HadCM3Q0-RCMs - in the case of extremes - mainly project decreases. This structure is, to some extent, reversed when considering the situation in NE. Here, ECHAM5-RCMs show slight increases, whereas HadCM3Q0-models are rather uncertain and disperse. In S, slight increases in int and q90 are projected with quite good model agreement. Extremes in S are simulated to not change considering ECHAM5-driven RCMs, HadCM3Q0-models tend to project slight increases.

Spring
Spring (Figure 3-9 and Table 3.1-2) is the season showing the most similar change structure across all three sub-regions. In general, spring-projections relate to projected change found in summer integrations, but in an alleviated character. Most conspicuous projections are thereby found for the mean and frequency, which tend to decrease in the projections of a majority of models and in all regarded sub-regions. Intense and extreme diagnostics rather tend to be quite stable, whereas a leaning towards slight decreases in ECHAM5-projections and a leaning towards increases in HadCM3Q0-projections is obvious.

Summer
In summer, the most pronounced changes are simulated for frequency and the mean in all three subregions (Figure 3-10 and Table 3.1-3). The most striking decreases in the mean are projected in the South (S) and in the Northwest (NW). In the Northeast (NE), decreases in the

mean are balanced out by marked increases in intensity and heavy rainfall events that compensate for the loss through projected decreases in frequency.
Regarding the sub-regional change structure in more detail, one can highlight the most prominent findings as follows. Especially in terms of frequency and the mean, inter-model spread in all three sub-regions is large. Even so, most models simulate significant decreases in frequency and the mean. Change signals for the mean are afflicted with the largest inter-model spread, covering the positive and negative value range (in NE: -9% [MetNo-HIRHAM] to +14% [VMGO-RRCM]; in NW: -35% [HC-HadRM] to +7%[DMI-HIRHAM] and in S: -34% [MetNo-HIRHAM] to +15% [ICTP-RegCM]). This spread reflects the large model uncertainty associated with projections of precipitation in summer (see also *Frei et al. (2006)*), which is likely due to very small-scale and short-lived precipitation events that are demanding to capture in RCMs. In summer-projections, HadCM3Q0 driven models tend to simulate more considerable decreases than ECHAM5 RCMs. Uncertainties (range of confidence intervals) related to the individual model-projections of mean and frequency are largest in the southern sub-region, where one could expect the largest inter-annual variability in summer precipitation. Projections of intensity and q90 do not demonstrate articulate change signals for mid-21st century integrations: likewise for extreme diagnostics. Exceptional in this regard is NE, where most models simulate an intensification of extremes and slightly increasing signals for int and q90. The most considerable model is thereby ETHZ-CLM simulating significant increases in int (+6%), q90 (+6%) and extremes (e.g. x1d.5: +13%). Extremes in S, more or less cluster depending on the driving GCM, whereas ECHAM5 models rather simulate decreases (e.g. x1d.50, value-range: -9% to -3%) and HadCM3Q0 driven models increases (e-g- x1d.50, value-range: -4% to +16%). As can be seen, the projected increases in HadCM3Q0 driven models in S are afflicted with larger inter-model spread. In NW change-signals for extremes, oscillate around a no-change signal. The stable trends in int, q90 and extremes (representing the tail of the frequency distribution) in connection with decreases in the mean imply a broadening of the precipitation frequency distribution and therefore an enhanced variability of summer-precipitation in general.

Fall
As is illustrated by Figure 3-11 (and Table 3.1-4), fall is the season showing the most prominent projected changes for extreme and moderate extreme precipitation diagnostics. As in winter-projections, RCM-projections in fall consistently and highly cluster depending on their underlying driving GCM. The most noticeable projections are generally characterized by striking intensifications of heavy rainfall events in the two northern sub-regions (NE and NW) and decreases in frequency and the mean in the south, whereas intense rainfall in S is mainly simulated to not considerably change.
On sub-regional level, the RCMs mainly simulate stable frequencies in NE and NW and slight decreases in S. Simultaneously all models simulate increases in the mean in NW and NE. In S, the mean is simulated to significantly decrease. According to HadCM3Q0 driven projections for instance, projected decreases in mea lie in the range of -14 to -31% (in S). Other model projections (ECHAM5 and the CNRM-Arpege model) highly vary in sign, more or less around stable conditions (0% change). Considering intensity, q90 and extremes one detects impressive results. In NW and NE, the majority of models simulate significant increases in intensity and the 90%-quantile in a magnitude around +10% (e.g. q90 in NW by HC-HadRM: +18%). In S, the direction of change in int and q90 highly depends on the driving GCM (similar to mea). ECHAM5-RCMs simulate decreases, whereas HadCM3Q0 models, at the same time, simulate increases. The same GCM-dependent inter-relation is seen for projections of extreme precipitation events in S. In NW and NE, striking intensifications are simulated to take place for extreme events. As is also illustrated in Figure 3-5, the exact

location of largest projected increases in models along the Alpine North-side highly depends on the driving GCM. While HadCM3Q0 models project increases in the Northwestern Alpine region, ECHAM5-models simulate strong increases in the Northeastern Alpine region. As Figure 3-11 presents, projected changes in NE and NW are then significant. However, nearly all models, independent of the GCM, simulate increases in these two regions, in a dimension up to 25% in NW (HC-HadRM, x1d.10) and 41% in NE (ICTP-RegCM, x1d.50). Note that the large inter-RCM spread is, to a large degree, governed by the GCM dependence and the spread implied by this relationship.

Summary

Some general concluding remarks can be given concerning the results presented in this section.

In general, RCMs robustly and consistently coincide in the sign and to a certain degree in the magnitude of projected change for the different precipitation diagnostics across the three sub-regions and seasons regarded. However, inter-model spread and a GCM-arrangement of RCM-projections is obvious throughout all seasons. Most pronounced GCM-arrangement is seen in winter and fall, where GCM-spread largely contributes to the overall inter-RCM spread, markedly in the northern Alpine region (NW & NE). Particularly in summer, GCM arrangement is weak, but inter-model spread is large. The investigation of inter-model spread also reveals that projections of intensity and q90 are afflicted with the weakest dispersion across models. Projections of the mean change signal show the largest spread, possibly due to the fact that the mean integrates across several diagnostics. Considering extremes, dispersion of model projections highly depends on the season and region regarded.

Uncertainty, expressed by the width of confidence intervals, is - in most seasons - largest in the southern sub-region. However, projections in the S are most, showing least inter-model spread, across all considered diagnostics. In this regard one should note that the size of the southern region, being roughly as large as the two northern regions in aggregate, might spatially average out inter-model spread.

Considering the uncertainty of single models, it is largest for the CNRM-RM model, which is the only (single) model driven by the Arpege GCM. Together with the VMGO-RRCM (HadCM3Q0 driven), CNRM-RM also deviates most from the other RCM projections. From the ECHAM5-RCM group, the DMI-HIRHAM RCM shows most deviating behavior.

Uncertainty in regard of single diagnostics is largest for the mean, followed by frequency and extreme diagnostics. For intensity and q90 quite small uncertainty ranges are calculated and inter-model spread very small.

Further inter-model assessment

Another inter-model assessment addressing simulated return values is given in two appendix figures. The figures show domain-mean changes for events with reoccurrences between 2 and 100 years, as individually simulated by the 10 RCMs on a seasonal level and for each sub-region considered.

Table 3.1-1: Best estimate of change (ratio SCEN1/CTRL) in domain mean precipitation diagnostics and 5-day precipitation extremes in winter (DJF) as simulated by 10 RCMs for period 2021-2050 (SCEN1) wrt 1961-1990 (CTRL).

NORTHWESTERN ALPS [NW]

RCM	fre	mea	int	q90	x5d.5	x5d.10	x5d.50
Arpege							
CNRM-RM	**0.90**	**0.88**	**0.94**	**0.95**	0.92	0.92	0.94
ECHAM5							
DMI-HIRHAM	**1.05**	**1.06**	0.99	0.98	0.98	0.99	1.00
KNMI-RACMO	**1.04**	1.00	**1.09**	**1.07**	**1.12**	**1.14**	**1.18**
MPI-REMO	1.02	**1.06**	**1.06**	**1.05**	1.10	**1.14**	**1.20**
SMHI-RCA	**1.05**	**1.29**	**1.09**	**1.06**	**1.11**	**1.13**	**1.16**
ICTP-RegCM	1.01	1.11	**1.05**	**1.04**	**1.09**	**1.12**	**1.18**
HadCM3Q0							
ETHZ-CLM	0.98	0.99	1.02	1.01	0.97	0.95	0.94
HC-HadRM	0.96	0.99	**1.04**	**1.06**	0.99	0.99	0.97
METNO-HIRHAM	0.99	**1.13**	1.00	0.99	0.97	0.95	0.94
VMGO-RRCM	**1.08**	**1.12**	**1.12**	**1.10**	**1.20**	**1.19**	**1.18**

NORTHEASTERN ALPS [NW]

RCM	fre	mea	int	q90	x5d.5	x5d.10	x5d.50
Arpege							
CNRM-RM	**0.86**	**0.83**	**0.96**	0.95	0.88	0.89	0.90
ECHAM5							
DMI-HIRHAM	**1.03**	1.03	1.01	1.02	1.07	1.09	1.11
KNMI-RACMO	**1.05**	**1.11**	1.02	1.05	0.98	0.98	0.97
MPI-REMO	**1.05**	1.01	0.99	0.96	0.93	0.94	0.96
SMHI-RCA	**1.05**	**1.06**	0.99	0.97	0.97	0.97	0.99
ICTP-RegCM	1.01	1.04	0.97	**0.94**	0.93	0.94	0.96
HadCM3Q0							
ETHZ-CLM	1.03	1.02	**1.07**	**1.05**	1.07	1.06	1.04
HC-HadRM	1.02	1.03	1.04	1.02	0.94	0.91	**0.86**
METNO-HIRHAM	1.03	1.03	**1.06**	**1.06**	**1.09**	1.07	1.05
VMGO-RRCM	**1.11**	**1.34**	**1.12**	**1.12**	1.07	1.01	0.92

SOUTHERN ALPS [S]

RCM	fre	mea	int	q90	x5d.5	x5d.10	x5d.50
Arpege							
CNRM-RM	0.97	1.08	1.01	1.05	1.01	0.99	0.96
ECHAM5							
DMI-HIRHAM	1.00	**0.86**	0.97	0.97	1.02	1.00	0.97
KNMI-RACMO	1.02	0.98	1.04	1.06	1.02	1.02	1.03
MPI-REMO	1.02	1.01	1.02	1.02	1.00	1.01	1.01
SMHI-RCA	1.01	0.99	1.03	1.05	1.01	1.01	1.01
ICTP-RegCM	0.97	0.95	1.02	1.03	0.99	0.99	0.98
HadCM3Q0							
ETHZ-CLM	0.94	0.85	1.02	1.01	1.04	1.03	1.06
HC-HadRM	0.97	0.91	1.02	1.02	1.08	1.07	1.07
METNO-HIRHAM	**0.97**	0.98	**1.04**	1.05	1.01	0.99	0.97
VMGO-RRCM	**1.08**	**1.13**	**1.14**	**1.12**	**1.12**	**1.10**	1.05

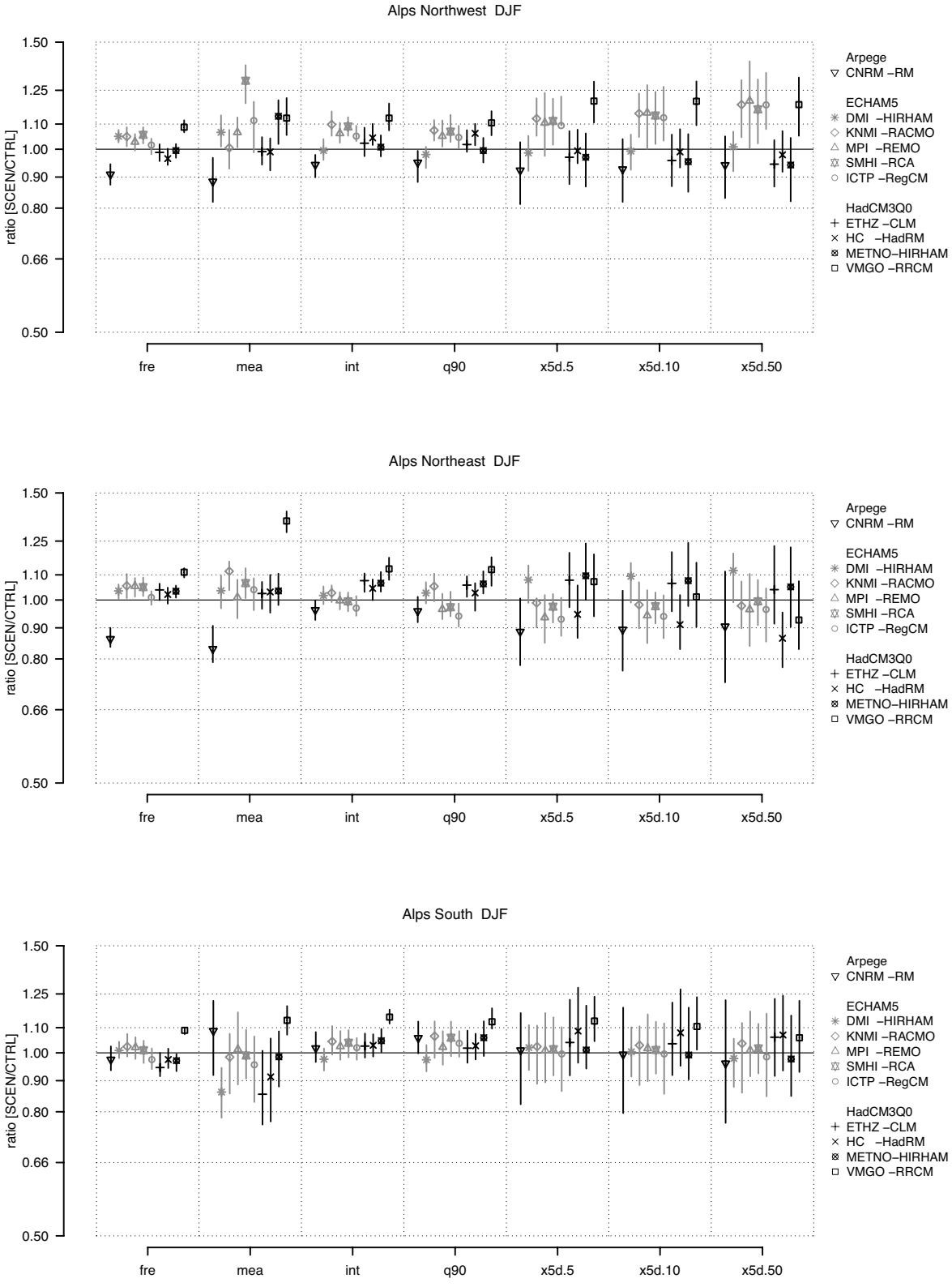

Figure 3-8: Simulated change (ratio SCEN1/CTRL) in domain-mean precipitation diagnostics and extremes in winter (DJF) for Northwestern Alps (top), Northeastern Alps (middle) and Southern Alps (bottom) as simulated by 10 RCMs for period 2021-2050 (SCEN1) wrt 1961-1990 (CTRL). Symbols depict the best-estimate, lines the 90%-confidence interval associated with simulated change.

Table 3.1-2: Best estimate of change (ratio SCEN1/CTRL) in domain mean precipitation diagnostics and 1-day precipitation extremes in spring (MAM) as simulated by 10 RCMs for period 2021-2050 (SCEN1) wrt 1961-1990 (CTRL).

NORTHWESTERN ALPS [NW]

RCM	fre	mea	int	q90	x1d.5	x1d.10	x1d.50
Arpege							
CNRM-RM	**1.02**	1.03	1.01	1.01	**1.07**	**1.07**	**1.08**
ECHAM5							
DMI-HIRHAM	**0.96**	**0.89**	1.02	1.02	0.99	1.01	1.04
KNMI-RACMO	**0.89**	**0.91**	1.00	1.02	0.99	0.99	0.97
MPI-REMO	**0.89**	**0.86**	**0.96**	0.98	**0.89**	**0.88**	**0.86**
SMHI-RCA	**0.93**	**0.83**	0.98	0.99	1.00	1.00	1.00
ICTP-RegCM	**0.93**	**0.84**	**0.94**	**0.94**	0.99	1.00	1.00
HadCM3Q0							
ETHZ-CLM	**0.89**	**0.82**	1.00	0.99	0.99	0.98	0.95
HC-HadRM	**0.95**	0.99	1.02	**1.03**	1.04	1.04	1.04
METNO-HIRHAM	**0.94**	**0.92**	0.98	0.99	0.96	0.96	0.96
VMGO-RRCM	**fre**	**1.09**	**1.04**	**1.06**	1.04	1.04	1.03

NORTHEASTERN ALPS [NW]

RCM	fre	mea	int	q90	x1d.5	x1d.10	x1d.50
Arpege							
CNRM-RM	**1.04**	**1.13**	**1.03**	1.02	**1.11**	**1.12**	**1.11**
ECHAM5							
DMI-HIRHAM	0.97	1.04	1.02	1.03	1.02	1.01	1.00
KNMI-RACMO	**0.90**	**0.91**	1.01	1.02	**1.07**	**1.08**	**1.12**
MPI-REMO	**0.91**	**0.90**	1.00	1.00	0.96	0.95	0.95
SMHI-RCA	**0.96**	**0.90**	0.98	0.99	1.00	1.00	0.99
ICTP-RegCM	**0.95**	**0.85**	0.97	0.97	0.97	0.97	0.96
HadCM3Q0							
ETHZ-CLM	**0.94**	**0.93**	1.02	1.03	1.02	1.02	1.03
HC-HadRM	0.99	1.01	**1.07**	**1.08**	**1.11**	**1.12**	**1.13**
METNO-HIRHAM	**0.95**	**0.86**	1.01	1.00	1.02	1.03	1.05
VMGO-RRCM	**1.02**	**1.19**	**1.09**	**1.09**	**1.11**	**1.10**	**1.07**

SOUTHERN ALPS [S]

RCM	fre	mea	int	q90	x1d.5	x1d.10	x1d.50
Arpege							
CNRM-RM	1.01	**1.01**	1.02	1.01	**1.07**	1.06	1.06
ECHAM5							
DMI-HIRHAM	**0.91**	**0.91**	**1.04**	**1.09**	1.05	1.05	1.03
KNMI-RACMO	**0.89**	0.89	1.03	1.05	1.01	1.00	0.99
MPI-REMO	**0.90**	0.97	**1.05**	**1.06**	1.00	1.00	1.00
SMHI-RCA	**0.91**	0.92	1.01	1.02	1.00	0.99	0.97
ICTP-RegCM	**0.94**	0.88	1.02	1.03	1.02	1.02	1.02
HadCM3Q0							
ETHZ-CLM	**0.92**	**0.79**	1.00	1.01	1.03	1.03	1.02
HC-HadRM	**0.96**	1.00	1.03	1.01	1.08	1.09	1.09
METNO-HIRHAM	**0.94**	0.92	1.03	1.04	1.02	1.02	1.02
VMGO-RRCM	**1.03**	**1.10**	**1.08**	**1.08**	**1.10**	**1.09**	**1.06**

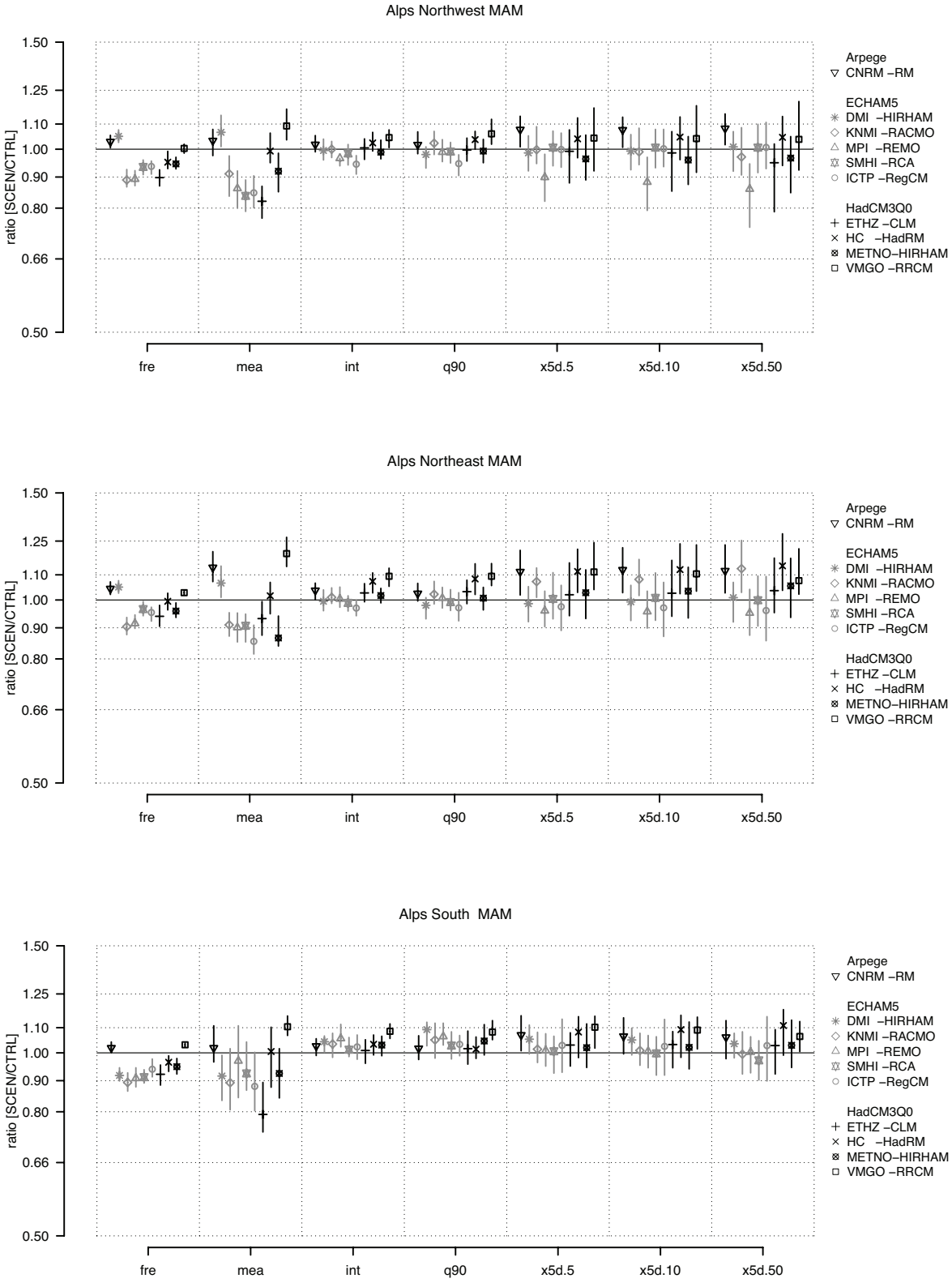

Figure 3-9: Simulated change (ratio SCEN1/CTRL) in domain-mean precipitation diagnostics and extremes in spring (MAM) for Northwestern Alps (top), Northeastern Alps (middle) and Southern Alps (bottom) as simulated by 10 RCMs for period 2021-2050 (SCEN1) wrt 1961-1990 (CTRL). Symbols depict the best-estimate, lines the 90%-confidence interval associated with simulated change.

Table 3.1-3: Best estimate of change (ratio SCEN1/CTRL) in domain mean precipitation diagnostics and 1-day precipitation extremes in summer (JJA) as simulated by 10 RCMs for period 2021-2050 (SCEN1) wrt 1961-1990 (CTRL).

NORTHWESTERN ALPS [NW]

RCM	fre	mea	int	q90	x1d.5	x1d.10	x1d.50
Arpege							
CNRM-RM	0.97	0.96	1.01	1.02	1.07	**1.08**	**1.11**
ECHAM5							
DMI-HIRHAM	0.99	1.07	1.00	1.00	0.97	0.96	0.94
KNMI-RACMO	**0.92**	0.89	0.96	0.97	1.00	0.98	0.96
MPI-REMO	**0.95**	**0.85**	0.96	0.97	1.02	0.98	1.02
SMHI-RCA	**0.94**	0.91	0.95	0.96	0.97	1.04	1.02
ICTP-RegCM	0.98	**0.88**	**0.95**	**0.93**	1.03	1.06	**1.11**
HadCM3Q0							
ETHZ-CLM	**0.82**	**0.65**	0.97	0.99	1.01	1.02	1.04
HC-HadRM	**0.88**	**0.75**	**0.93**	0.95	0.98	0.99	1.01
METNO-HIRHAM	**0.89**	**0.74**	1.01	1.01	1.03	1.04	1.06
VMGO-RRCM	**0.94**	0.99	1.00	1.01	1.04	1.04	1.03

NORTHEASTERN ALPS [NW]

RCM	fre	mea	int	q90	x1d.5	x1d.10	x1d.50
Arpege							
CNRM-RM	1.02	**1.10**	**1.04**	1.00	**1.19**	**1.20**	**1.19**
ECHAM5							
DMI-HIRHAM	**1.04**	1.02	**1.04**	1.04	1.11	1.10	1.10
KNMI-RACMO	**0.95**	0.96	**1.06**	1.05	1.12	**1.14**	**1.18**
MPI-REMO	**0.95**	1.02	1.00	1.01	1.01	1.02	1.04
SMHI-RCA	0.98	**0.93**	0.99	0.99	1.04	1.04	1.05
ICTP-RegCM	0.98	0.94	0.98	0.99	1.03	1.05	1.05
HadCM3Q0							
ETHZ-CLM	**0.89**	**1.07**	**1.06**	**1.06**	**1.13**	**1.14**	**1.16**
HC-HadRM	**0.89**	0.96	1.04	**1.08**	**1.09**	**1.08**	1.05
METNO-HIRHAM	**0.89**	**0.91**	1.02	1.01	1.07	1.08	**1.10**
VMGO-RRCM	**0.98**	**1.14**	1.02	**1.04**	1.01	0.99	0.96

SOUTHERN ALPS [S]

RCM	fre	mea	int	q90	x1d.5	x1d.10	x1d.50
Arpege							
CNRM-RM	0.99	0.95	1.01	1.02	1.05	1.06	1.09
ECHAM5							
DMI-HIRHAM	**1.03**	0.92	1.00	1.00	1.03	1.01	0.97
KNMI-RACMO	**0.92**	**0.71**	1.00	0.99	0.94	0.95	0.98
MPI-REMO	**0.94**	**0.74**	0.99	0.99	0.97	0.98	0.99
SMHI-RCA	**0.95**	1.04	**0.95**	1.00	0.94	0.93	0.91
ICTP-RegCM	**1.04**	1.15	0.97	0.97	0.97	0.96	0.94
HadCM3Q0							
ETHZ-CLM	**0.83**	**0.81**	1.00	0.99	0.97	0.99	1.02
HC-HadRM	**0.87**	**0.80**	0.98	0.97	1.08	1.09	1.11
METNO-HIRHAM	**0.82**	**0.66**	1.00	1.00	0.96	0.97	0.96
VMGO-RRCM	**0.99**	**0.92**	1.00	1.01	1.04	**1.13**	**1.16**

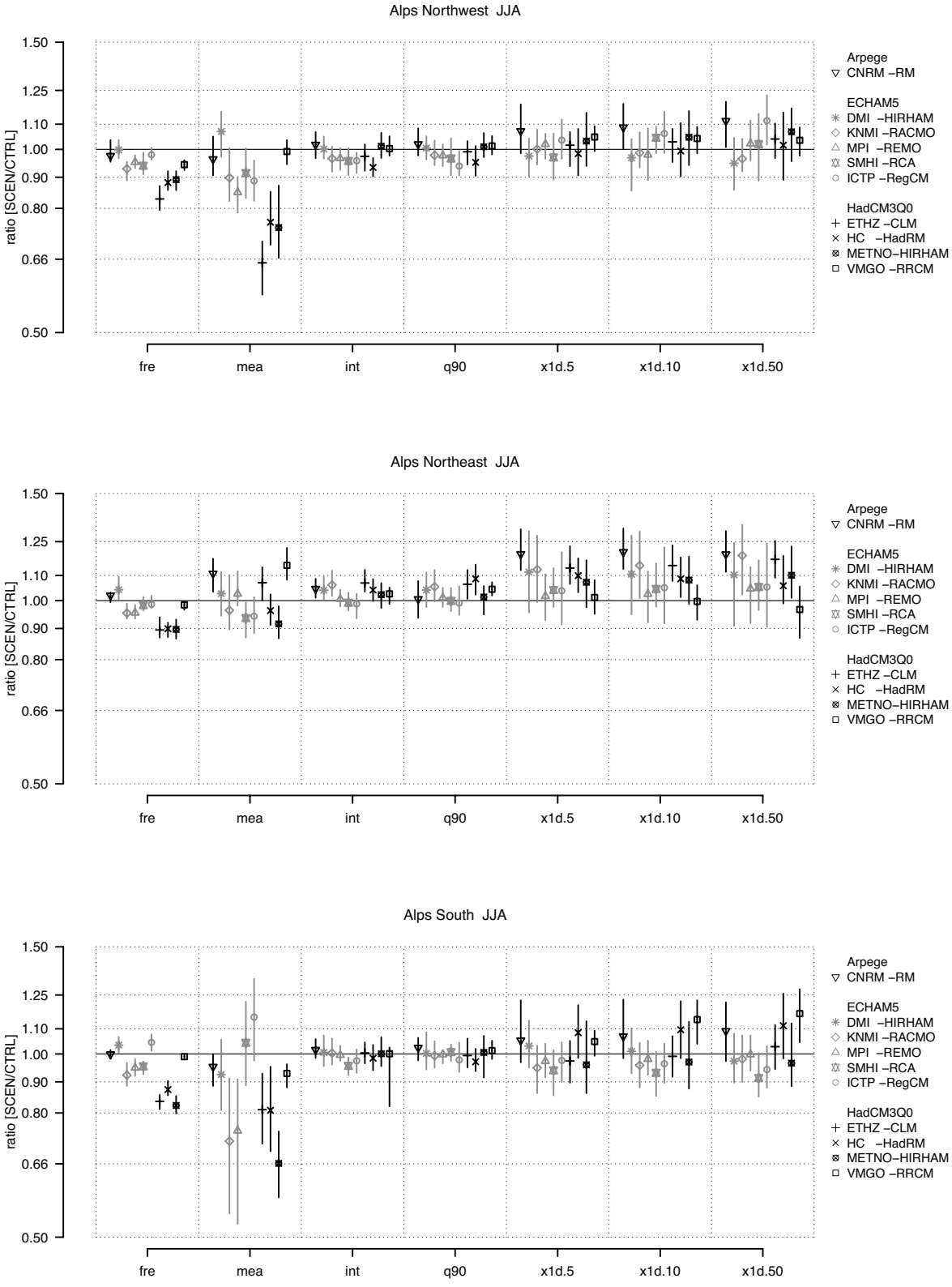

Figure 3-10: Simulated change (ratio SCEN1/CTRL) in domain-mean precipitation diagnostics and extremes in summer (JJA) for Northwestern Alps (top), Northeastern Alps (middle) and Southern Alps (bottom) as simulated by 10 RCMs for period 2021-2050 (SCEN1) wrt 1961-1990 (CTRL). Symbols depict the best-estimate, lines the 90%-confidence interval associated with simulated change.

Table 3.1-4: Best estimate of change (ratio SCEN1/CTRL) in domain mean precipitation diagnostics and 1-day precipitation extremes in fall (SON) as simulated by 10 RCMs for period 2021-2050 (SCEN1) wrt 1961-1990 (CTRL).

NORTHWESTERN ALPS [NW]

RCM	fre	mea	int	q90	x1d.5	x1d.10	x1d.50
Arpege							
CNRM-RM	0.98	1.05	**1.12**	**1.15**	**1.19**	**1.20**	**1.23**
ECHAM5							
DMI-HIRHAM	1.01	1.01	1.03	**1.03**	**1.10**	**1.10**	**1.10**
KNMI-RACMO	0.99	1.09	1.04	**1.07**	**1.18**	**1.10**	1.00
MPI-REMO	1.01	1.05	**1.05**	**1.06**	1.07	1.05	1.04
SMHI-RCA	1.04	1.10	**1.03**	**1.06**	1.07	1.06	1.05
ICTP-RegCM	**1.02**	1.01	1.02	1.02	0.99	0.99	1.00
HadCM3Q0							
ETHZ-CLM	0.98	1.01	**1.10**	**1.11**	**1.15**	**1.15**	**1.16**
HC-HadRM	0.99	**1.14**	**1.15**	**1.18**	**1.24**	**1.25**	**1.16**
METNO-HIRHAM	1.00	**1.09**	**1.13**	**1.14**	1.05	**1.18**	**1.17**
VMGO-RRCM	1.01	**1.12**	**1.09**	**1.10**	1.08	1.06	1.04

NORTHEASTERN ALPS [NW]

RCM	fre	mea	int	q90	x1d.5	x1d.10	x1d.50
Arpege							
CNRM-RM	1.01	**1.16**	**1.15**	**1.15**	**1.16**	**1.15**	**1.14**
ECHAM5							
DMI-HIRHAM	1.02	**1.08**	1.03	**1.05**	1.02	1.02	1.02
KNMI-RACMO	0.98	1.03	**1.10**	**1.14**	**1.14**	**1.15**	**1.17**
MPI-REMO	0.98	**1.10**	**1.09**	**1.13**	**1.16**	**1.18**	**1.23**
SMHI-RCA	1.02	1.05	**1.06**	**1.09**	**1.18**	**1.20**	**1.21**
ICTP-RegCM	1.01	**1.11**	**1.11**	**1.11**	**1.26**	**1.31**	**1.41**
HadCM3Q0							
ETHZ-CLM	1.00	1.03	**1.05**	1.04	1.07	1.06	1.06
HC-HadRM	0.99	1.03	1.03	1.04	1.06	1.06	1.07
METNO-HIRHAM	0.99	1.03	**1.04**	**1.14**	0.98	0.98	0.98
VMGO-RRCM	**1.05**	**1.17**	**1.10**	**1.11**	1.07	1.04	1.01

SOUTHERN ALPS [S]

RCM	fre	mea	int	q90	x1d.5	x1d.10	x1d.50
Arpege							
CNRM-RM	1.00	0.96	**1.09**	**1.09**	**1.19**	**1.18**	**1.15**
ECHAM5							
DMI-HIRHAM	**0.93**	**0.80**	**0.94**	**0.96**	0.98	0.99	1.01
KNMI-RACMO	**0.92**	**0.86**	0.97	0.95	0.96	0.97	0.98
MPI-REMO	**0.92**	**0.69**	1.00	1.06	0.98	1.00	1.05
SMHI-RCA	0.98	**0.85**	0.94	**0.91**	1.07	0.99	0.99
ICTP-RegCM	0.97	**0.78**	0.97	0.97	0.95	0.95	0.97
HadCM3Q0							
ETHZ-CLM	**0.95**	1.08	1.04	**1.10**	1.06	1.06	1.05
HC-HadRM	**0.95**	0.90	1.00	1.01	1.04	1.03	1.01
METNO-HIRHAM	**0.94**	1.00	**1.06**	**1.07**	**1**.08	**1.09**	**1.09**
VMGO-RRCM	**1.04**	**1.08**	**1.18**	**1.21**	**1.15**	**1.11**	**1.14**

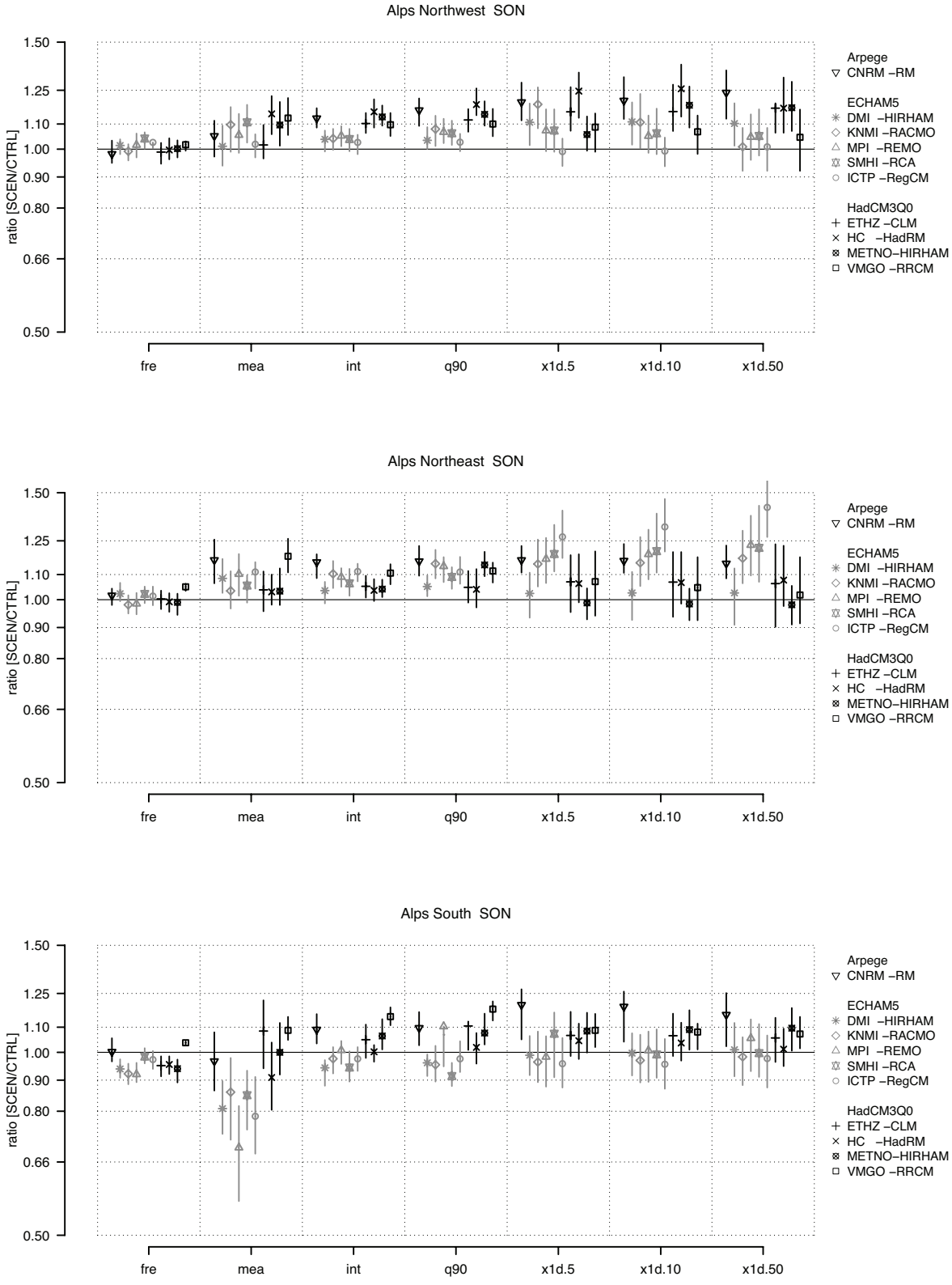

Figure 3-11: Simulated change (ratio SCEN1/CTRL) in domain-mean precipitation diagnostics and extremes in fall (SON) for Northwestern Alps (top), Northeastern Alps (middle) and Southern Alps (bottom) as simulated by 10 RCMs for period 2021-2050 (SCEN1) wrt 1961-1990 (CTRL). Symbols depict the best-estimate, lines the 90%-confidence interval associated with simulated change.

3.2 Long-Term Change

This chapter addresses change-projections for late 21st century conditions, represented by period 2070-2099 (SCEN2). As for SCEN1, change is expressed with respect to conditions in the control-period 1961-1990 (CTRL). Analyses are performed on a reduced subset of 5 RCMs (see labeled models in Table 2.1-1) and results are presented comparative to results obtained for SCEN1-integrations. This confrontation allows assessing systematic changes in the course of the 21st century. The first sub-section focuses on the evolution of the spatial distribution of change across the studied diagnostics. A second sub-section presents sub-regional changes as individually simulated by the 5 considered RCMs for SCEN2.

3.2.1 Evolution of the Spatial Distributions of Change

The evolution of the spatial distributions of change for the studied diagnostics in the course of the 21st century is depicted in Figures 3-2.1 to 3.2-6. Similar to Figures 3.1-1 to 3.1-3 the median of a multi-model ensemble is shown. Here, an ensemble of a reduced subset of 5 RCMs is used and the time horizon is additionally extended to period 2070-2099 (SCEN2), For reasons of direct comparison, the presented figures also show the change for period 2021-2050 (SCEN1), likewise based on the reduced subset of 5 RCMs. In this context it is worth noting, that the patterns shown by the 5-member ensemble do perform remarkably good in reproducing the patterns shown by the 10-member ensemble in Figures 3.1-1 to 3.1-6. As before, stippled regions show model-agreement (here, 4 out of 5 RCMs, resp. 80%, agree in sign).

In general, most change signals seen in mid-21st century projections (2021-2050 wrt 1961-1990) amplify in late-21st century simulations (2070-2099). Coevally, regions showing model agreement spread out. Locally, however, conspicuous, non-linear trends are found. For instance, some areas experience weakened trends or even reversals in the projected sign of change in the course of the 21st century.

In terms of **frequency** (fre) (Figure 3-12) the most remarkable amplification of simulated changes is seen in summer, where a very widespread and serious decrease amplifies and is simulated across the entire Alpine region and central Europe. Regions south of the Alpine main crest (~46°N) show a comprehensive decrease larger than -30%. A northward spread of regions with model agreement concerning a decrease in the occurrence of precipitation is also simulated in fall, vice versa a southern spread of regions affected by increasing frequency is seen in winter. Winter increases in frequency by the end of the century are very remarkable south of the Alps (resp. the southern Alps). Along the northern rim of the Alps and northward, noteworthy changes occur for spring projections, where decreases in SCEN1-integrations balance out to no change in late 21st-century integrations with respect to present-day conditions. Elsewhere, amplifying decreasing signals, similar to summer projections, are seen for spring.

Changes in the **mean** (mea) (Figure 3-13) precipitation highly correlate with the projected patterns for frequency (fre). Remarkable decreases amplify and spread out in summer, whereas increases in fall become much larger north of the Alps. In general, the magnitudes in seasonal changes are greater for the mean when compared to changes in fre, especially increasing signals deviate towards greater values of change. For instance, slight differences

with respect to the patterns found for fre can be found, above all, in spring and fall. Then, some regions on the North-side of the Alps experience considerable increases in the mean, while frequency is simulated to decrease. This implies that precipitation intensity has to markedly increase to balance out for the loss by the frequency decrease. Peculiar is the sign reversal in projected change along the northern rim of the Alps in spring, where a decrease in mea is simulated for SCEN1- followed by increases in SCEN2-integrations. Also, a very remarkable amplification of increases in the mean is found on the Alpine Southside and along the eastern slopes of the Alps in winter. Southeast of the Alpine main crest, winter increases in the mean by the end of the 21st century are simulated to comprehensively lie above +20%. Mostly, mean winter precipitation is simulated to largely increase across the entire domain presented: as stated earlier, this increase is very pronounced in the east.

The spatial distribution of seasonal changes for **intensity** (int) and the **90%-percentile** (q90) at SCEN1-conditions do highly correlate (see Figure 3-2): as does also the evolution of the change patterns for both when considering SCEN2-integrations (int: Figure 3-14, q90: Figure 3-15). Contrary to the complex and highly variable spatial change structure simulated for fre and mea, a distinct outspread and amplification of regions affected by increases in int and q90 can be seen throughout all seasons, independent of the change behavior shown for the mean and frequency. As for mean winter precipitation, very distinct intensifications are projected for eastern Alpine regions and regions south of the main-crest in winter. The weakest increases are simulated in spring, strongest in winter and fall. Worth mentioning is the also very strong intensification of increases in intensity and q90 along the northern Alpine foreland in summer. Here, a remarkable intensification of precipitation intensity is a robust feature across all RCMs, most prominent in the northeastern Alpine foreland. In fall, one sees a widespread amplification and outspread of increases, very prominent north of the Alps and in southern Germany.

It is noteworthy that the characters of change for intensity and q90 are remarkably different to the patterns simulated for frequency and the mean. Most areas experience a summer- and spring decrease in frequency and the mean, while coevally intensity and q90 are simulated to mostly increase at the same time. Visually, this is seen by the widespread model-agreement and bluish colors in the plots showing changes in intensity and q90, whereas fre and mea, at the same time, show variable colors and hence logically variable signs of change across the study domain. Different directions in sign (fre/mea[-] compared to int/q90[+]) are for example seen in spring projections (SCEN2) across France.

Regarding future projections of extremes, as mentioned before (3.1.1.) one can see slight differences between changes in the 5-year return value of **one-** (x1d.5, Figure 3-16) and **multi-day precipitation extremes** (x5d.5) (Figure 3-17). Change patterns for one-day events are spatially more variable than those for multi-day precipitation episodes. Nevertheless, the patterns found for both are related to each other and similar to changes projected for int and q90. The most pronounced changes in extremes are seen in a widespread intensification of extremes in winter, especially in the southeastern parts of the Alpine region. Multi-day precipitation events are thereby simulated to intensify more than one-day events, showing widespread increases larger than +30% in the southeastern Alpine region. Interestingly, this strong feature of increasing precipitation does not appear within the Southern Alps until the late 21st century pointing out a non-linear change behavior. A similar magnitude of intensification is found in fall: most pronounced on the Alpine North-side and most notably for short-lived events. In spring, regions affected by decreases in heavy rainfall events amplify and spread out from the Mediterranean towards the Alps. However, along the

northwestern slopes of the Alps, an intensification of heavy rainfall events is found in spring. Summertime extremes are projected to distinctly decrease in vicinity of the Mediterranean (e.g. Po-Valley and very southern Alps). Exceptional in summer is the quite remarkable increase of single-day extremes along and north of the northern Alpine rim. Similar to the pattern found for intensity and q90, these increases distinctly amplify in their magnitude in the course of the 21st century.

Concentrating the most striking findings obtained throughout this part of the study, one can summarize that the Alps, on a very small spatial scale, emerge as a sharp divide between regions affected by distinctly different characteristics of change in precipitation and precipitation extremes in the course of the 21st century.
Considering all indices comparatively, one recognizes a different change behavior between basic climatological measures (mean and frequency) and indices representing the strength of precipitation and extreme precipitation (q90 and extremes; x1d.5 and x5d.5). This implies that most probably different physical processes drive changes in mean and extreme precipitation independently of each other in a warming climate.
The findings furthermore point to increased precipitation variability in future climatic conditions.

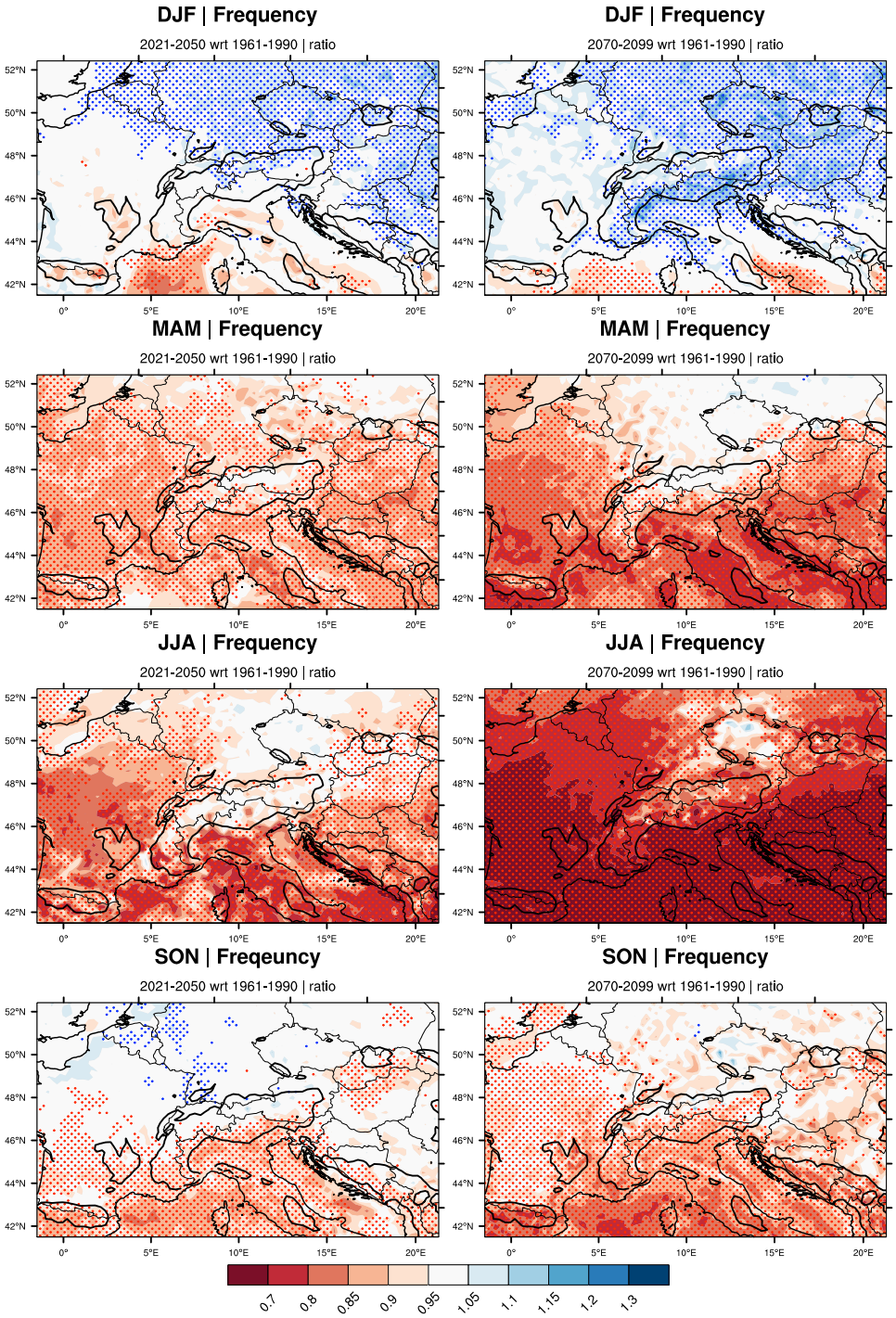

Figure 3-12: Projected change (ratio SCEN/CTRL) in precipitation frequency as simulated by a multi-model ensemble of 5 RCMs on seasonal level for period 2021-2050 wrt 1961-1990 (left column) and period 2070-2099 wrt 1961-1990 (right column). Depicted is the ensemble-median change signal. Stippling denotes model agreement (80%) in increases (blue) and decreases (red). Thick lines illustrate the 700m a.s.l.-isoline as represented by the ENSEMBLES E-OBS topography.

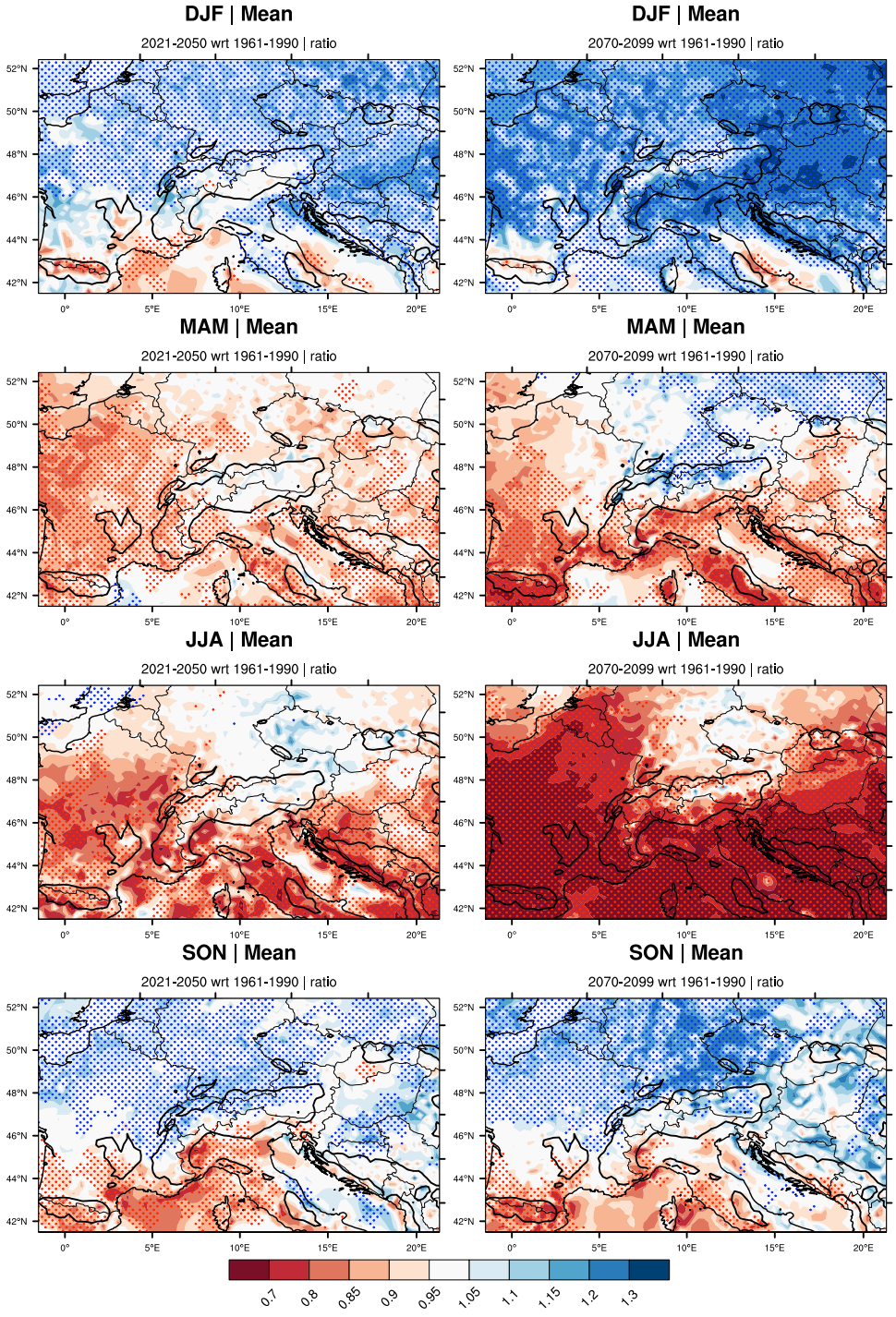

Figure 3-13: Projected change (ratio SCEN/CTRL) in mean precipitation as simulated by a multi-model ensemble of 5 RCMs on seasonal level for period 2021-2050 wrt 1961-1990 (left column) and period 2070-2099 wrt 1961-1990 (right column). Depicted is the ensemble-median change signal. Stippling denotes model agreement (80%) in increases (blue) and decreases (red). Thick lines illustrate the 700m a.s.l.-isoline as represented by the ENSEMBLES E-OBS topography.

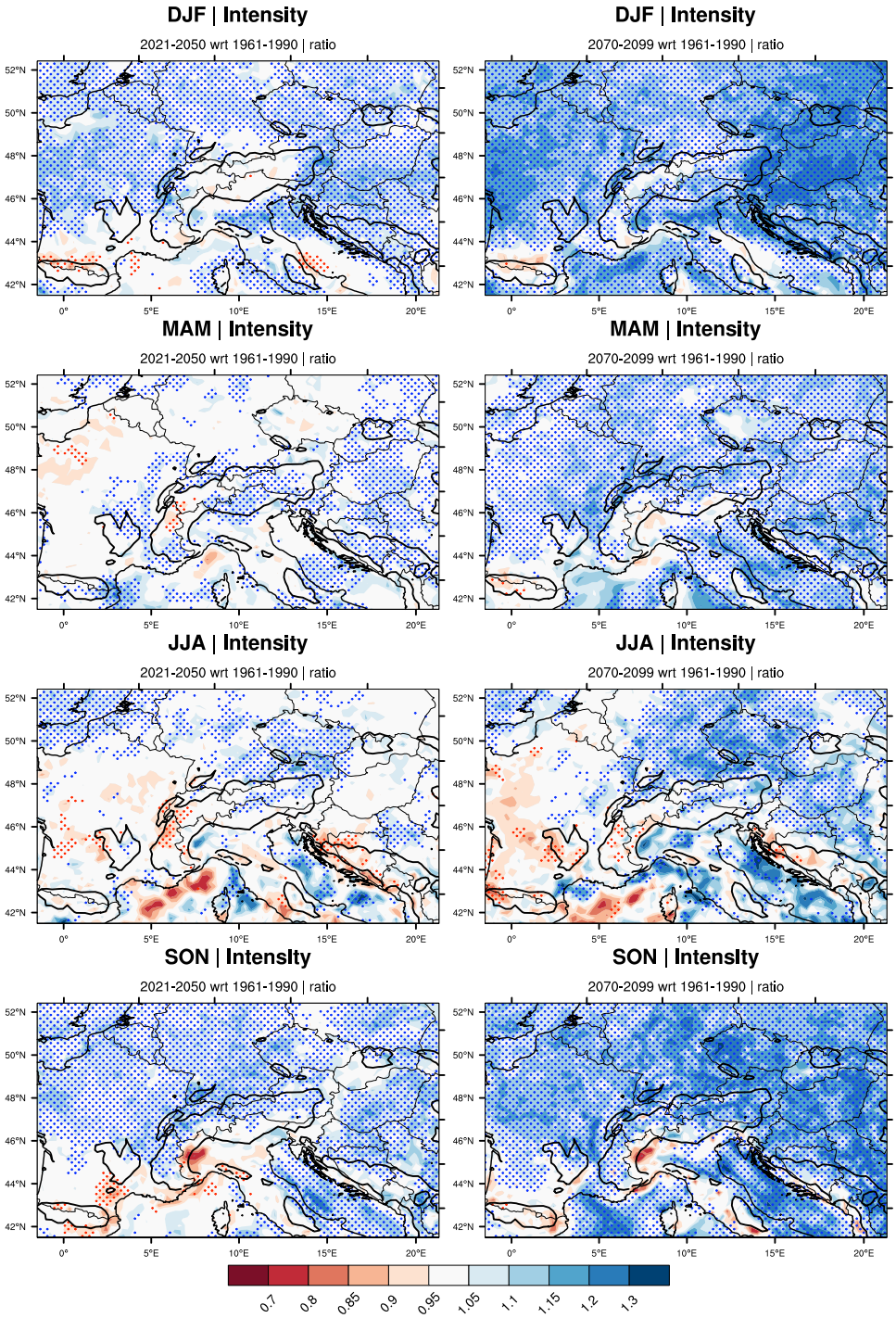

Figure 3-14: Projected change (ratio SCEN/CTRL) in precipitation intensity as simulated by a multi-model ensemble of 5 RCMs on seasonal level for period 2021-2050 wrt 1961-1990 (left column) and period 2070-2099 wrt 1961-1990 (right column). Depicted is the ensemble-median change signal. Stippling denotes model agreement (80%) in increases (blue) and decreases (red). Thick lines illustrate the 700m a.s.l.-isoline as represented by the ENSEMBLES E-OBS topography.

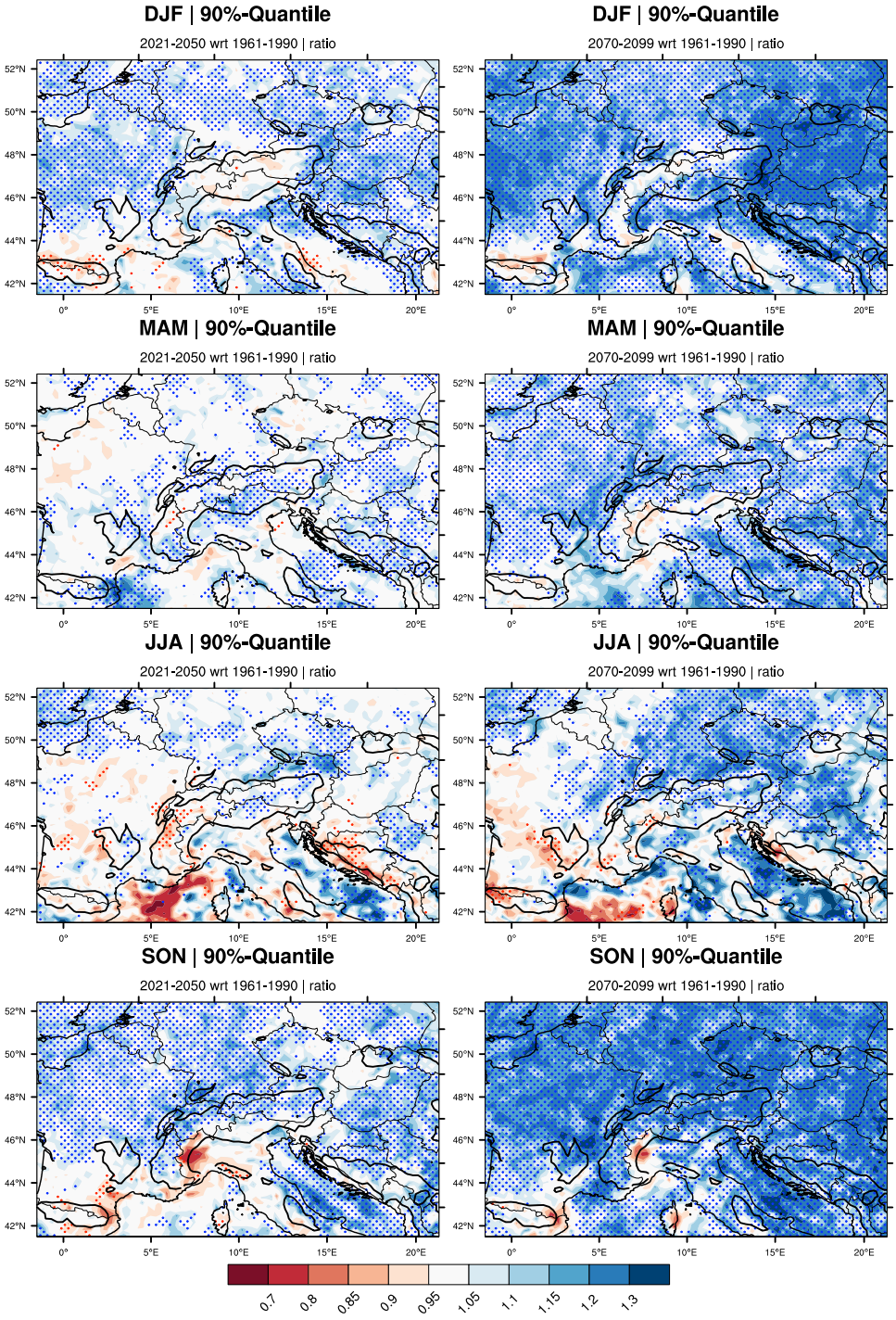

Figure 3-15: Projected change (ratio SCEN/CTRL) in the 90%-quantile as simulated by a multi-model ensemble of 5 RCMs on seasonal level for period 2021-2050 wrt 1961-1990 (left column) and period 2070-2099 wrt 1961-1990 (right column). Depicted is the ensemble-median change signal. Stippling denotes model agreement (80%) in increases (blue) and decreases (red). Thick lines illustrate the 700m a.s.l.-isoline as represented by the ENSEMBLES E-OBS topography.

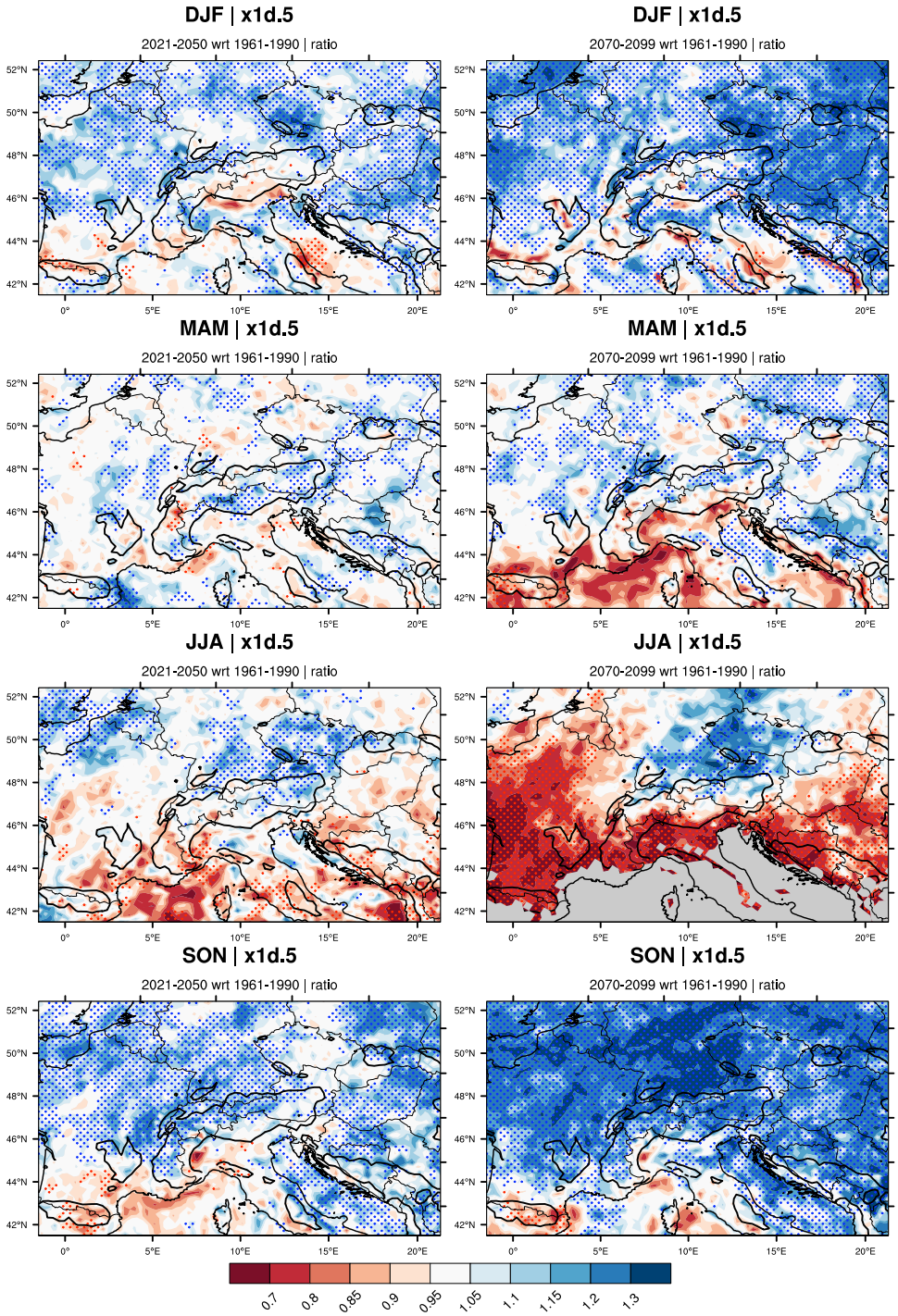

Figure 3-16: Projected change (ratio SCEN/CTRL) in the 5-year return value of 1-day precipitation events as simulated by a multi-model ensemble of 5 RCMs on seasonal level for period 2021-2050 wrt 1961-1990 (left column) and period 2070-2099 wrt 1961-1990 (right column). Depicted is the ensemble-median change signal. Stippling denotes model agreement (80%) in increases (blue) and decreases (red). Grid-cells too dry for extreme value analysis are masked out. Thick lines illustrate the 700m a.s.l.-isoline as represented by the ENSEMBLES E-OBS topography.

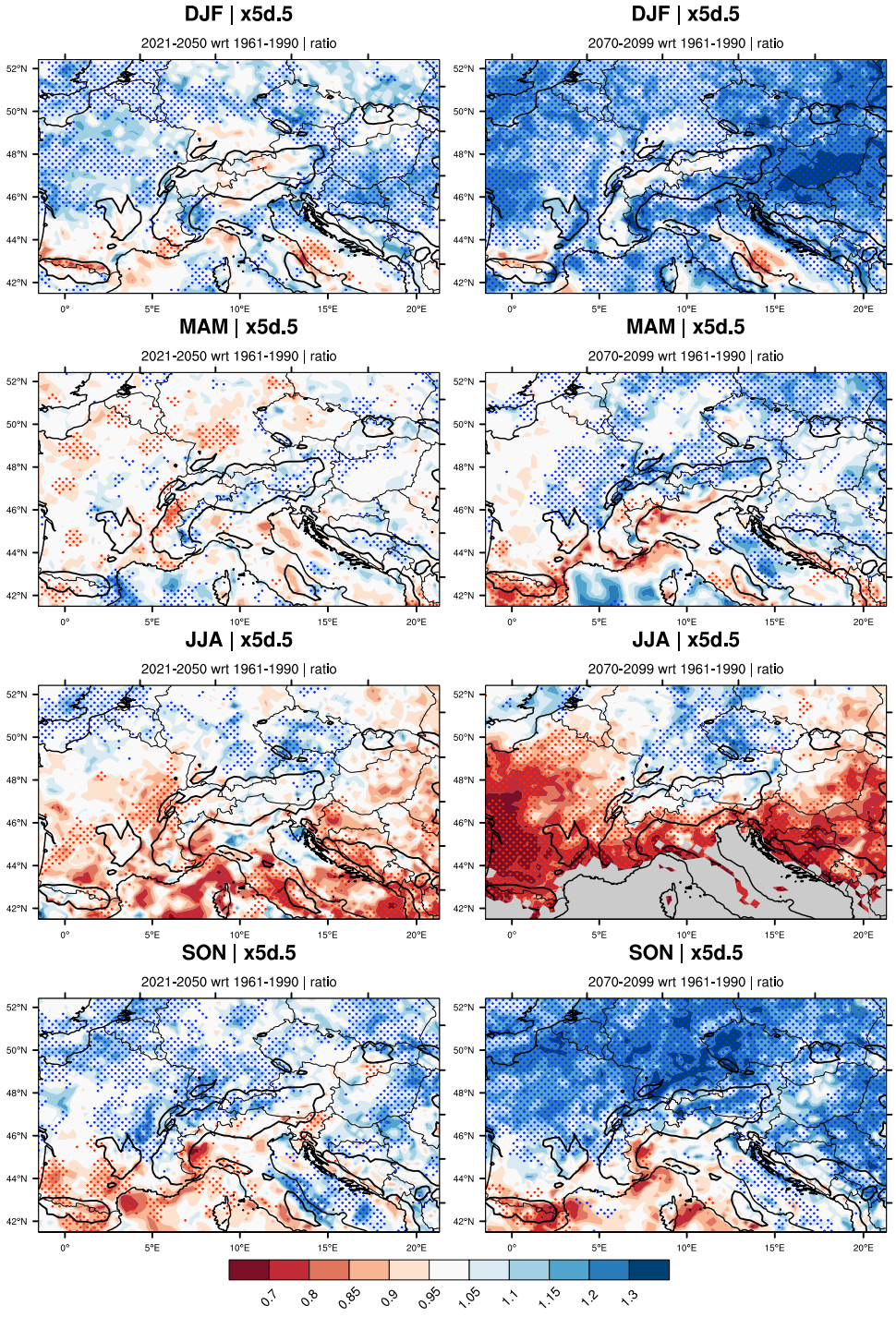

Figure 3-17: Projected change (ratio SCEN/CTRL) in the 5-year return value of 5-day precipitation events as simulated by a multi-model ensemble of 5 RCMs on seasonal level for period 2021-2050 wrt 1961-1990 (left column) and period 2070-2099 wrt 1961-1990 (right column). Depicted is the ensemble-median change signal. Stippling denotes model agreement (80%) in increases (blue) and decreases (red). Grid-cells too dry for extreme value analysis are masked out. Thick lines illustrate the 700m a.s.l.-isoline as represented by the ENSEMBLES E-OBS topography.

3.2.2 Simulated Change Structure across RCMs

The highly complex seasonal change structure across diagnostics on sub-regional level was already mentioned in this report for mid 21st century projections. Inter-model differences in simulating changes in period 2021-2050 with respect to (wrt) 1961-1990 were shown, taking 10 RCMs into account (Figures 3.1-8 to 3.1-11). This section aims to extend the time horizon and presents results on the change found for period 2070-2099 wrt 1961-1990, performed on a reduced subset of 5 RCMs (Table 2.1-1). SCEN2-results (in red) are shown in direct comparison to results obtained for SCEN1 (in black) in order to better assess amplifications, reductions, reversals or stabilizations of change signals during the 21st century.

In general, the findings of this sub-section show that change signals amplify, meaning that decreases / increases become larger in late 21st century simulations when compared with results for mid-21st-century changes. Furthermore, many change signals thereby become significant for late-21st century projections. Nevertheless, some signals weaken in magnitude, stabilize at certain levels or even reverse.
As already obvious from the results presented before, systematic changes across RCMs are mainly governed by the driving GCMs and only secondary by individual RCM formulations. This GCM-arrangement is especially obvious in winter and fall. This character is consistent throughout the entire 21st century. In this regard, most exceptional are the results obtained for summer, where GCM-grouping is weaker.
In the following, only the most prominent findings are shortly addressed and changes in between SCEN1- and SCEN2-integrations elucidated. All the figures and tables presented can be can be examined to get a more detailed overview.

Winter
In winter (Figure 3-18 and Table 3.2-1), amplifications of increasing change signals are an obvious feature, especially for climatological (descriptive) diagnostics and in the Southern Alpine region. Changes in extremes show, in NE and NW, a varied and highly disperse change structure in between RCMs for late 21st century projections. This might have something to do with the general tendency of models to simulate decreases in the severity of multi-day precipitation episodes, as also shown and addressed in Figure 3-7. The intensifications seen in the Southern Alpine region are also worth noting. Here, quite stable projections of diagnostics (in the case of mea even decreases) in mid-21st century integrations turn into robustly simulated striking increases in late-21st century projections.
Other characteristics seen in late 21st century results are shortly described in the following. Consistent across all RCMs, each diagnostic experiences a clear amplification of distinct increasing change signals. Except the ETHZ-CLM RCM, each RCM simulates significant increases in frequency (fre), intensity (int) and the 90%-Percentile (q90), in a dimension of around +10% and in each sub-region. Such increases are also simulated for extremes, however, they are mostly not significant. Only in the Southern region are increases and small inter-model spread a robust feature across all RCMs. Taking change in the 5-year return value as an example, increases in the southern region range from +8% to +15% for late 21st century conditions. Projections of the mean are, as also seen in other seasons, afflicted with largest inter-model spread.

Spring
Spring results are shown in Figure 3-19 and Table 3.2-2. Results presented earlier pointed out a related change structure for spring and summer projections. Similarity between spring and

summer is also obvious for late 21st first century integrations. Interestingly and obvious is a non-linear change for the mean in the course of the 21st century in all three sub-regions. Having seen substantial reductions in SCEN1-projections, these reductions reduce in character for SCEN2-integrations. Especially intense and extreme diagnostics in the two northern regions experience larger positive change signals, which in a majority turn out to be significant, by the end of the 21st century. In S amplifications are generally weak: however, one sees more pronounced reductions in frequency. Inter-model spread is obviously larger in the two northern sub-regions (e.g. range in x1d.5: NW: -3%- +19%; NE: +6%- +15%; S: +5%- +9%).

Summer

The already described and very remarkable change structure in summer is strongly amplified in its character for late 21st century conditions (Figure 3-20 and Table 3.2-3). This is expressed by further - partially significant - increases in extreme indices and quite remarkable - mostly significant - decreases in frequency and the mean. This tendency is found throughout all three Alpine sub-regions. Most prominent decreases in the mean and frequency are found in the Southern Alps. Here, RCMs simulate amplifying reductions in the mean reaching reductions between -29% and -49% by the end of the 21st century (compared to a range between -8% to -34%, by the same 5 RCMs in SCEN1). Further decreases in the mean and frequency are also found in NE and NW.

Regarding extremes, NW experiences very pronounced intensifying increases in summertime precipitation extremes up to +33%. Noteworthy and exemplary is the projection of the MPI-REMO model in NW, showing an increase of +33% for the 50-year return value and simultaneously a decrease of -39% in the mean and -26% for fre. Regarding the intensification of extremes, ECHAM5-driven models tend to more pronouncedly amplify the signals seen in SCEN1-integrations. Nevertheless, inter-model differences are obviously seen, even between RCMs driven by the same GCM - especially in the case of the two HadCM3Q0 driven RCMs. This supports the conclusion (found in 3.1.3) that individual RCM formulations become prominent when regarding summer projections and hence generate large inter-model variability in projecting future climatic conditions.

Fall

Most prominent changes concerning extremes in SCEN1-integrations were found in fall. Projected increases clearly amplify for SCEN2-conditions, most impressive in NW and NE. In NW, for instance, all RCMs simulate significant increases in int (+8 to +18%), q90 (+8 to 28%) and all considered return values (e.g. x1d.5: +12 to +28%). In NE, change signals among ECHAM5-RCMs even reach higher percentages of change. For instance, the MPI-REMO model simulates an increase of +33% for the 5-year return value. Nevertheless, inter-model variability in extreme-projections for SCEN2 in NE is large. Interestingly, oppositional to results in NE, HadCM3Q0-RCMs simulate significant increases for extremes in the South.

Another interesting fact is, that all models (except of two ECHAM5-RCMs in NE) simulate decreases in frequency. Compared to SCEN1-conditions, serious decreases are projected by HadCM30-driven models, which account for projected decreases in the mean even though precipitation events clearly intensify in strength.

Table 3.2-1: Best estimate of change (ratio SCEN1/CTRL) in domain mean precipitation diagnostics and 1-day precipitation extremes in winter (DJF) as simulated by 5 RCMs for period 2070-2099 (SCEN2) wrt 1961-1990 (CTRL).

			NORTHWESTERN ALPS [NW]				
RCM	**fre**	**mea**	**int**	**q90**	**x5d.5**	**x5d.10**	**x5d.50**
ECHAM5							
DMI-HIRHAM	**1.07**	**1.13**	**1.03**	1.01	0.97	0.98	1.02
KNMI-RACMO	**1.09**	**1.21**	**1.13**	**1.13**	**1.10**	**1.11**	**1.11**
MPI-REMO	**1.07**	**1.19**	**1.07**	**1.06**	**1.10**	**1.11**	**1.12**
HadCM3Q0							
ETHZ-CLM	0.98	0.98	1.02	1.01	0.97	0.97	0.98
HC-HadRM	0.97	**1.05**	**1.07**	**1.08**	1.05	**1.06**	**1.08**

			NORTHEASTERN ALPS [NE]				
RCM	**fre**	**mea**	**int**	**q90**	**x5d.5**	**x5d.10**	**x5d.50**
ECHAM5							
DMI-HIRHAM	**1.05**	**1.06**	**1.04**	**1.04**	1.03	1.02	0.98
KNMI-RACMO	**1.08**	**1.21**	**1.12**	**1.11**	**1.10**	1.10	1.09
MPI-REMO	**1.06**	1.01	**1.07**	**1.08**	0.98	0.96	0.90
HadCM3Q0							
ETHZ-CLM	1.02	**0.92**	**1.08**	**1.08**	1.06	1.04	0.98
HC-HadRM	1.02	0.99	**1.08**	**1.09**	1.02	1.00	0.93

			SOUTHERN ALPS [S]				
RCM	**fre**	**mea**	**int**	**q90**	**x5d.5**	**x5d.10**	**x5d.50**
ECHAM5							
DMI-HIRHAM	**1.06**	0.99	**1.07**	**1.07**	1.11	1.10	1.10
KNMI-RACMO	**1.12**	1.00	**1.09**	**1.13**	1.13	1.11	1.03
MPI-REMO	**1.09**	1.09	**1.10**	**1.13**	**1.15**	**1.14**	**1.16**
HadCM3Q0							
ETHZ-CLM	1.02	1.00	1.12	**1.12**	1.08	1.06	1.04
HC-HadRM	**1.06**	1.14	**1.13**	**1.14**	**1.14**	1.12	1.09

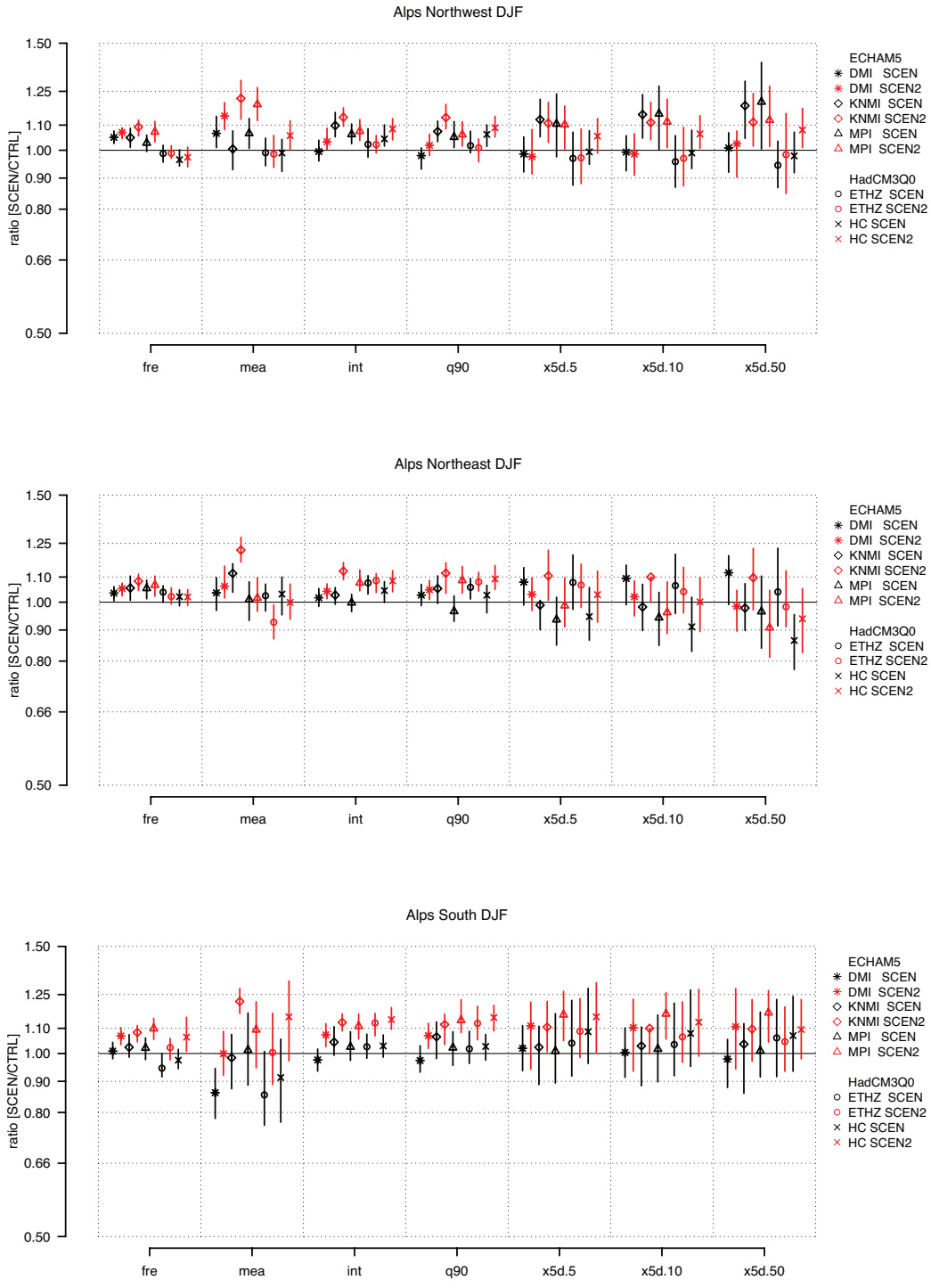

Figure 3-18: Simulated change (ratio SCEN/CTRL) in domain-mean precipitation diagnostics and extremes in winter for Northwestern Alps (top), Northeastern Alps (middle) and Southern Alps (bottom) as simulated by 5 RCMs for period 2021-2050 (SCEN1, in black) and period 2070-2099 (SCEN2, in red) wrt 1961-1990. Symbols depict the best-estimate, lines the 90%-confidence interval associated with simulated change.

Table 3.2-2: Best estimate of change (ratio SCEN1/CTRL) in domain mean precipitation diagnostics and 1-day precipitation extremes in spring (MAM) as simulated by 5 RCMs for period 2070-2099 (SCEN2) wrt 1961-1990 (CTRL).

NORTHWESTERN ALPS [NW]

RCM	fre	mea	int	q90	x1d.5	x1d.10	x1d.50
ECHAM5							
DMI-HIRHAM	1.01	0.96	**1.09**	**1.10**	**1.08**	**1.07**	**1.07**
KNMI-RACMO	**0.92**	0.96	**1.11**	**1.13**	**1.07**	**1.06**	1.06
MPI-REMO	**0.90**	0.95	**1.07**	**1.10**	0.97	0.97	0.95
HadCM3Q0							
ETHZ-CLM	**0.90**	**0.88**	1.02	**1.05**	1.07	**1.07**	1.06
HC-HadRM	**0.87**	1.00	**1.10**	**1.11**	**1.19**	**1.19**	**1.19**

NORTHEASTERN ALPS [NE]

RCM	fre	mea	int	q90	x1d.5	x1d.10	x1d.50
ECHAM5							
DMI-HIRHAM	**1.03**	**1.10**	**1.07**	**1.07**	**1.14**	**1.15**	**1.18**
KNMI-RACMO	**0.93**	0.98	**1.11**	**1.14**	**1.15**	**1.16**	**1.18**
MPI-REMO	**0.94**	1.00	**1.07**	**1.10**	1.06	1.05	1.04
HadCM3Q0							
ETHZ-CLM	**0.96**	0.96	**1.05**	**1.04**	**1.14**	**1.16**	**1.19**
HC-HadRM	**0.95**	1.04	**1.14**	**1.15**	**1.14**	**1.16**	**1.18**

SOUTHERN ALPS [S]

RCM	fre	mea	int	q90	x1d.5	x1d.10	x1d.50
ECHAM5							
DMI-HIRHAM	**0.85**	**0.72**	1.02	**1.06**	**1.07**	**1.08**	**1.07**
KNMI-RACMO	**0.82**	**0.65**	1.00	1.00	**1.07**	**1.08**	**1.07**
MPI-REMO	**0.83**	**0.64**	1.03	1.03	1.05	1.07	1.09
HadCM3Q0							
ETHZ-CLM	**0.93**	0.92	**1.05**	**1.05**	**1.07**	**1.08**	**1.08**
HC-HadRM	**0.88**	0.90	**1.07**	1.04	**1.09**	**1.11**	**1.14**

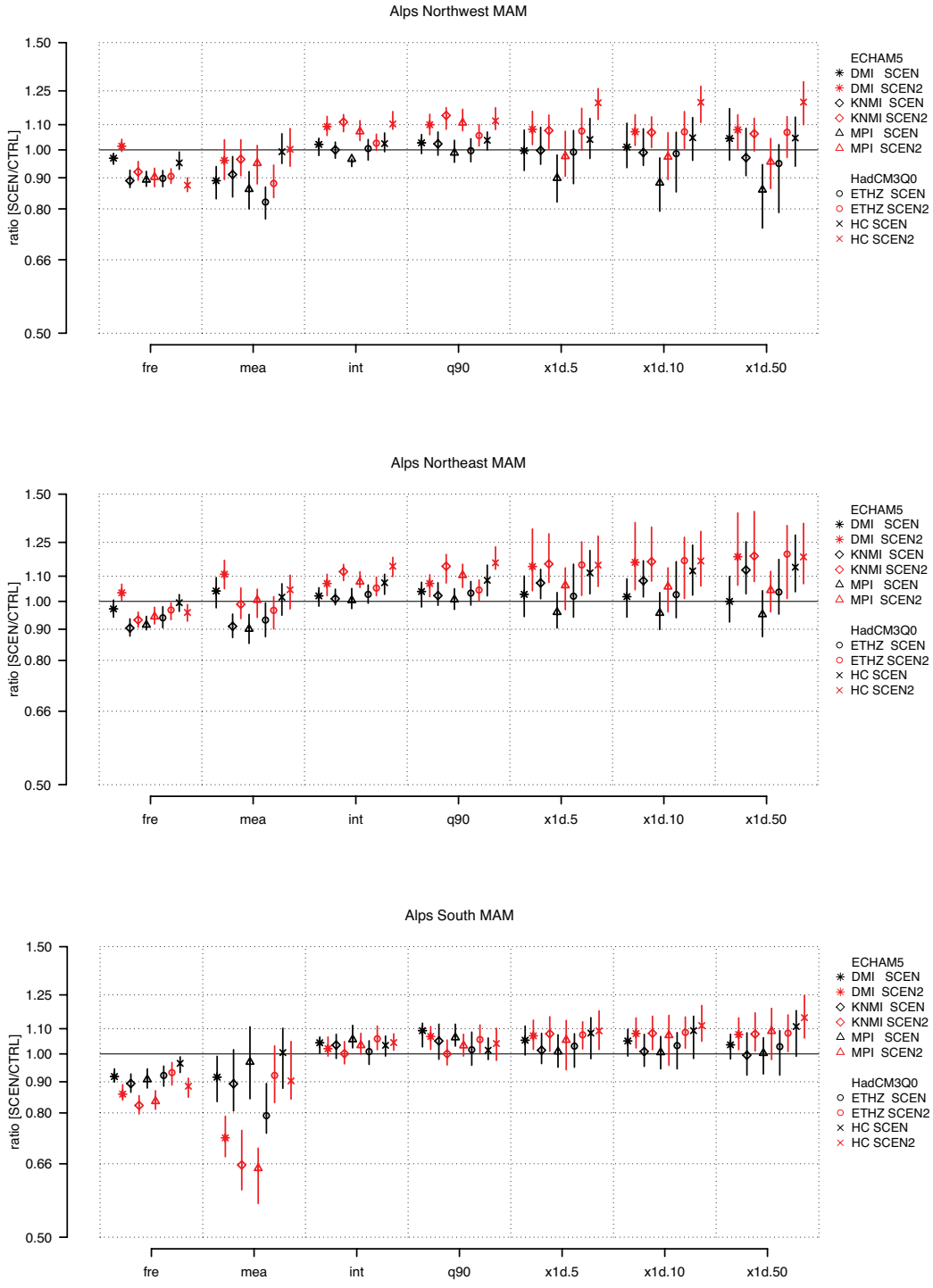

Figure 3-19: Simulated change (ratio SCEN/CTRL) in domain-mean precipitation diagnostics and extremes in spring for Northwestern Alps (top), Northeastern Alps (middle) and Southern Alps (bottom) as simulated by 5 RCMs for period 2021-2050 (SCEN1, in black) and period 2070-2099 (SCEN2, in red) wrt 1961-1990. Symbols depict the best-estimate, lines the 90%-confidence interval associated with simulated change.

Table 3.2-3: Best estimate of change (ratio SCEN1/CTRL) in domain mean precipitation diagnostics and 1-day precipitation extremes in summer (JJA) as simulated by 5 RCMs for period 2070-2099 (SCEN2) wrt 1961-1990 (CTRL).

NORTHWESTERN ALPS [NW]

RCM	fre	mea	int	q90	x1d.5	x1d.10	x1d.50
ECHAM5							
DMI-HIRHAM	**0.91**	**0.83**	**0.96**	0.98	1.00	1.00	1.00
KNMI-RACMO	**0.72**	**0.67**	**1.05**	**1.07**	**1.12**	**1.14**	**1.18**
MPI-REMO	**0.74**	**0.61**	1.00	1.04	**1.16**	**1.21**	**1.33**
HadCM3Q0							
ETHZ-CLM	**0.71**	**0.52**	1.01	1.04	0.97	0.98	0.99
HC-HadRM	**0.79**	**0.69**	1.02	**1.04**	**1.10**	**1.12**	**1.18**

NORTHEASTERN ALPS [NE]

RCM	fre	mea	int	q90	x1d.5	x1d.10	x1d.50
ECHAM5							
DMI-HIRHAM	1.00	0.96	**1.05**	1.07	1.07	1.08	1.06
KNMI-RACMO	**0.80**	**0.84**	**1.14**	**1.18**	**1.23**	**1.24**	**1.27**
MPI-REMO	**0.81**	**0.83**	**1.06**	**1.09**	**1.14**	**1.16**	**1.19**
HadCM3Q0							
ETHZ-CLM	**0.77**	1.01	**1.07**	**1.06**	**1.10**	**1.12**	**1.15**
HC-HadRM	**0.82**	0.94	**1.07**	**1.12**	**1.15**	**1.16**	**1.14**

SOUTHERN ALPS [S]

RCM	fre	mea	int	q90	x1d.5	x1d.10	x1d.50
ECHAM5							
DMI-HIRHAM	**0.85**	**0.71**	**1.07**	1.03	1.02	1.04	1.08
KNMI-RACMO	**0.69**	**0.53**	1.03	1.05	0.95	1.00	1.09
MPI-REMO	**0.74**	**0.61**	1.03	**1.07**	1.01	1.04	**1.09**
HadCM3Q0							
ETHZ-CLM	**0.68**	**0.51**	0.99	1.00	**0.88**	0.91	0.95
HC-HadRM	**0.76**	**0.58**	0.95	0.96	0.91	0.93	0.95

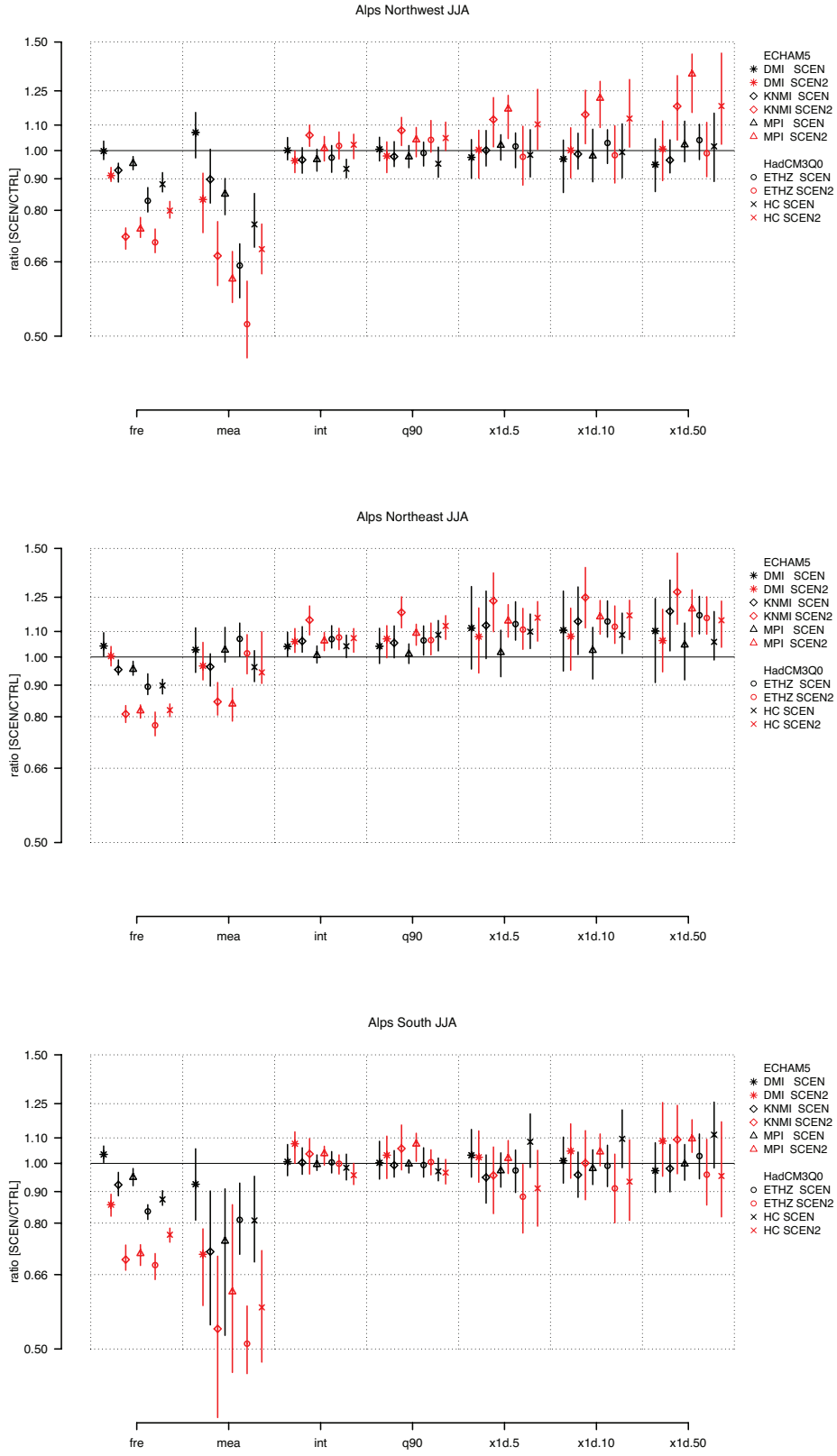

Figure 3-20: Simulated change (ratio SCEN/CTRL) in domain-mean precipitation diagnostics and extremes in summer for Northwestern Alps (top), Northeastern Alps (middle) and Southern Alps (bottom) as simulated by 5 RCMs for period 2021-2050 (SCEN1, in black) and period 2070-2099 (SCEN2, in red) wrt 1961-1990. Symbols depict the best-estimate, lines the 90%-confidence interval associated with simulated change. Note that axes had to be adjusted in order to capture the whole range of confidence intervals.

Table 3.2-4: Best estimate of change (ratio SCEN1/CTRL) in domain mean precipitation diagnostics and 1-day precipitation extremes in fall (SON) as simulated by 5 RCMs for period 2070-2099 (SCEN2) wrt 1961-1990 (CTRL).

			NORTHWESTERN ALPS [NW]				
RCM	**fre**	**mea**	**int**	**q90**	**x1d.5**	**x1d.10**	**x1d.50**
ECHAM5							
DMI-HIRHAM	0.99	**1.07**	**1.08**	**1.08**	**1.24**	**1.26**	**1.30**
KNMI-RACMO	0.98	**1.10**	**1.12**	**1.16**	**1.28**	**1.29**	**1.30**
MPI-REMO	**0.96**	1.05	**1.14**	**1.17**	**1.20**	**1.22**	**1.25**
HadCM3Q0							
ETHZ-CLM	**0.83**	**0.89**	**1.11**	**1.14**	**1.12**	**1.11**	**1.10**
HC-HadRM	**0.90**	1.04	**1.19**	**1.28**	**1.26**	**1.28**	**1.31**

			NORTHEASTERN ALPS [NE]				
RCM	**fre**	**mea**	**int**	**q90**	**x1d.5**	**x1d.10**	**x1d.50**
ECHAM5							
DMI-HIRHAM	1.01	**1.10**	**1.10**	**1.13**	**1.18**	**1.18**	**1.18**
KNMI-RACMO	1.00	**1.14**	**1.22**	**1.27**	**1.27**	**1.27**	**1.31**
MPI-REMO	0.96	**1.18**	**1.23**	**1.26**	**1.33**	**1.35**	**1.38**
HadCM3Q0							
ETHZ-CLM	**0.87**	0.91	**1.14**	**1.14**	**1.22**	**1.24**	**1.24**
HC-HadRM	0.99	1.03	1.03	1.04	1.06	1.06	1.07

			SOUTHERN ALPS [S]				
RCM	**fre**	**mea**	**int**	**q90**	**x1d.5**	**x1d.10**	**x1d.50**
ECHAM5							
DMI-HIRHAM	**0.92**	**0.77**	1.03	**1.05**	**1.12**	**1.13**	**1.15**
KNMI-RACMO	**0.91**	**0.85**	**1.05**	1.07	1.04	1.04	1.02
MPI-REMO	**0.92**	**0.73**	1.04	1.02	1.03	1.06	1.08
HadCM3Q0							
ETHZ-CLM	**0.88**	0.97	**1.16**	**1.19**	**1.23**	**1.23**	**1.20**
HC-HadRM	**0.86**	0.95	**1.09**	**1.09**	**1.13**	**1.15**	**1.17**

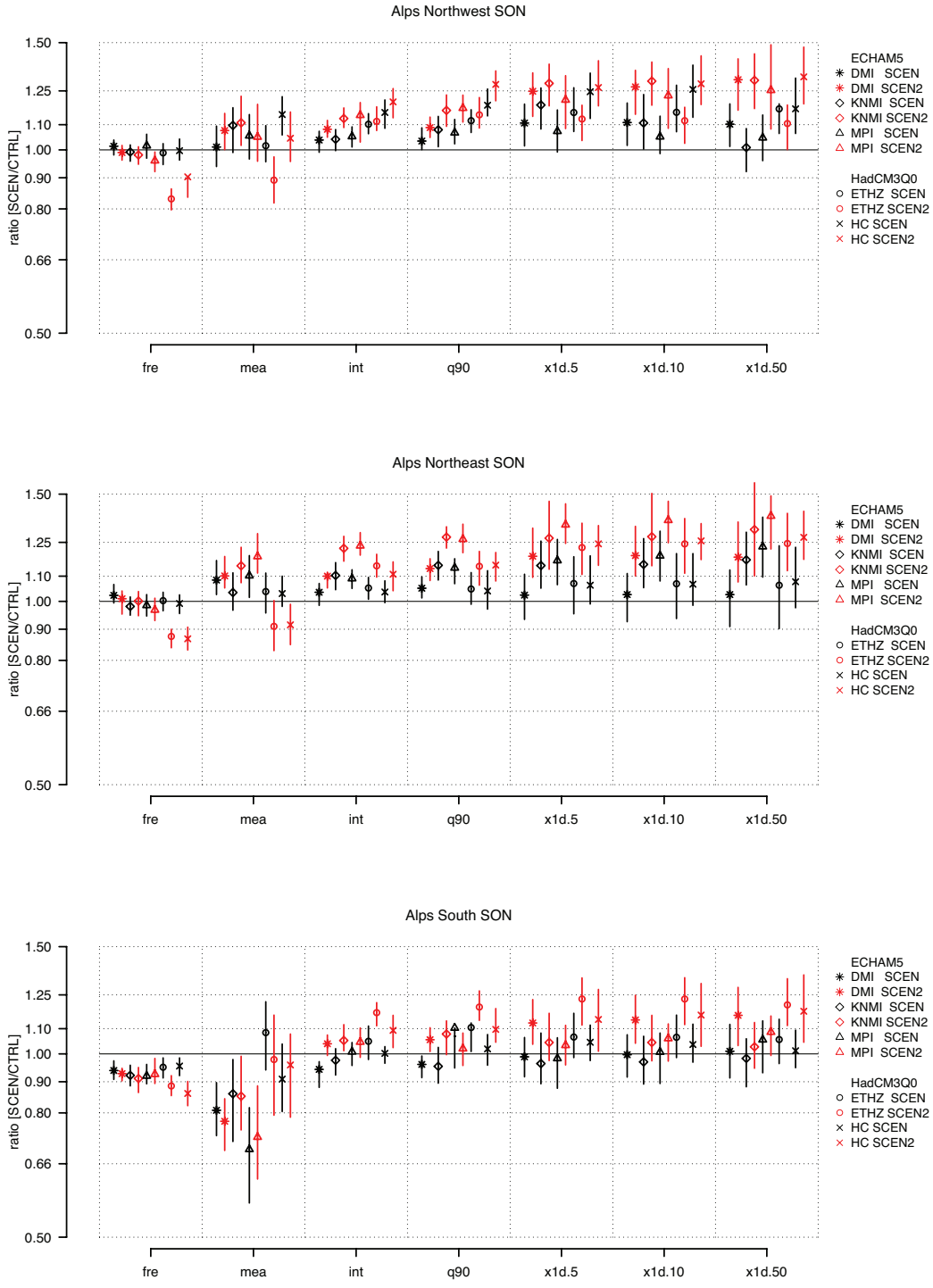

Figure 3-21: Simulated change (ratio SCEN/CTRL) in domain-mean precipitation diagnostics and extremes in fall for Northwestern Alps (top), Northeastern Alps (middle) and Southern Alps (bottom) as simulated by 5 RCMs for period 2021-2050 (SCEN1, in black) and period 2070-2099 (SCEN2, in red) wrt 1961-1990. Symbols depict the best-estimate, lines the 90%-confidence interval associated with simulated change.

3.3 Change in Return Values

3.3.1 Introduction

An additional case study is presented in this section. The studies intention is to present absolute return values and related uncertainties in these values. It relies on a multi-model ensemble of 5 RCMs, and focuses on three Swiss sub-regions for present day conditions (CTRL, 1961-1990) and for two future scenarios, 2021-2050 (SCEN1) and 2070-2099 (SCEN2). For comparison and validation with observations at approximately present-day conditions (1971-1998), the analysis is additionally performed on a gridded observational precipitation dataset for the Alpine region, assembled by *Frei and Schär (1998)* (see also section 2.1.2).
The regions of interest are depicted in Figure 3-22. Basing on the Swiss domains defined in context of the CH2011-initiative [1], the regions represent Northwestern (NW-CH), Northeastern (NE-CH) and Southern (S-CH) Switzerland. Their definition is based on a grid-point correlation analysis of gridded temperature and precipitation fields. Hence, the three regions characterize different climatic regimes within Switzerland.

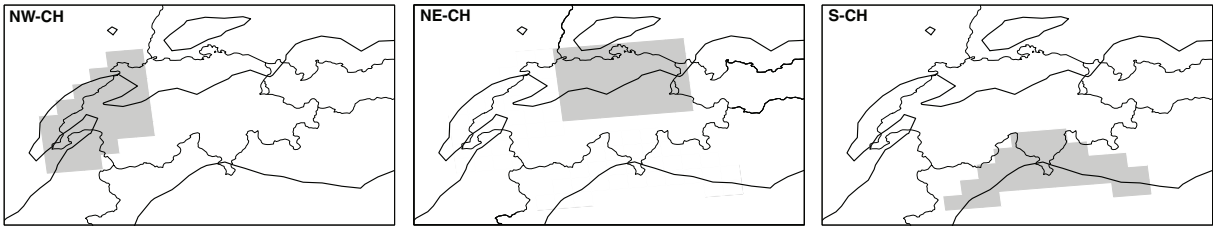

Figure 3-22: Sub-regions used in the additional study on absolute return values in Switzerland. Definitions adopted from the CH2011-initiative. Thin black lines depict country borders, thicker lines the ENSEMBLES-grid 700m-isoline.

The 5 RCMs used to form the multi-model ensemble, comply with the five models used to investigate late 21st century projections presented before (see also labeled in Table 2.1-1). The methodological approach behind this investigation is a modification and further development of the bootstrapping / resampling procedure described in section 2.2.4. Here, 50 estimates of absolute return values of seasonal precipitation extremes are individually resampled for each one of the 5 RCMs. Subsequently, the generated samples are aggregated to one single frequency distribution of 250 samples, containing 50 samples from each RCM. The median of the resulting distribution is assumed to be the best estimate for a return value associated with a certain return period in a sub-region. Moreover, the range between the 95%- and 5%-percentiles of the frequency distribution denotes the uncertainty range associated with a return value. Associated with the width of the uncertainty range one is able to draw conclusions about uncertainty and variability in the projections of return values. For the observational reference, as performed for each single model, only 50 bootstrap samples are resampled to form the distribution from which the best estimate (median) and uncertainty range (range between 5%- and 95%-percentile) is derived.

[1] The CH2011 initiative is a consortium of several Swiss climate research institutions that provide a report with updated and high quality climate scenarios for Switzerland.
(URL: http://www.c2sm.ethz.ch/services/CH2011).

3.3.2 Results

Figure 3-23 (NW-CH), Figure 3-24 (NE-CH) and Figure 3-25 (S-CH) depict the results of the analysis. The left column in each figure depicts the observational reference, whereas the green area depicts the uncertainty range and the black line, the best estimate. The mid-column presents results for period 2021-2050 (SCEN1), compared to 1961-1990 (CTRL). The right column presents projected conditions in 2070-2099 (SCEN2) and also CTRL for reasons of comparison. Results for control-simulations are colored in blue, those for scenario integrations in red. The best estimates are depicted by solid lines.

Comparing CTRL with FS1998, one sees quite a good reproduction of seasonal characteristics and magnitude associated with return values in the three sub-regions. Generally, winter and fall events tend to be overestimated by models. On a seasonal level, one also sees distinct differences in the character and strength of heavy rainfall events between the three regions. Especially S-CH distinguishes itself from the two northern domains. For instance, return values are partly more than twice as large, when compared to NW- and NE-CH. Nevertheless, one should note that there is only an overlap of 20 years between CTRL and FS1998: so that a direct comparison should be treated carefully.
Comparing the ***best estimates*** of control and scenario integrations reveals what changes in return values mean in regard to changes in return periods and the frequency of extremes under future climatic conditions. Referring to the best estimate, only the most pronounced changes are described in the following. A very remarkable intensification of precipitation extremes is simulated in fall for the two northern sub-domains (NE-CH and NW-CH). This intensification distinctly amplifies throughout the 21st century. For instance, in NE-CH, events with a recurrence of 20 years at present-day conditions will occur once in 10 years in period 2021-2050. At the end of the 21st century, this shift becomes even more dramatic. Heavy rainfall events that occur once in 100 years will then occur once in 20 years. In NE-CH and NW-CH, strong intensifications of extreme rainfall events are also simulated to occur in summer. The southern sub-region is not affected by increases / decreases as large in magnitude as in the two northern sub-domains. However, return values in S are large in general.
In association with adaptation to climate change, one has to pay attention to the ***uncertainty range*** associated with simulated return values / periods, as they depict the most extreme events that could potentially occur. A look at the uncertainty ranges obtained in this study, reveal serious implications for particular regions and in particular seasons; in particular when considering the high costs attached to adapting to the simulated climatic conditions and their uncertainties. The most noteworthy cases are found when the upper bound of the uncertainty range for scenario integrations greatly exceeds the upper bound of associated control integrations. The most extreme example for such a case is found in northeastern Switzerland (NE-CH) in fall. The lower bound of the future uncertainty range even distinctly exceeds the best estimate obtained for present-day conditions. On the other hand, the best estimate for future conditions is simulated to fall together with the upper bound of CTRL-conditions. This implies that heavy rainfall events are most likely to strongly intensify. Moreover, the upper uncertainty bound obtained for future conditions very highly exceeds the upper uncertainty bound representative for present day climatic conditions. In absolute values, this is expressed by a shift from 115mm/day at present-day conditions to 170mm/d at late 21st century conditions for an event occurring once in 100years (~40% change). Adapting infrastructure to such an intensification to avoid severe damage in the case of a 100yr-event would implicate large expenses.

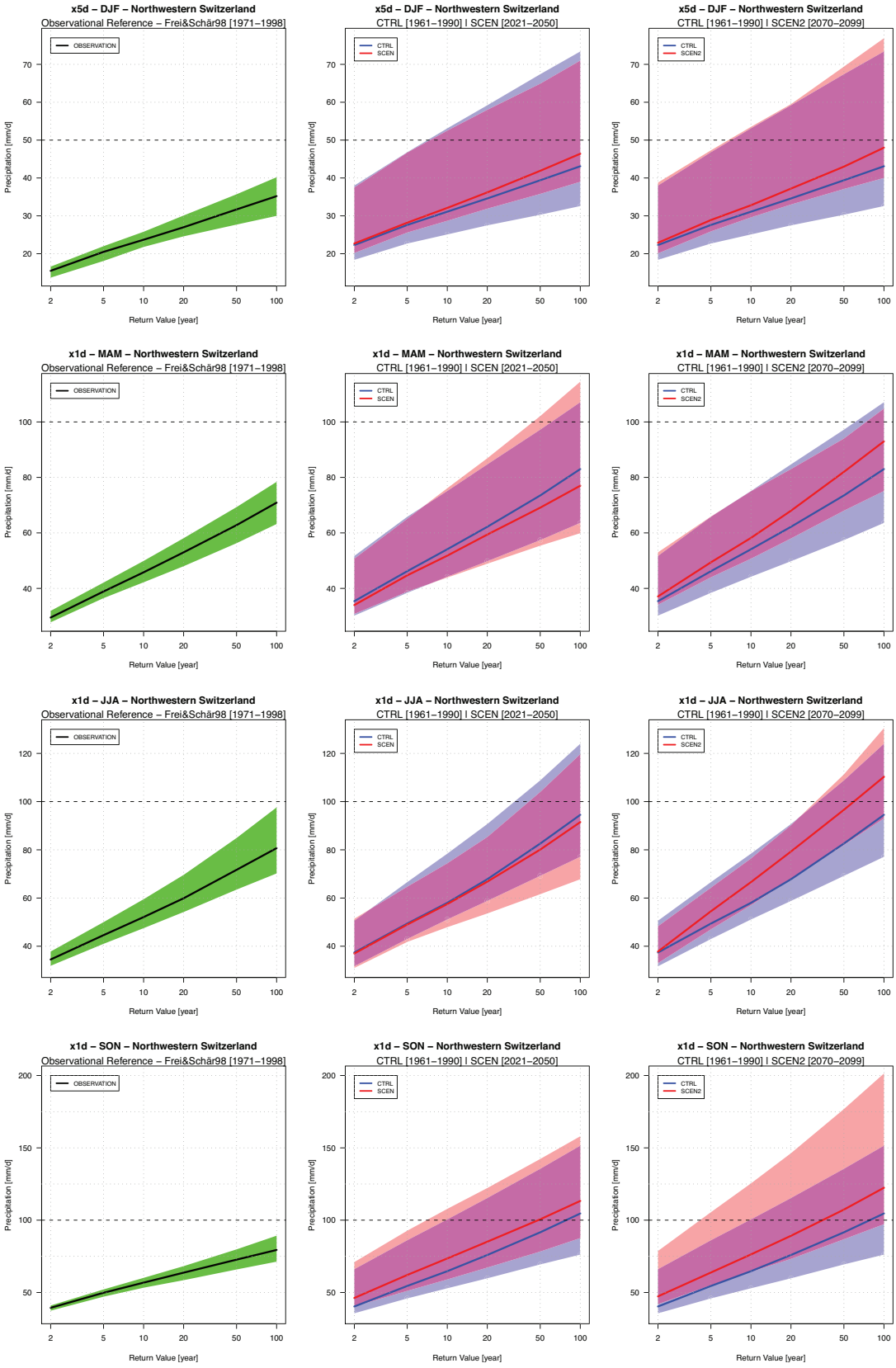

Figure 3-23: Absolute return values for heavy rainfall events with return periods between 2 and 100 years on a seasonal level for Northwestern Switzerland. The left column shows observational records (FreiSchär1998), for period 1971-1998. The middle column depicts absolute values for SCEN1 (2021-2050, in red) and CTRL (1961-1990, in blue) based on a 5 RCM-member ensemble. The right column presents results for SCEN2 (2070-2099, in red) and CTRL. Shaded areas depict the 90%-uncertainty range, the bold-lines best estimates.

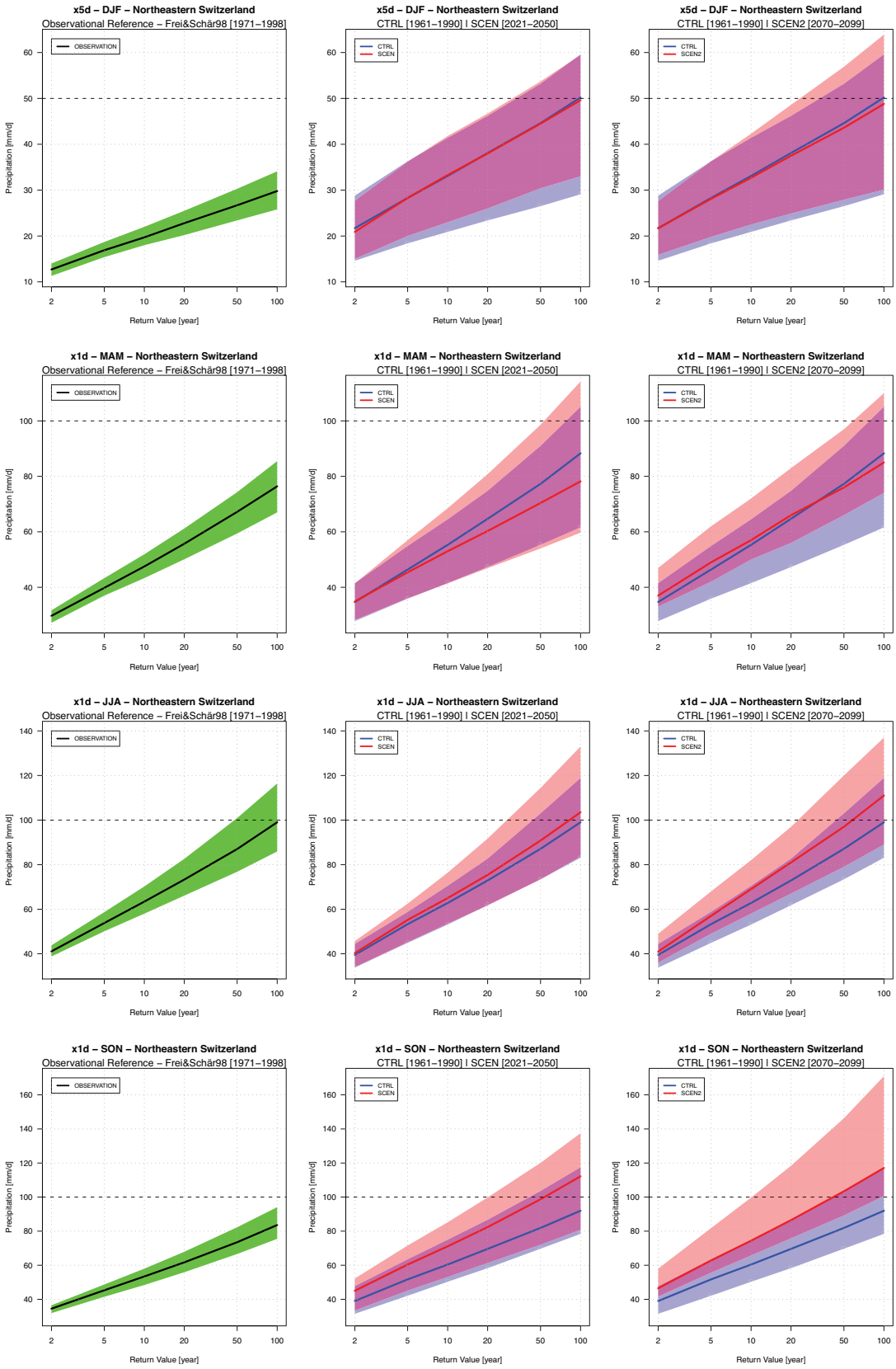

Figure 3-24: Absolute return values for heavy rainfall events with return periods between 2 and 100 years on a seasonal level for Northeastern Switzerland. The left column shows observational records (FreiSchär1998), for period 1971-1998. The middle column depicts absolute values for SCEN1 (2021-2050, in red) and CTRL (1961-1990, in blue) based on a 5 RCM-member ensemble. The right column presents results for SCEN2 (2070-2099, in red) and CTRL. Shaded areas depict the 90%-uncertainty range, the bold-lines best estimates.

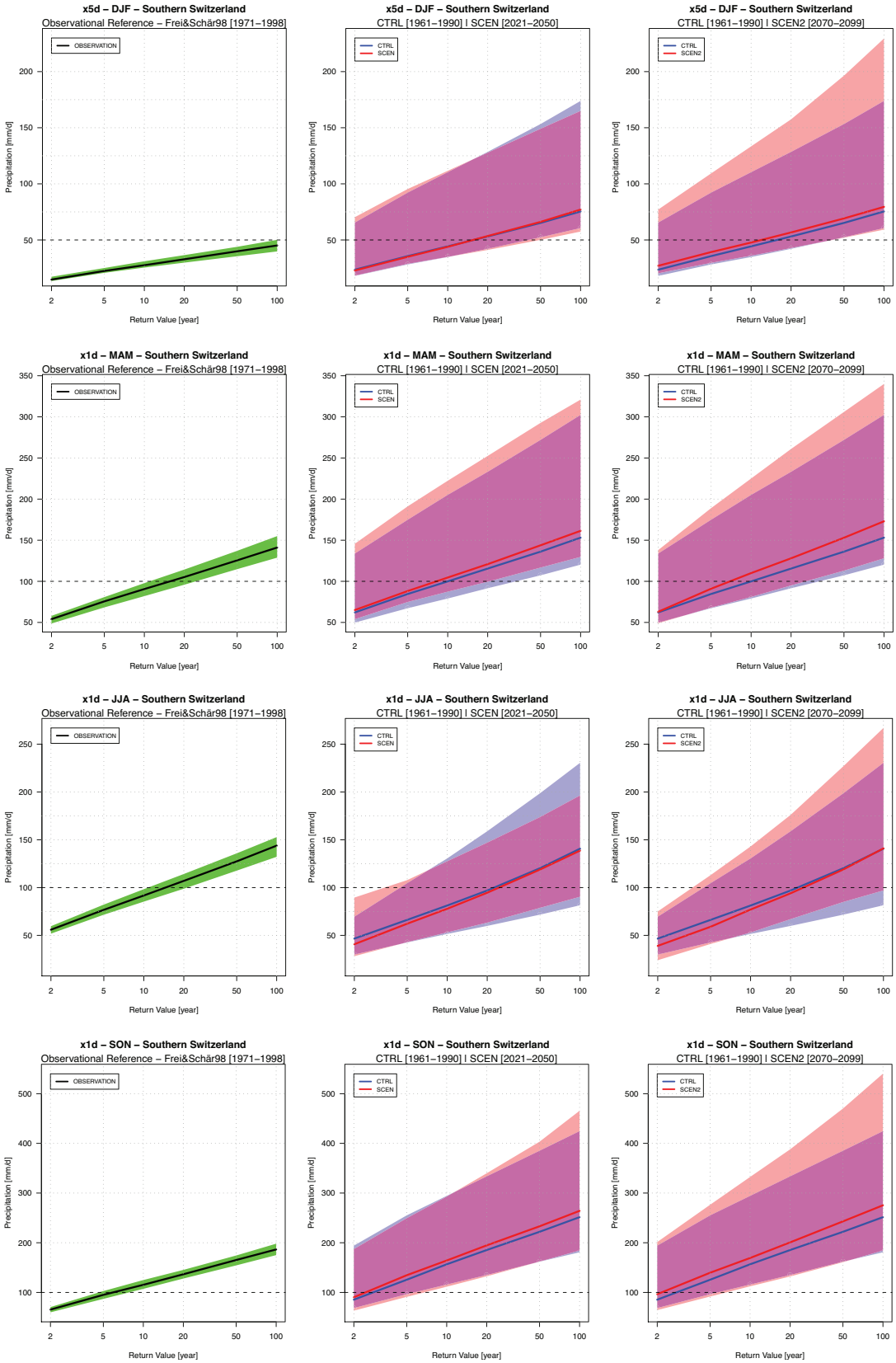

Figure 3-25: Absolute return values for heavy rainfall events with return periods between 2 and 100 years on a seasonal level for Southern Switzerland. The left column shows observational records (FreiSchär1998), for period 1971-1998. The middle column depicts absolute values for SCEN1 (2021-2050, in red) and CTRL (1961-1990, in blue) based on a 5 RCM-member ensemble. The right column presents results for SCEN2 (2070-2099, in red) and CTRL. Shaded areas depict the 90%-uncertainty range, the bold-lines best estimates.

4 Conclusion

The presented study analyzed 21st century projections of extreme and basic precipitation diagnostics for the Alpine region with respect to present-day climatic conditions as simulated by a set of 10 regional climate models stemming from the EU-ENSEMBLES project. The results obtained imply that serious changes in the character of precipitation and changes in precipitation extremes are subject to 21st century climate change in central Europe and the Alps in particular. Although the morphology of the seasonal change structure is a robustly simulated feature throughout the whole set of considered RCMs, marked inter-model variability and spread has been shown. The range of inter-model spread thereby depends on the season and diagnostic regarded. Moreover, models tend to cluster in dependence of the underlying driving GCM, which thus contributes to additional inter-model spread in the whole set of considered RCM simulations.

Change Assessment

Considering the intended assessment of changes, the results obtained indicate that serious changes are likely to occur in the Alpine and central European region. Not only heavy rainfall events are projected to increase in severity: the basic precipitation climatology is likely to face changes that bear severe potential to cause impact. The obtained seasonal change structure also implies that under future climatic conditions a more variable precipitation climate is about to set in.

Focusing on projected changes in extreme precipitation events, most remarkable intensifications are simulated in the Northern Alps and generally across the northern parts of central Europe in fall. The Southern Alps and southeastern central Europe are likely to experience most pronounced intensifications of heavy rainfall events in winter. These findings are in line with earlier studies [*Frei et al.*, 2006; *Solomon et al.*, 2007].

The driving factors that contribute to the projected increases in winter and fall extreme events remain an open question and should be addressed in future research. One should consider an increased frequency and intensity of VB cyclones as well as shifted and modified large-scale weather and circulation patterns causing the simulated increases in heavy precipitation events as possible driving processes. Especially regions facing the most considerable winter increases coincide with regions typically affected by VB cyclones (Genoa-cyclones). On the other hand, regions facing the most marked increases in fall (northwestern Alpine region) are commonly influenced by synoptic disturbances of Atlantic origin. On account of this, an increased frequency of synoptic-disturbances or shifted storm-tracks might cause the projected increases. For example, [*Jacobeit et al.*, 2009]) have recently examined the link between large-scale atmospheric circulation patterns and precipitation extremes over central Europe.

In general, however, the projected changes in heavy rainfall, especially in fall, are of a complex nature. There is, to some degree, a tendency for 1-day events to increase considerably more than 5-day events. The question is raised whether the contribution of convective events to heavy rainfall in fall (and winter) increases under future climatic conditions. This would imply a combined effect of circulation and moisture uptake capacity changes.

Apart from the most pronounced projected changes in heavy rainfall, this study shows, that in summer and also spring, severe decreases in precipitation frequency and the mean are a robust feature in model projections across the entire central European region, most prominently in the southern parts. In conjunction with projected increases in the occurrence of heat waves [*Fischer and Schar*, 2010; *Schar et al.*, 2004], these projections bear the potential to imply very serious hazards. Also, the projected reduced frequency and hence future lack of summer-precipitation implies an enhanced probability of persisting and extreme heat-waves like that of 2003 due to soil-drying [*Fischer et al.*, 2007]. At the same time, projections show a stable or even an increased trend in the intensity of summer rainfall events, particularly along the northern Alps and in southern Germany. This implies that precipitation events become less but more intense under future climatic conditions.
Throughout all seasons, but especially in summer, changes in the mean and in extreme diagnostics scale disproportionately. These findings are in line with observations, experiments and future simulations. In summer, the signs of change in mean/frequency and extremes/intense precipitation are even opposed. Specifically in summer, the increased moisture uptake capacity in a warmed climate might be an important factor contributing to the projected increases in extremes and intense diagnostics.
In summary, the findings of this study evidently imply that the event of precipitation is about to intensify as the hydrologic cycle will intensify in a warming climate. The results reveal and confirm *Alexander et al. (2006)* that large areas will be afflicted with less wet days but an increase in the intensity of single wet days. The intensification of precipitation is a reasonably robust feature across all seasons and regions, independent of projected changes in the mean and frequency. This implies that different physical and dynamical processes govern changes in precipitation diagnostics. Mean and frequency are thereby likely to be primarily governed by changes in the circulation, while intense precipitation diagnostics might be governed by thermo-dynamical properties of warmed air which supplies more water to be rained out during an event. Nevertheless, if increases in the mean are projected, they are mainly attributable to an intensification of precipitation.

Inter-model Assessment
The results also allow inference to be drawn with respect to the assessment of inter-model behavior (resp. model uncertainty) in the projections of future precipitation and its extremes. Ten models have been used to perform the analyses presented. These can be partitioned according to different driving GCMs: 5 RCMs are driven by the ECHAM5-, 4 models by the HadCM3Q0- and one single model by the Arpege-GCM.
Compared with the earlier and similar example-study by *Frei et al. (2006)* that only considered 6 HadCM-driven RCMs, the inclusion of additional RCM-GCM-groups comprises an added value in order to assess inter-model behavior more accurately. In the presented study, the increase of examined RCMs and expansion across different GCM-groups clearly enlarged inter-model spread and thus uncertainty about future changes. Moreover, the results reveal that RCM projections highly depend on the underlying GCM and its driving boundary conditions, conspicuously in winter and fall. A link to mainly large-scale and long-lived precipitation events occurring favorably in winter and fall, which are captured in GCMs, can potentially be drawn but remains an open question. This study has also shown that GCM arrangement is weaker in summer where sub-grid processes (e.g. convection) are a prominent source of precipitation and hence individual model-parameterizations become a crucial factor in the different projections and thereby raise uncertainties (see also *Frei et al. (2006)*). Nevertheless, the results show that RCM projections mainly seem to be individual interpretations of the large-scale GCM projection patterns (see Figure 3-4 and Figure 3-5). Covering only parts of the entire inter-model range, consideration of one single GCM-chain

can lead to misguiding results. For this reason, future studies should comprise several GCM-chains in order to assess climate change and possible impacts. An added value could also be achieved when taking several GCMs into account that drive the same RCM. This approach would allow investigating the influence of GCMs on a RCM simulation in more detail. This approach was not undertaken within the presented investigation.
Focusing on the results obtained throughout this study, one sees, besides GCM-grouping of RCMs, characteristic deviations of single models. Within the HadCM3Q0-model group, VMGO-RRCM shows very pronounced deviations. In the ECHAM5-driven integrations, DMI-HIRHAM shows the most deviant behavior. It is also obvious that the CNRM-Arpege model does not always match the systematic behavior of the two other GCM groups. CNRM-Arpege does also shows the largest uncertainties, expressed by the range of its confidence intervals within its projections.
When considering uncertainties in general, one sees the largest uncertainties in the projections of the mean, followed by frequency and extreme value diagnostics. Intensity and the 90%-quantile face markedly small uncertainties: model-spread for these two diagnostics is also small in all seasons.

Finally concluding the presented study, one can recapitulate that it displays a comprehensive morphological review on projected changes in the character of precipitation and its extremes for central Europe and the Alpine region in particular. Even though particular inter-model differences exist, the results demonstrate that changes are very likely to take place. The study does not investigate possible reasons for the simulated changes, but suggests future research directions to focus on these causes. Possible severe climatic risks are robustly shown in the simulated seasonal change structures. These risks include an intensification of heavy rainfall events and an increased risk of droughts in summer months.

Literature

Alexander, L. V., et al. (2006), Global observed changes in daily climate extremes of temperature and precipitation, *Journal of Geophysical Research-Atmospheres*, *111*(D5).

Allen, M. R., and W. J. Ingram (2002), Constraints on future changes in climate and the hydrologic cycle, *Nature*, *419*(6903), 224-+.

Arnold, J. (2009), Extreme Precipitation in the European Alps: Evaluating ENSEMBLES Regional Climate Model Simulations for Present-Day Climate, 63 pp, ETH Zürich, Zürich.

Arnold, J., P. Pall, S. Kotlarski, T. Bosshard, and C. Schar (2011), Extreme Precipitation in the European Alps: Evaluating ENSEMBLES Regional Climate Model Simulations for Present-Day Climate, edited, ETH Zürich.

Barry, R. G. (2008), *Mountain Weather and Climate*, Cambridge University Press.

Beniston, M. (2003), Climatic change in mountain regions: A review of possible impacts, *Climatic Change*, *59*(1-2), 5-31.

Beniston, M., et al. (2007), Future extreme events in European climate: an exploration of regional climate model projections, *Climatic Change*, *81*, 71-95.

Böhm, U. e. a. (2006), CLM - the climate version of LM: Brief description and long-term applications., *COSMO Newsletter No. 6, COSMO, Deutscher Wetterdienst, Offenbach am Main*.

Buonomo, E., R. Jones, C. Huntingford, and J. Hannaford (2007), On the robustness of changes in extreme precipitation over Europe from two high resolution climate change simulations, *Quarterly Journal of the Royal Meteorological Society*, *133*(622), 65-81.

Christensen, J. H. e. a. (2007), The HIRHAM Regional Climate Model Version 5, *Technical report 06-17. Danish Meteorological Institute DMI, Copenhagen*.

Coles, S. (2001), *An Introduction to Statistical Modeling of Extreme Values*, 224 pp., Springer

Collins, M., B. B. Booth, B. Bhaskaran, G. R. Harris, J. M. Murphy, D. M. H. Sexton, and M. J. Webb (2011), Climate model errors, feedbacks and forcings: a comparison of perturbed physics and multi-model ensembles, *Climate Dynamics*, *36*(9-10), 1737-1766.

Deque, M., C. Dreveton, A. Braun, and D. Cariolle (1994), THE ARPEGE/IFS ATMOSPHERE MODEL - A CONTRIBUTION TO THE FRENCH COMMUNITY CLIMATE MODELING, *Climate Dynamics*, *10*(4-5), 249-266.

Diaz, H. F., and R. J. Murnane (2008), *Climate Extremes and Society*, Cambridge University Press.

Emori, S., and S. J. Brown (2005), Dynamic and thermodynamic changes in mean and extreme precipitation under changed climate, *Geophysical Research Letters*, *32*(17).

Fischer, E. M., and C. Schar (2009), Future changes in daily summer temperature variability: driving processes and role for temperature extremes, *Climate Dynamics*, *33*(7-8), 917-935.

Fischer, E. M., and C. Schar (2010), Consistent geographical patterns of changes in high-impact European heatwaves, *Nature Geoscience*, *3*(6), 398-403.

Fischer, E. M., S. I. Seneviratne, P. L. Vidale, D. Luthi, and C. Schar (2007), Soil moisture - Atmosphere interactions during the 2003 European summer heat wave, *Journal of Climate*, *20*(20), 5081-5099.

Fowler, H. J., M. Ekstrom, S. Blenkinsop, and A. P. Smith (2007), Estimating change in extreme European precipitation using a multimodel ensemble, *Journal of Geophysical Research-Atmospheres*, *112*(D18).

Frei, C., and C. Schar (1998), A precipitation climatology of the Alps from high-resolution rain-gauge observations, *International Journal of Climatology*, *18*(8), 873-900.

Frei, C., and C. Schar (2001), Detection probability of trends in rare events: Theory and application to heavy precipitation in the Alpine region, *Journal of Climate*, *14*(7), 1568-1584.

Frei, C., and J. Schmidli (2006), Das Niederschlagsklima der Alpen: Wo sich Extreme nahekommen, in *ProMet: Meteorologische Fortbildung*, edited by D. WetterDienst.

Frei, C., C. Schar, D. Luthi, and H. C. Davies (1998), Heavy precipitation processes in a warmer climate, *Geophysical Research Letters*, *25*(9), 1431-1434.

Frei, C., R. Scholl, S. Fukutome, J. Schmidli, and P. L. Vidale (2006), Future change of precipitation extremes in Europe: intercomparison of scenarios from regional climate models, *Journal of Geophysical Research-Atmospheres*, *111*(D06105).

Frei, C., J. H. Christensen, M. Deque, D. Jacob, R. G. Jones, and P. L. Vidale (2003), Daily precipitation statistics in regional climate models: Evaluation and intercomparison for the European Alps, *Journal of Geophysical Research-Atmospheres*, *108*(D3).

Frich, P., L. V. Alexander, P. Della-Marta, B. Gleason, M. Haylock, A. Tank, and T. Peterson (2002), Observed coherent changes in climatic extremes during the second half of the twentieth century, *Climate Research*, *19*(3), 193-212.

Giorgi, F. (2008), Regionalization of climate change information for impact assessment and adaptation, *WMO Bulletin*, *57*(2), 86-92.

Giorgi, F., and L. O. Mearns (1999), Introduction to special section: Regional climate modeling revisited, *Journal of Geophysical Research-Atmospheres*, *104*(D6), 6335-6352.

Gordon, C., C. Cooper, C. A. Senior, H. Banks, J. M. Gregory, T. C. Johns, J. F. B. Mitchell, and R. A. Wood (2000), The simulation of SST, sea ice extents and ocean heat transports in a version of the Hadley Centre coupled model without flux adjustments, *Climate Dynamics*, *16*(2-3), 147-168.

Haerter, J. O., P. Berg, and S. Hagemann (2010), Heavy rain intensity distributions on varying time scales and at different temperatures, *Journal of Geophysical Research-Atmospheres*, *115*.

Hanel, M., and T. A. Buishand (2011), Analysis of precipitation extremes in an ensemble of transient regional climate model simulations for the Rhine basin, *Climate Dynamics*, *36*(5-6), 1135-1153.

Haugen, J., and H. Haakenstrand (2006), The development of HIRHAM version 2 with 50km and 25km resolution, *RegClim General Technical Report No. 9, 159-173*.

Hawkins, E., and R. Sutton (2009), THE POTENTIAL TO NARROW UNCERTAINTY IN REGIONAL CLIMATE PREDICTIONS, *Bulletin of the American Meteorological Society*, *90*(8), 1095-+.

Held, I. M., and B. J. Soden (2006), Robust responses of the hydrological cycle to global warming, *Journal of Climate*, *19*(21), 5686-5699.

Hosking, J. R. M. (1985), Algorithm AS 215: Maximum-likelihood estimation of the paramater of the generalized extreme value distribution, *Applied Statistics*, *34*, 301-310.

Jacob, D., et al. (2007), An inter-comparison of regional climate models for Europe: model performance in present-day climate, *Climatic Change*, *81*, 31-52.

Jacobeit, J., J. Rathmann, A. Philipp, and P. D. Jones (2009), Central European precipitation and temperature extremes in relation to large-scale atmospheric circulation types, *Meteorologische Zeitschrift*, *18*(4), 397-410.

Katz, R. W., and B. G. Brown (1992), EXTREME EVENTS IN A CHANGING CLIMATE - VARIABILITY IS MORE IMPORTANT THAN AVERAGES, *Climatic Change*, *21*(3), 289-302.

Katz, R. W., M. B. Parlange, and P. Naveau (2002), Statistics of extremes in hydrology, *Advances in Water Resources*, *25*(8-12), 1287-1304.

Kendon, E. J., D. P. Rowell, R. G. Jones, and E. Buonomo (2008), Robustness of future changes in local precipitation extremes, *Journal of Climate*, *21*(17), 4280-4297.

Kharin, V. V., and F. W. Zwiers (2000), Changes in the extremes in an ensemble of transient climate simulations with a coupled atmosphere-ocean GCM, *Journal of Climate*, *13*(21), 3760-3788.

Kharin, V. V., and F. W. Zwiers (2005), Estimating extremes in transient climate change simulations, *Journal of Climate*, *18*(8), 1156-1173.

Kharin, V. V., F. W. Zwiers, X. B. Zhang, and G. C. Hegerl (2007), Changes in temperature and precipitation extremes in the IPCC ensemble of global coupled model simulations, *Journal of Climate*, *20*(8), 1419-1444.

Kjellström, E. e. a. (2005), A 140-year simulation of European climate with the new version of the Rossby Centre regional atmospheric climate model (RCA3). *SMHI Reports Meteorology and Climatology No. 108, Norrköping, Sweden*.

Klein Tank, A. M. G., and G. P. Konnen (2003), Trends in indices of daily temperature and precipitation extremes in Europe, 1946-99, *Journal of Climate*, *16*(22), 3665-3680.

Klein Tank, A. M. G., and F. W. Zwiers (2009), Guidelines on Analysis of extremes in a changing climate in support of informed decisions for adaptation*Rep*., World Meteorological Organization.

Kotz, S., and S. Nadarajah (2001), *Extreme Value Distributions: Theory and Applications*, World Scientific Publishing Company.

Kundzewicz, Z. W., M. Radziejewski, and I. Pinskwar (2006), Precipitation extremes in the changing climate of Europe, *Climate Research*, *31*(1), 51-58.

Lenderink, G., and E. Van Meijgaard (2008), Increase in hourly precipitation extremes beyond expectations from temperature changes, *Nature Geoscience*, *1*(8), 511-514.

Liu, S. C., C. B. Fu, C. J. Shiu, J. P. Chen, and F. T. Wu (2009), Temperature dependence of global precipitation extremes, *Geophysical Research Letters*, *36*.

Martins, E. S., and J. R. Stedinger (2000), Generalized maximum-likelihood generalized extreme-value quantile estimators for hydrologic data, *Water Resources Research*, *36*(3), 737-744.

MeteoSchweiz (2006), Starkniederschläge August 2005, *Arbeitsberichte der MeteoSchweiz*, *211*, 63.

Min, S. K., X. B. Zhang, F. W. Zwiers, and G. C. Hegerl (2011), Human contribution to more-intense precipitation extremes, *Nature*, *470*(7334), 376-379.

Nakicenovic, N., and R. Swart (2000), *IPCC - Special Report on Emission Scenarios, Summary for Policy Makers*, Cambridge University Press.

Nott, J. (2006), *Extreme Events, A Physical Reconstruction and Risk Assessment*, 310 pp., Cambridge University Press.

O'Gorman, P. A., and T. Schneider (2009), The physical basis for increases in precipitation extremes in simulations of 21st-century climate change, *Proceedings of the National Academy of Sciences of the United States of America*, *106*(35), 14773-14777.

Pal, J. S., et al. (2007), Regional climate modeling for the developing world - The ICTP RegCM3 and RegCNET, *Bulletin of the American Meteorological Society*, *88*(9), 1395-+.

Pall, P., M. R. Allen, and D. A. Stone (2007), Testing the Clausius-Clapeyron constraint on changes in extreme precipitation under CO2 warming, *Climate Dynamics*, *28*(4), 351-363.

Pall, P., T. Aina, D. A. Stone, P. A. Stott, T. Nozawa, A. G. J. Hilberts, D. Lohmann, and M. R. Allen (2011), Anthropogenic greenhouse gas contribution to flood risk in England and Wales in autumn 2000, *Nature (London)*, *470*(7334), 380-384.

Radu, R., M. Deque, and S. Somot (2008), Spectral nudging in a spectral regional climate model, *Tellus Series a-Dynamic Meteorology and Oceanography*, *60*(5), 898-910.

Roeckner, E., K. Arpe, L. Bengtsson, M. Christoph, M. Claussen, L. Dumenil, M. Esch, M. Giorgetta, U. Schlese, and U. Schulzweida (1996), Atmospheric general circulation model ECHAM-4: model description and simulation of present-day climate, *Atmospheric general circulation model ECHAM-4: model description and simulation of present-day climate*, 96 pp.

Schar, C., P. L. Vidale, D. Luthi, C. Frei, C. Haberli, M. A. Liniger, and C. Appenzeller (2004), The role of increasing temperature variability in European summer heatwaves, *Nature*, *427*(6972), 332-336.

Schmidli, J., and C. Frei (2005), Trends of heavy precipitation and wet and dry spells in Switzerland during the 20th century, *International Journal of Climatology*, *25*(6), 753-771.

Schmidli, J., C. Frei, and C. Schar (2001), Reconstruction of mesoscale precipitation fields from sparse observations in complex terrain, *Journal of Climate*, *14*(15), 3289-3306.

Shkolnik, I. M., E. M. Molkentkin, E. D. Nadezhina, E. I. Khlebovnika, and I. A. Sall (2008), Temperature extremes and wild fires in Siberia in 21st century: the VMGO RCM simulation., *Rus. Meteorol. Hydrol.*, *3*, 5-15.

Solomon, S., D. Qin, M. Manning, Z. Chen, M. Maquis, K. B. Averyt, M. Tignor, and H. L. Miller (2007), *Climate Change 2007: The Physical Science Basis. Contribution of Working Group 1 to the Fourth Assessment Report of the Intergovernmental Panel on Climate Change*, Cambridge University Press, Cambridge, UK.

van der Linden, P., and J. F. B. Mitchell (2009), *ENSEMBLES: Climate Change and its Impacts: Summary of research and results from the ENSEMBLES project.* , 160 pp., MetOffice Hadlex Centre, Exeter.

Van Meijgaard, E. e. a. (2008), The KNMI regional atmospheric climate model RACMO, version 2.1, *KNMI technical report, 302, KNMI, De Bilt*.

Whiteman, D. C. (2000), *Mountain Meteorology: Fundamentals and Applications*, Oxford University Press.

Wilks, D. S. (2006), *Statistical Methods in the Atmospheric Sciences*, 648 pp., Academic Press.

Appendix

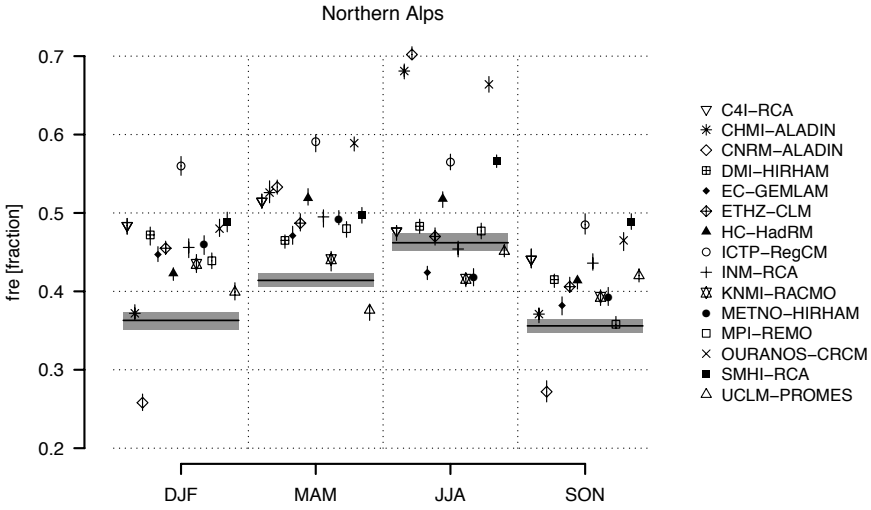

Figure A 1: Domain-mean values and 90% confidence intervals for precipitation frequency on seasonal level in period 1971-1998 in the Northern Alpine region as simulated by 15 EU-ENSEMBLES RCMs (depicted by symbols and lines) and as observed, based on the FS1998-dataset (depicted as grey shaded area). Source: Arnold et al (2011, in prep.)

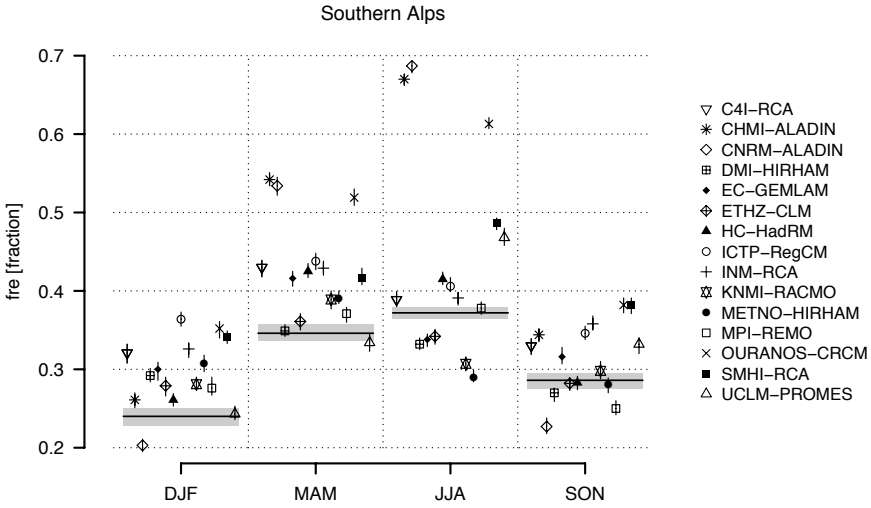

Figure A 2: Domain-mean values and 90% confidence intervals for precipitation frequency on seasonal level in period 1971-1998 in the Southern Alpine region as simulated by 15 EU-ENSEMBLES RCMs (depicted by symbols and lines) and as observed, based on the FS1998-dataset (depicted as grey shaded area). Source: Arnold et al (2011, in prep.)

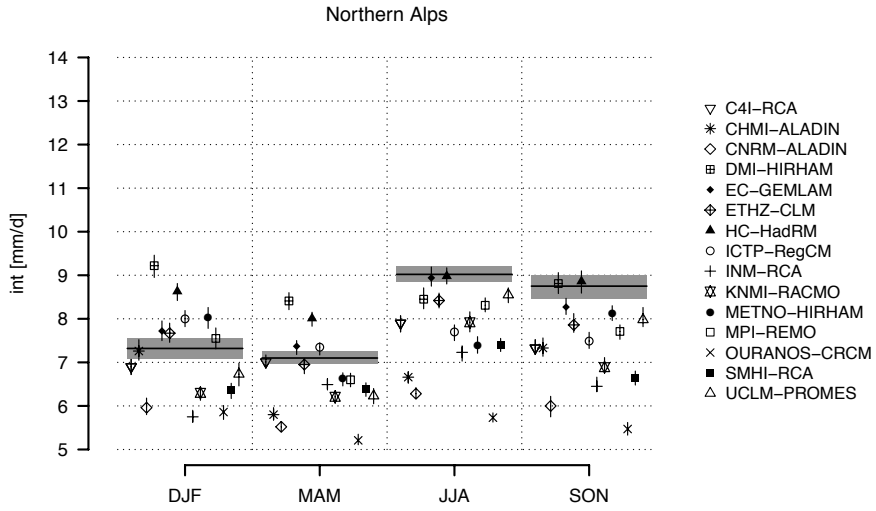

Figure A 3: Domain-mean values and 90% confidence intervals for precipitation intensity on seasonal level in period 1971-1998 in the Northern Alpine region as simulated by 15 EU-ENSEMBLES RCMs (depicted by symbols and lines) and as observed, based on the FS1998-dataset (depicted as grey shaded area). Source: Arnold et al (2011, in prep.)

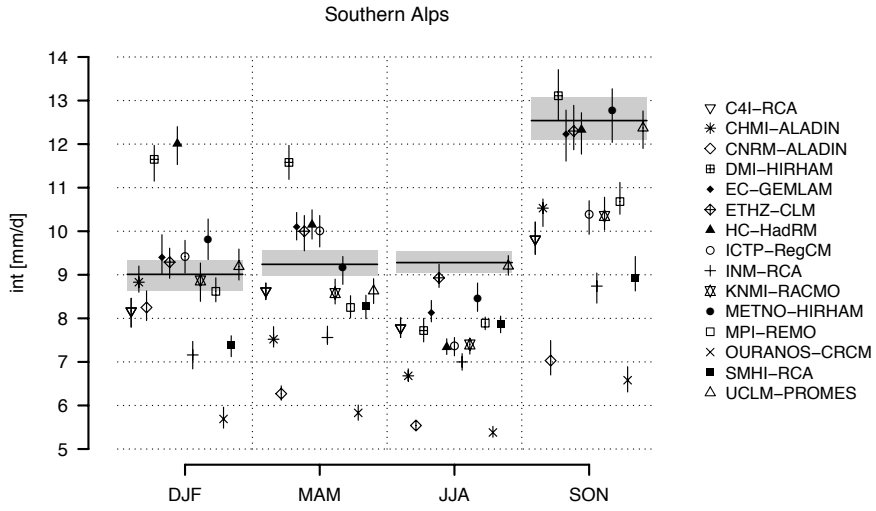

Figure A 4: Domain-mean values and 90% confidence intervals for precipitation intensity on seasonal level in period 1971-1998 in the Southern Alpine region as simulated by 15 EU-ENSEMBLES RCMs (depicted by symbols and lines) and as observed, based on the FS1998-dataset (depicted as grey shaded area). Source: Arnold et al (2011, in prep.)

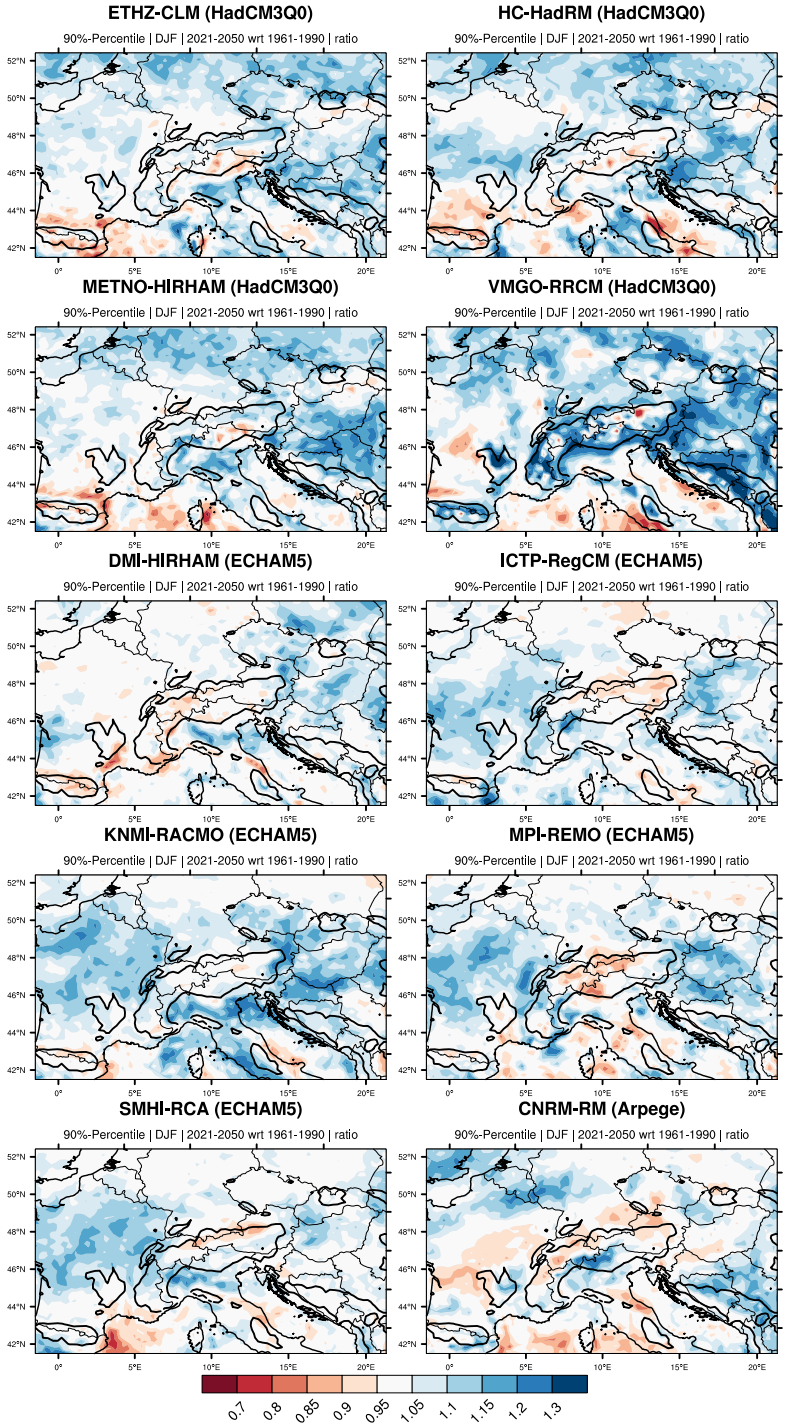

Figure A 5: Change (ratio SCEN/CTRL) in the 90%-quantile in winter as simulated by 10 RCMs for period SCEN1 (2021-2050) wrt CTRL (1961-1990). Thick lines illustrate the 700m a.s.l.-isoline as represented by the ENSEMBLES E-OBS topography.

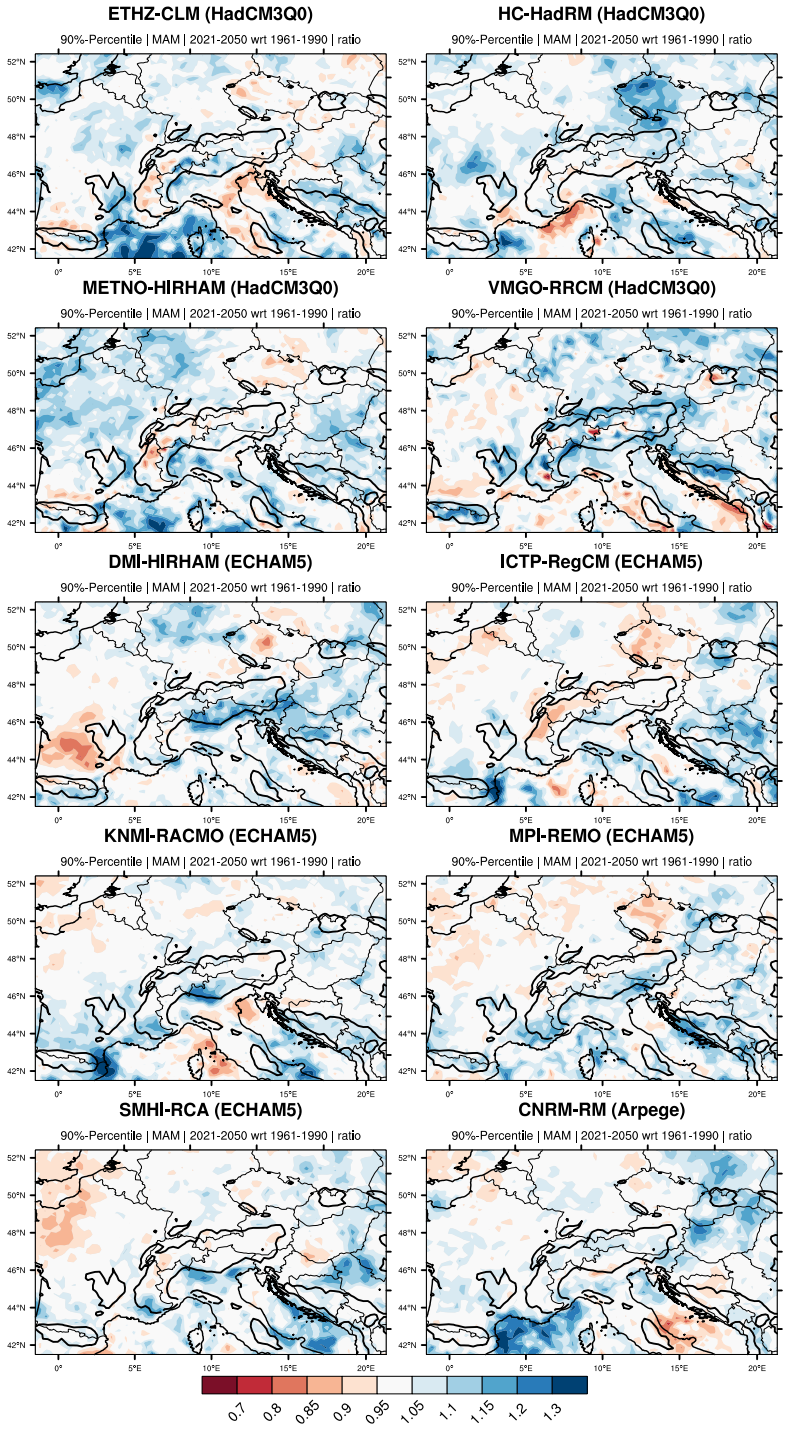

Figure A 6: Change (ratio SCEN/CTRL) in the 90%-quantile in spring as simulated by 10 RCMs for period SCEN1 (2021-2050) wrt CTRL (1961-1990). Thick lines illustrate the 700m a.s.l.-isoline as represented by the ENSEMBLES E-OBS topography.

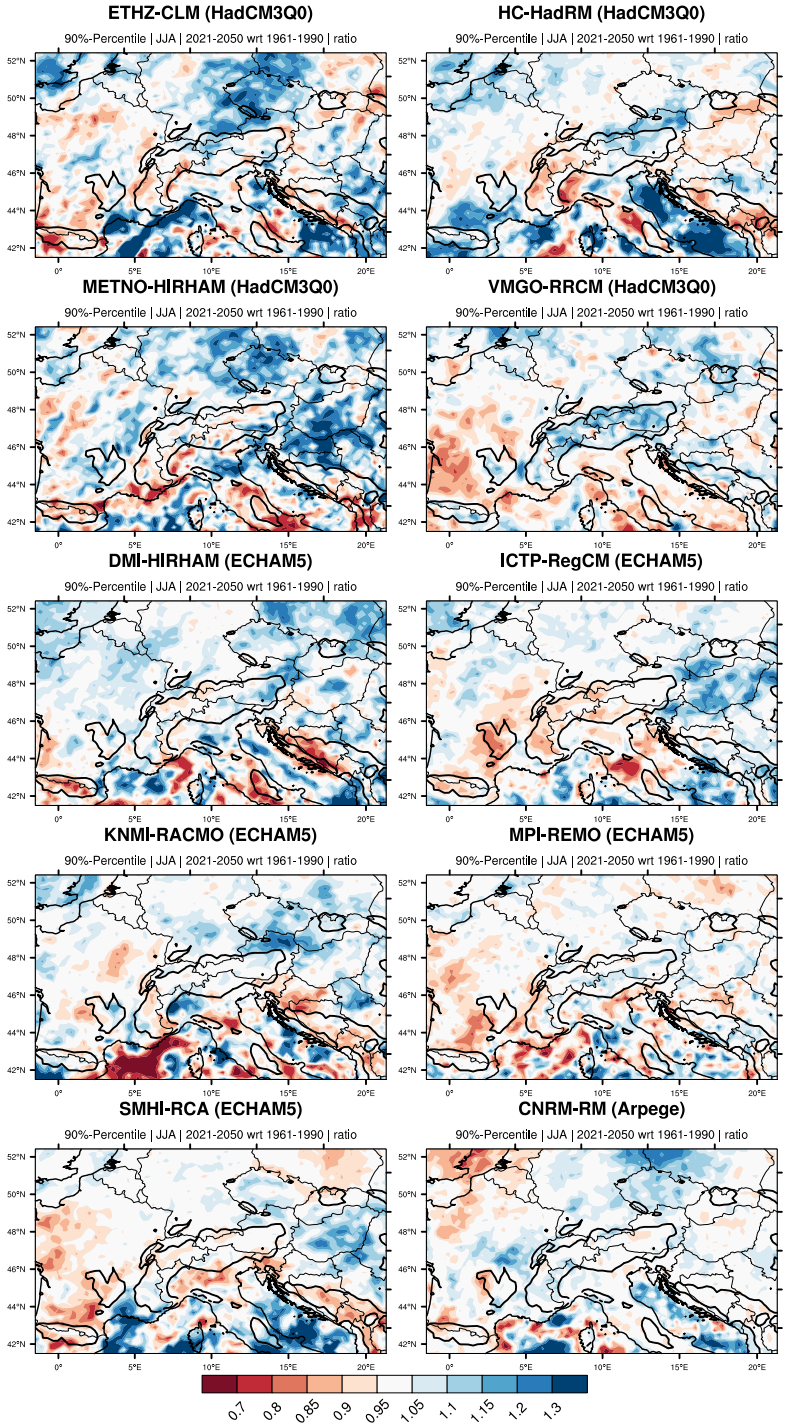

Figure A 7: Change (ratio SCEN/CTRL) in the 90%-quantile in summer as simulated by 10 RCMs for period SCEN1 (2021-2050) wrt CTRL (1961-1990). Thick lines illustrate the 700m a.s.l.-isoline as represented by the ENSEMBLES E-OBS topography.

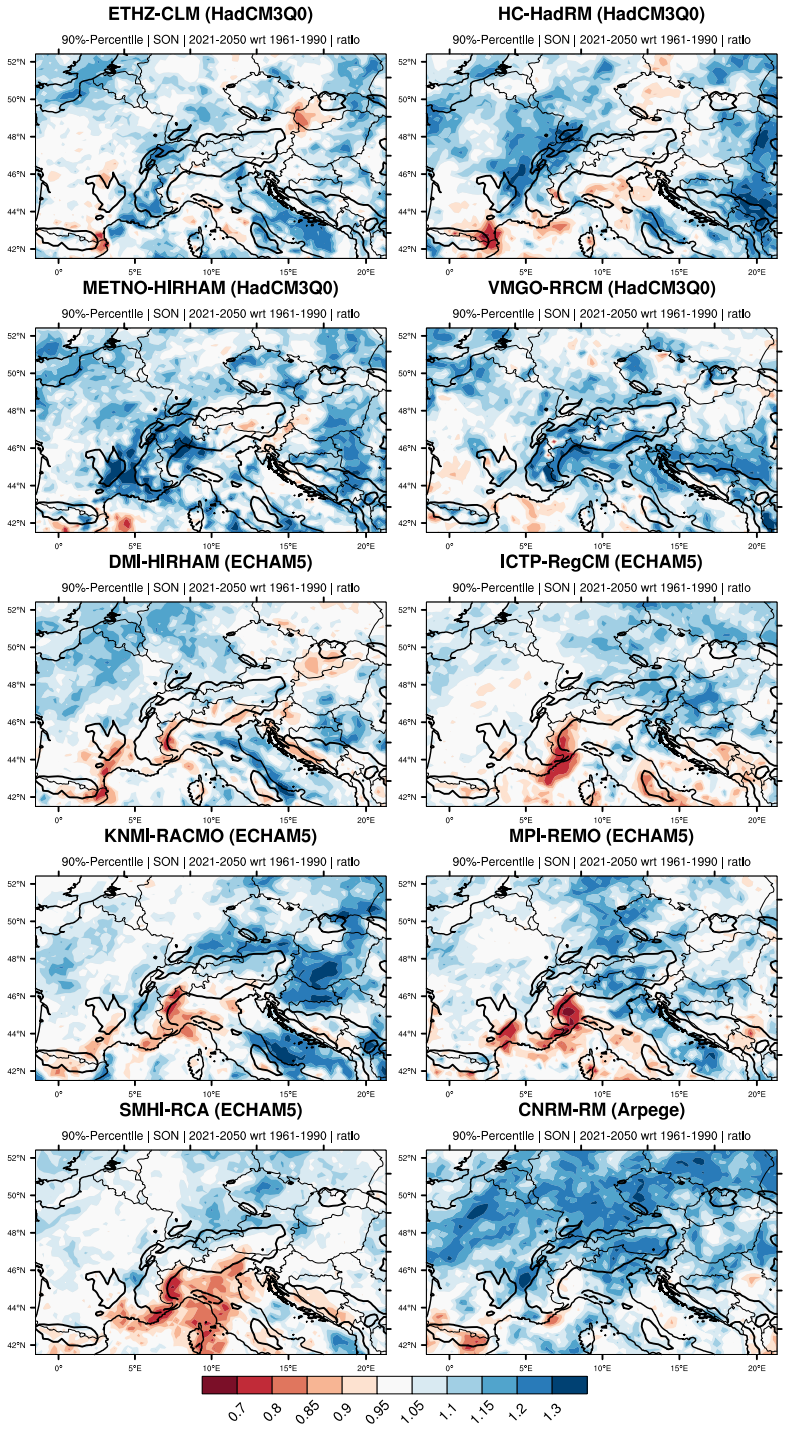

Figure A 8: Change (ratio SCEN/CTRL) in the 90%-quantile in fall as simulated by 10 RCMs for period SCEN1 (2021-2050) wrt CTRL (1961-1990). Thick lines illustrate the 700m a.s.l.-isoline as represented by the ENSEMBLES E-OBS topography.

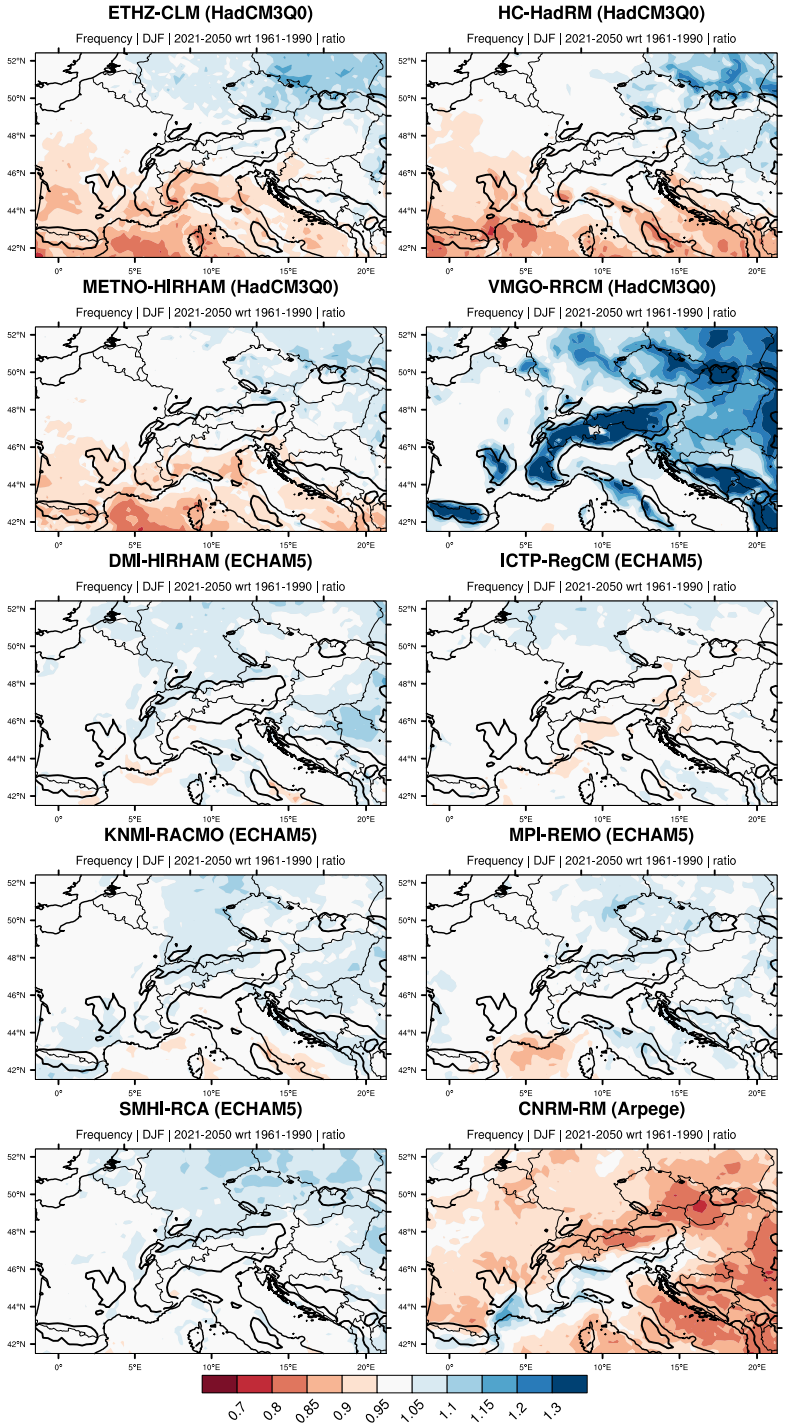

Figure A 9: Change (ratio SCEN/CTRL) in precipitation frequency in winter as simulated by 10 RCMs for period SCEN1 (2021-2050) wrt CTRL (1961-1990). Thick lines illustrate the 700m a.s.l.-isoline as represented by the ENSEMBLES E-OBS topography.

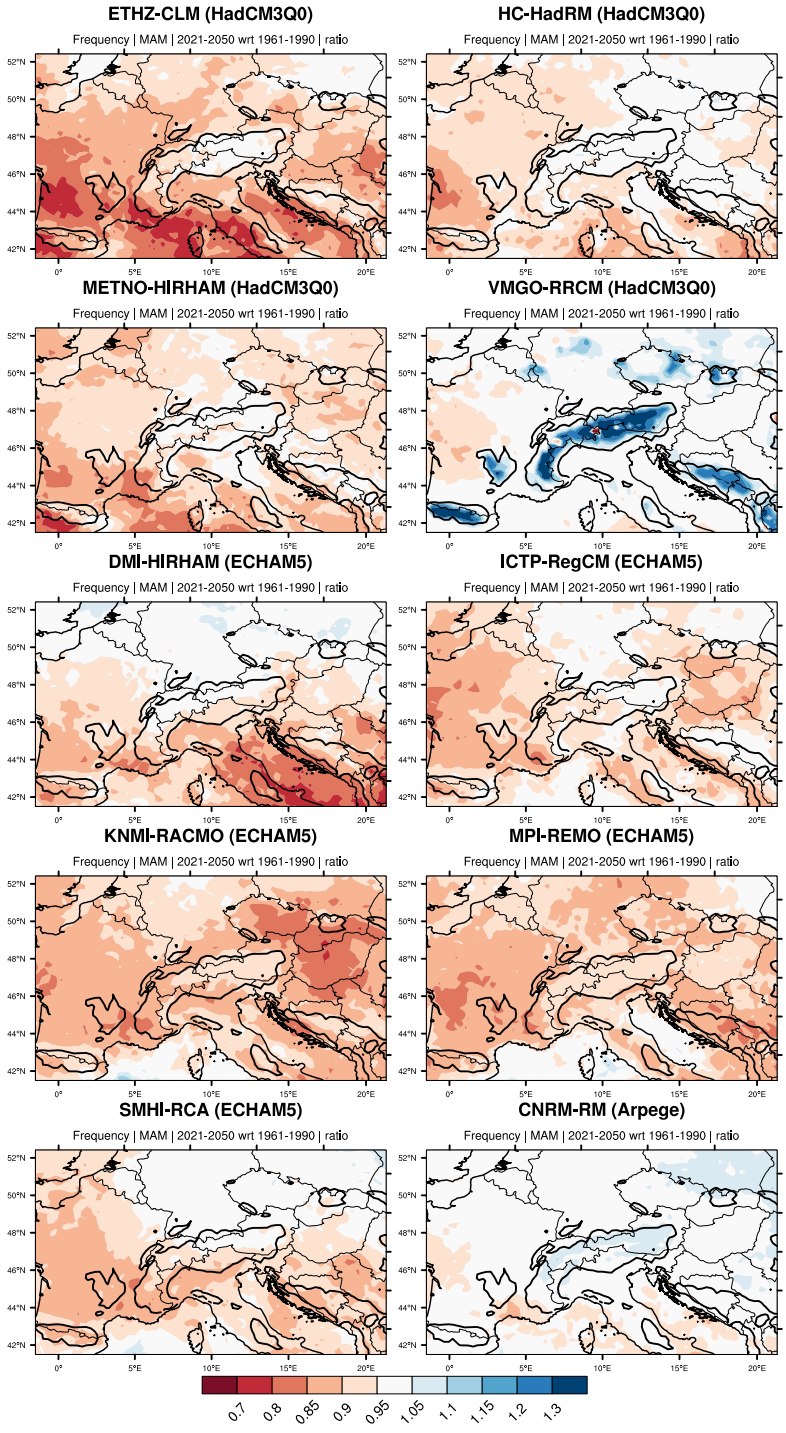

Figure A 10: Change (ratio SCEN/CTRL) in precipitation frequency in spring as simulated by 10 RCMs for period SCEN1 (2021-2050) wrt CTRL (1961-1990). Thick lines illustrate the 700m a.s.l.-isoline as represented by the ENSEMBLES E-OBS topography.

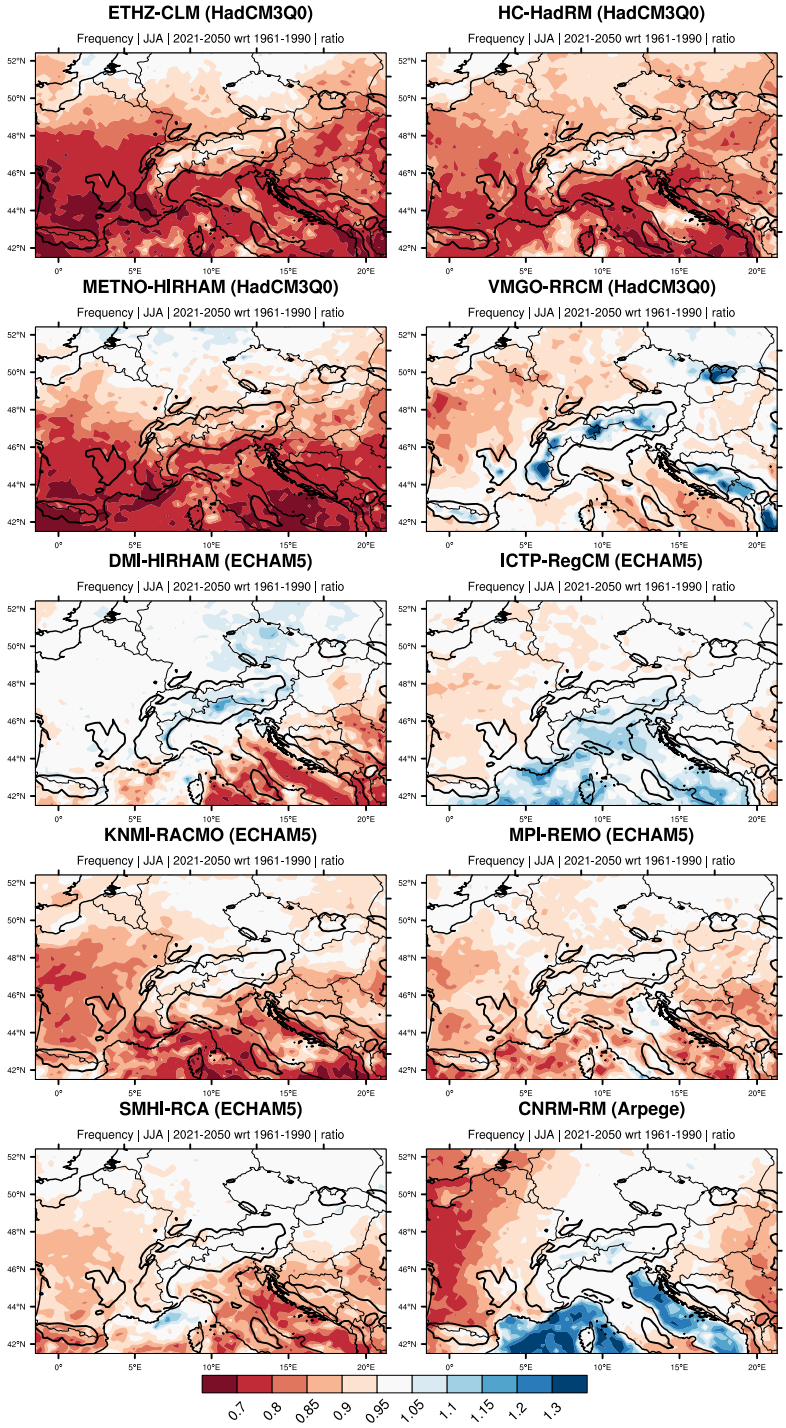

Figure A 11: Change (ratio SCEN/CTRL) in precipitation frequncy in summer as simulated by 10 RCMs for period SCEN1 (2021-2050) wrt CTRL (1961-1990). Thick lines illustrate the 700m a.s.l.-isoline as represented by the ENSEMBLES E-OBS topography.

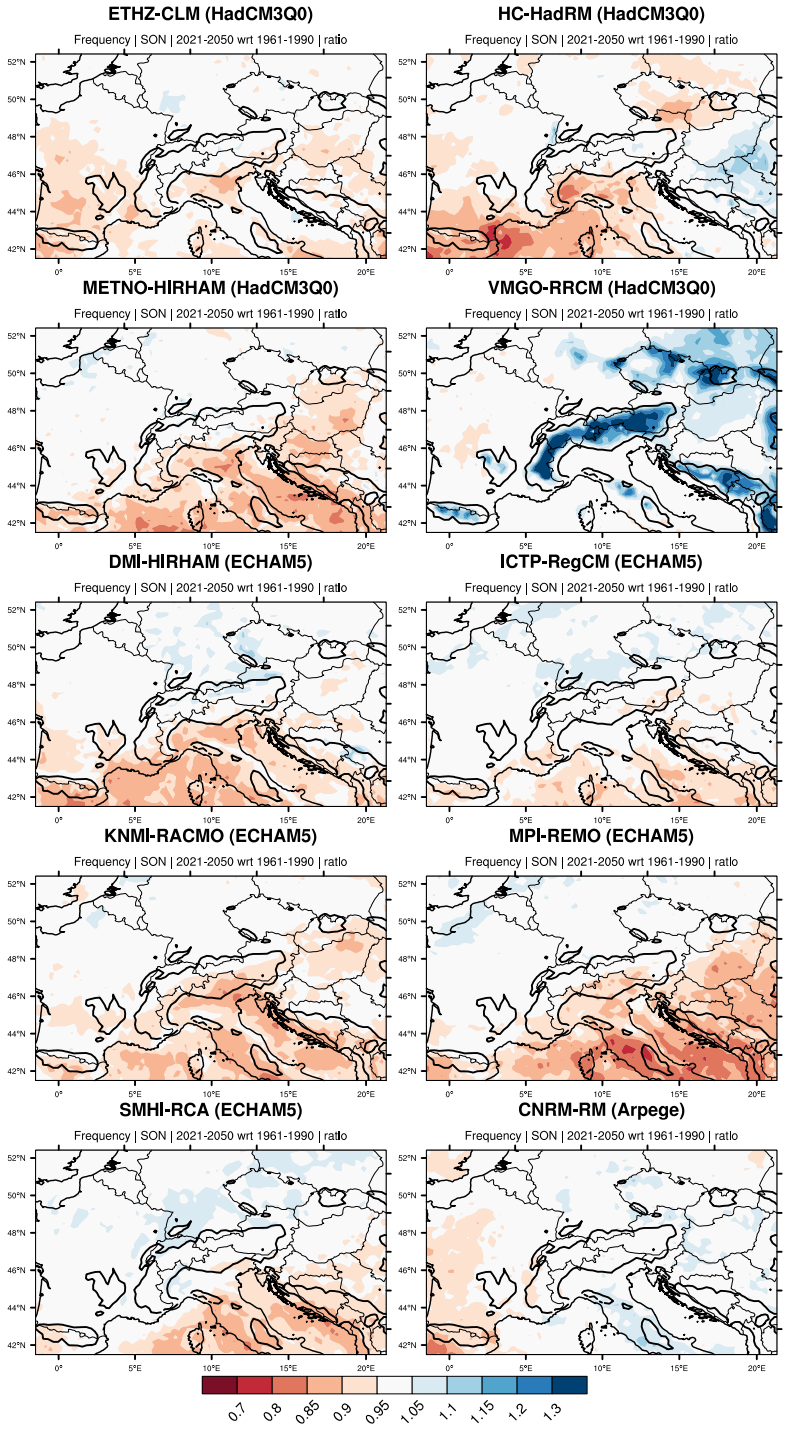

Figure A 12: Change (ratio SCEN/CTRL) in precipitation frequency in fall as simulated by 10 RCMs for period SCEN1 (2021-2050) wrt CTRL (1961-1990). Thick lines illustrate the 700m a.s.l.-isoline as represented by the ENSEMBLES E-OBS topography.

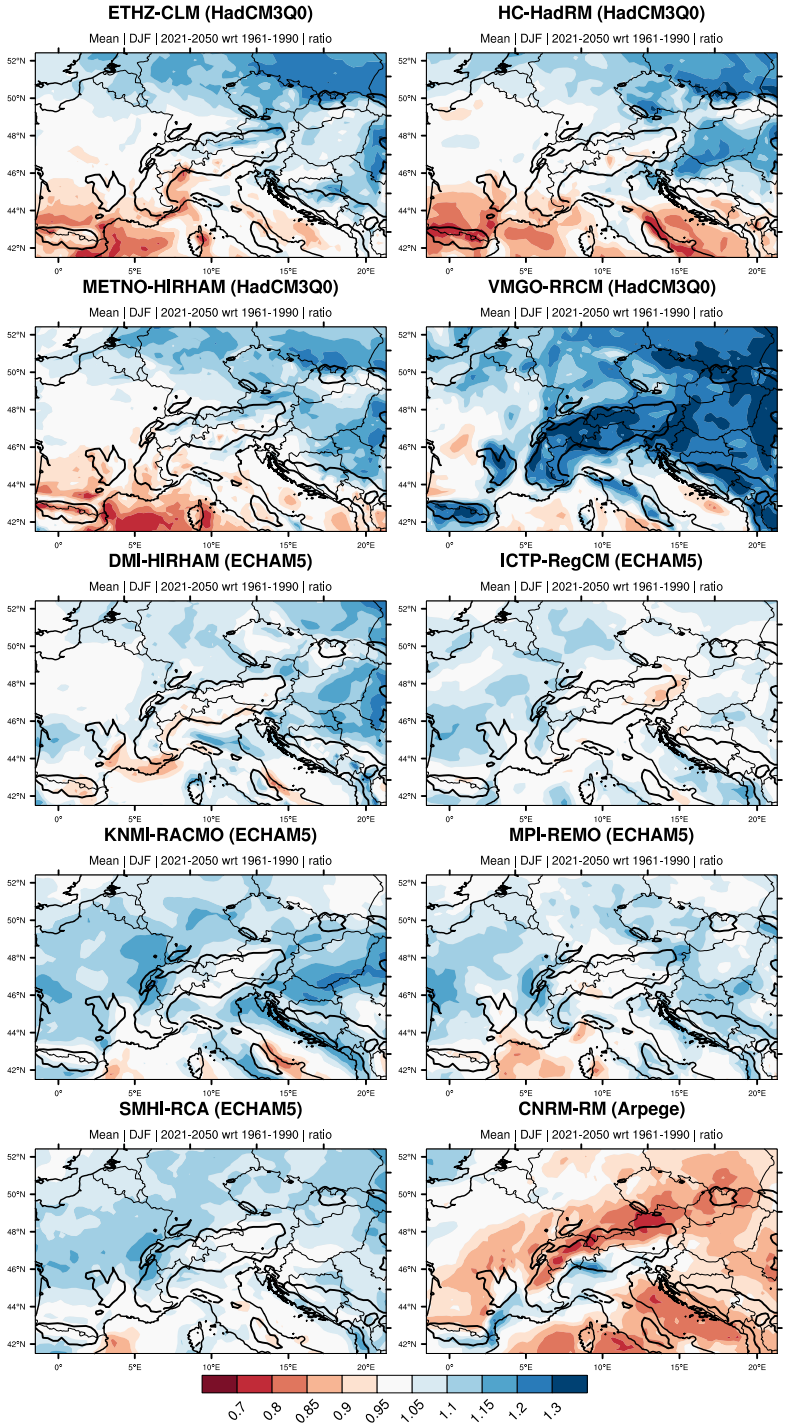

Figure A 13: Change (ratio SCEN/CTRL) in mean precipitation in winter as simulated by 10 RCMs for period SCEN1 (2021-2050) wrt CTRL (1961-1990). Thick lines illustrate the 700m a.s.l.-isoline as represented by the ENSEMBLES E-OBS topography.

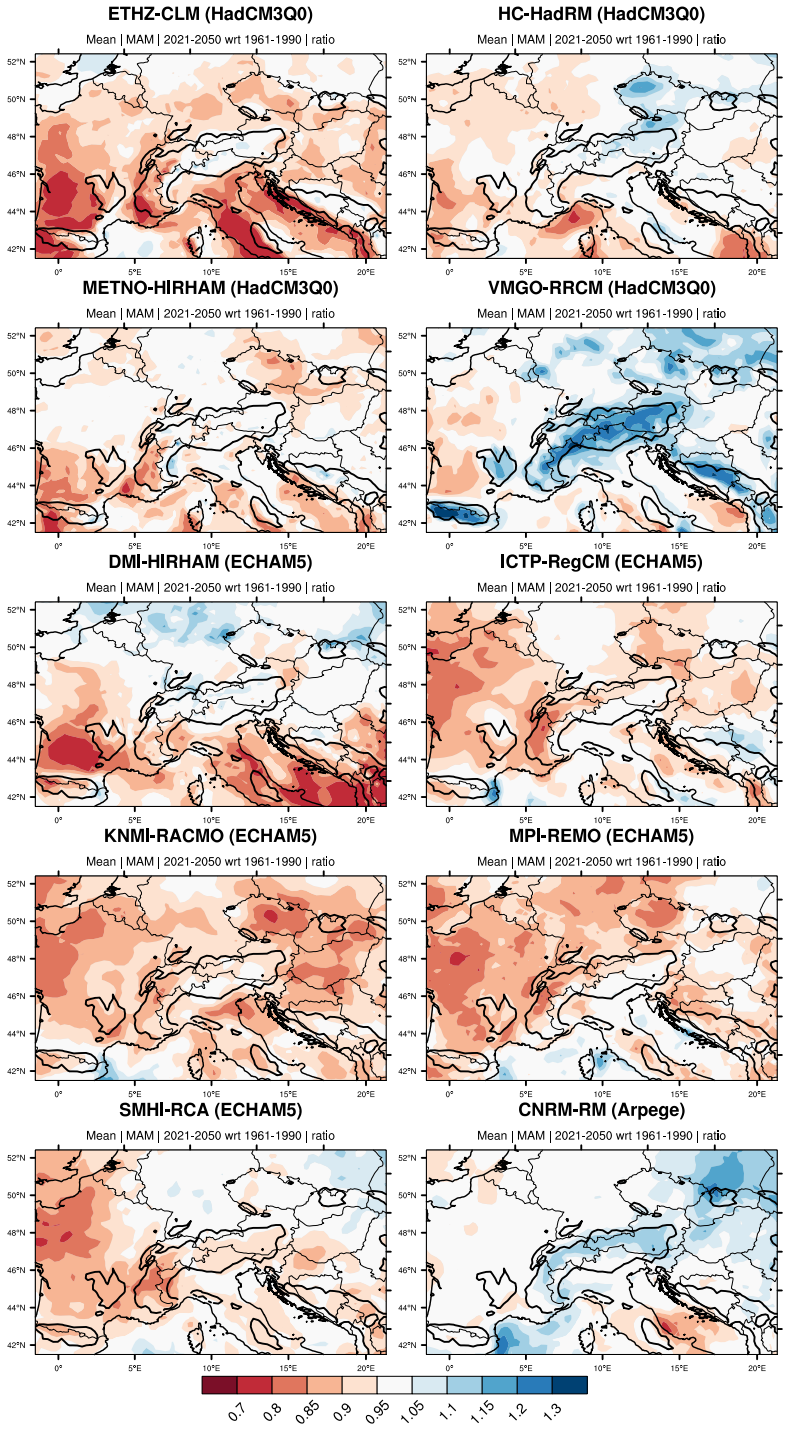

Figure A 14: Change (ratio SCEN/CTRL) in mean precipitation in spring as simulated by 10 RCMs for period SCEN1 (2021-2050) wrt CTRL (1961-1990). Thick lines illustrate the 700m a.s.l.-isoline as represented by the ENSEMBLES E-OBS topography.

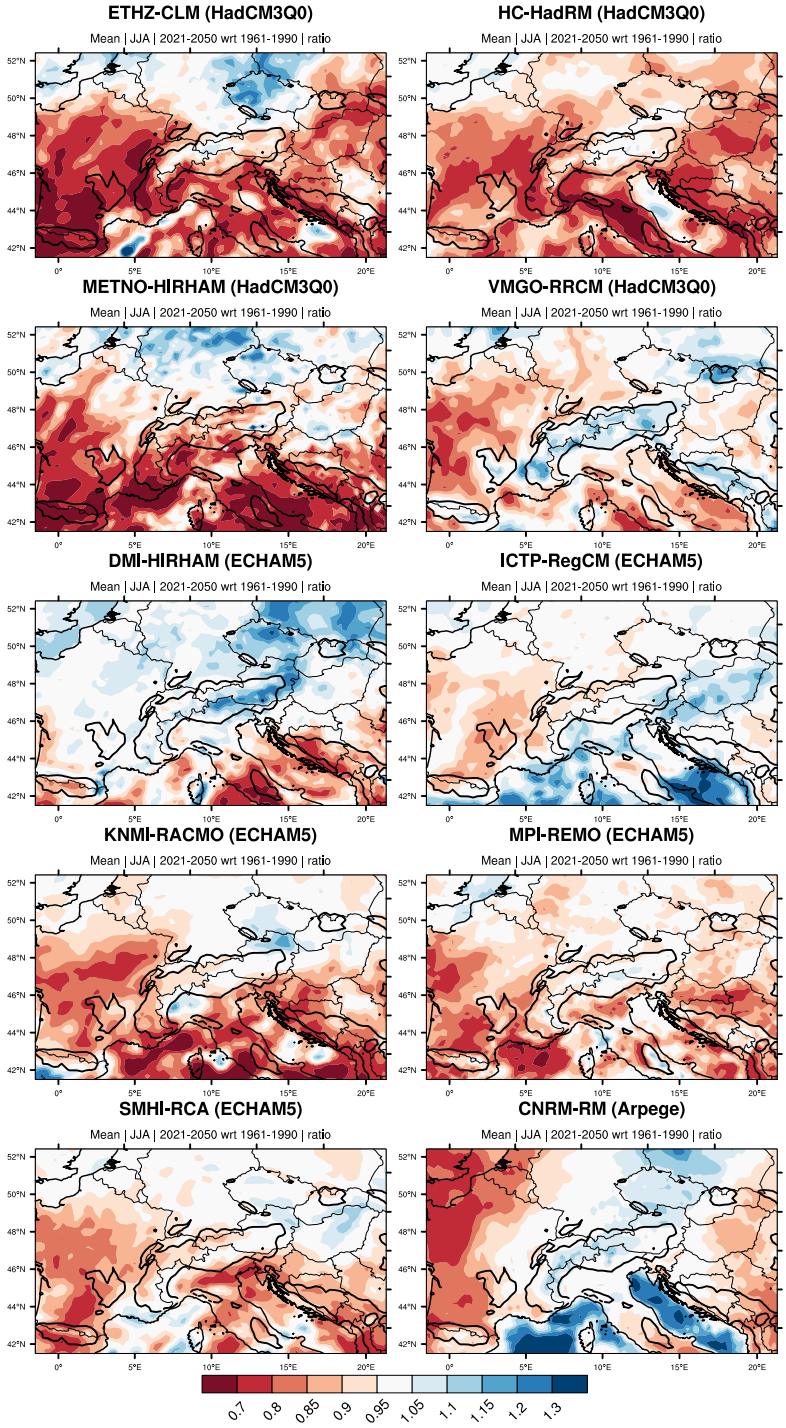

Figure A 15: Change (ratio SCEN/CTRL) in mean precipitation in summer as simulated by 10 RCMs for period SCEN1 (2021-2050) wrt CTRL (1961-1990). Thick lines illustrate the 700m a.s.l.-isoline as represented by the ENSEMBLES E-OBS topography.

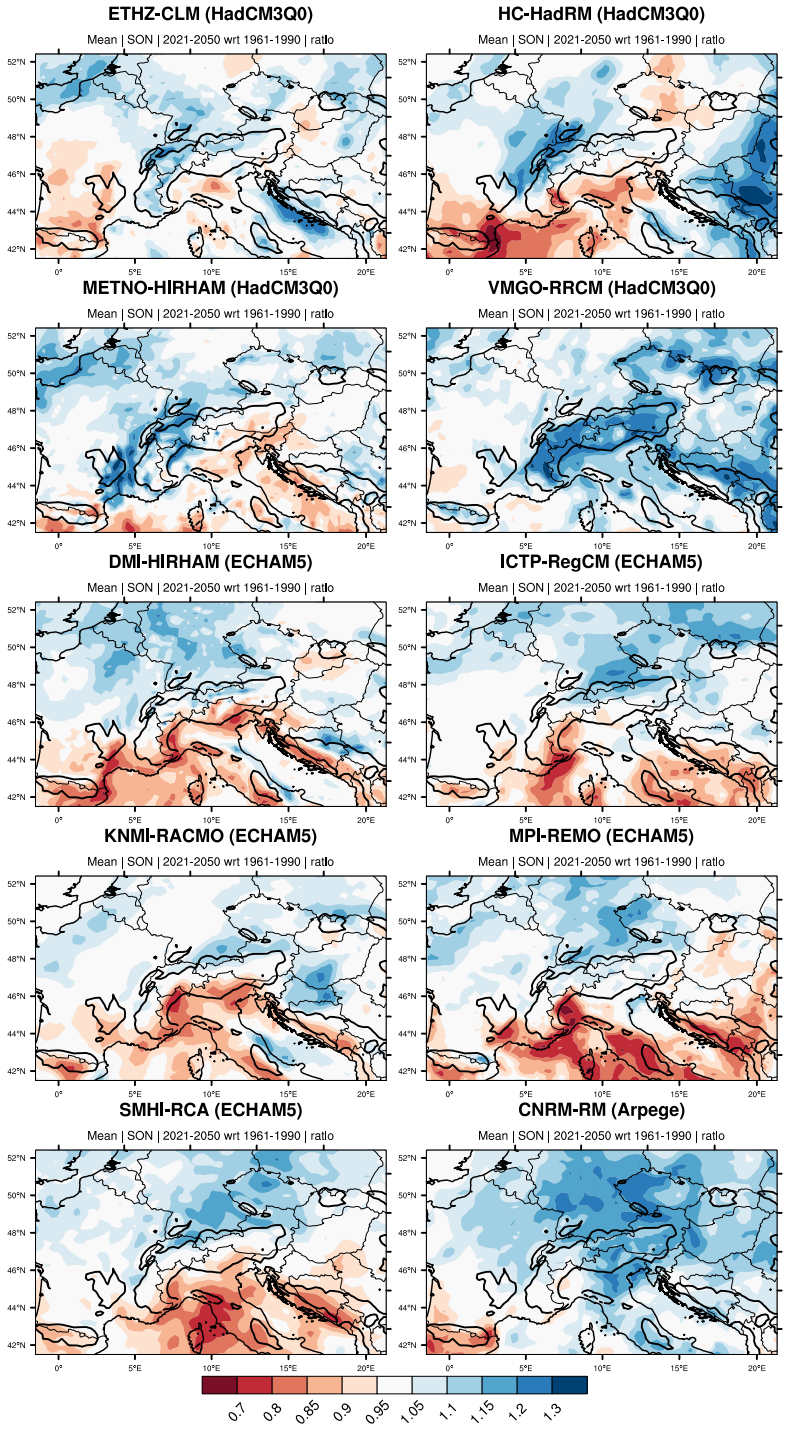

Figure A 16: Change (ratio SCEN/CTRL) in mean precipitation in fall as simulated by 10 RCMs for period SCEN1 (2021-2050) wrt CTRL (1961-1990). Thick lines illustrate the 700m a.s.l.-isoline as represented by the ENSEMBLES E-OBS topography.

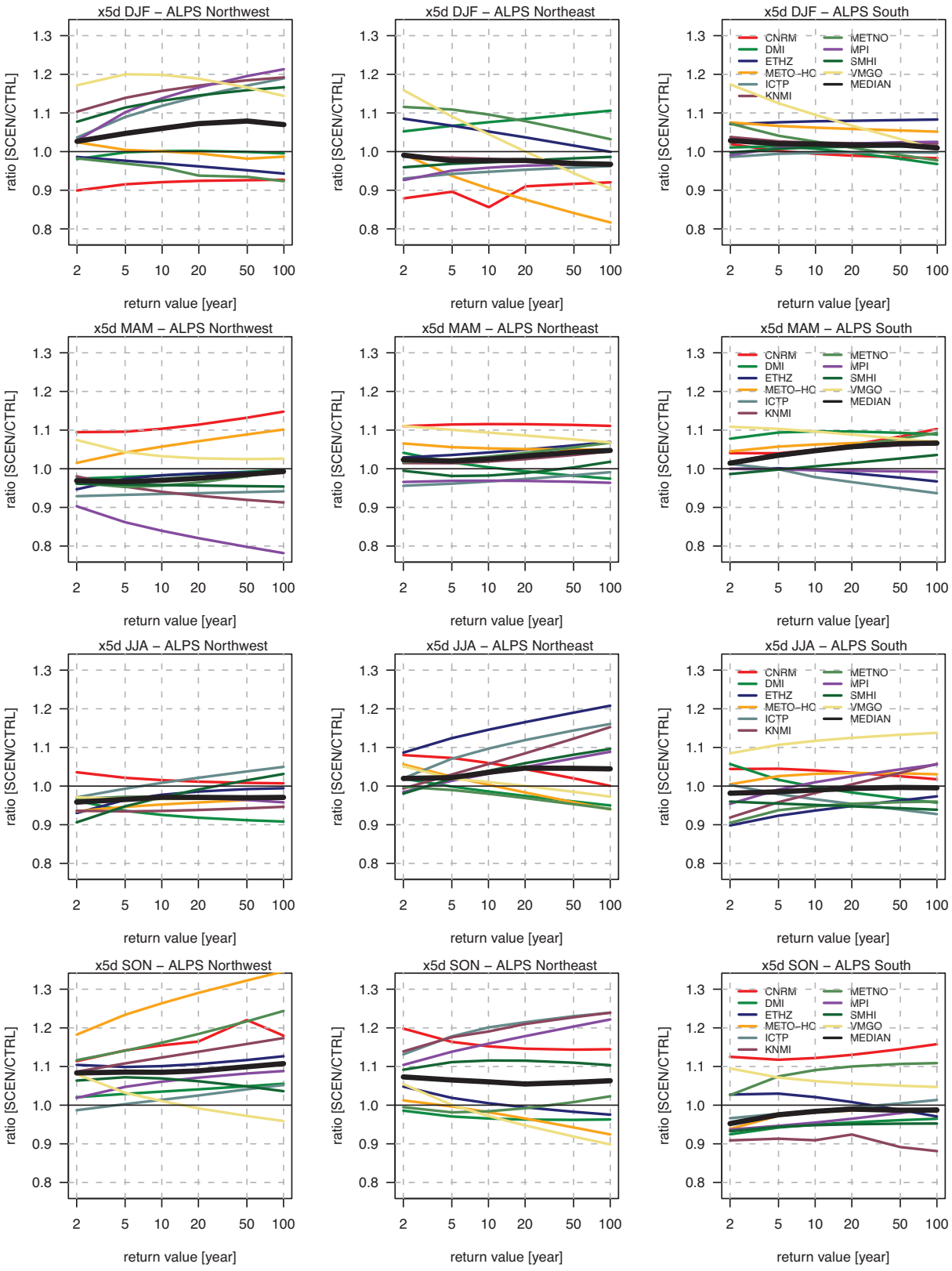

Figure A 17: Simulated change structure across increasing return periods (2 to 100 years) as simulated by 10 ENSEMBLES RCMs regarding 5-day precipitation extremes on sub-regional (columns) and seasonal level (ratios (SCEN/CTRL) depict domain-mean values, whereas SCEN: 2021-2050 & CTRL: 1961-1990).

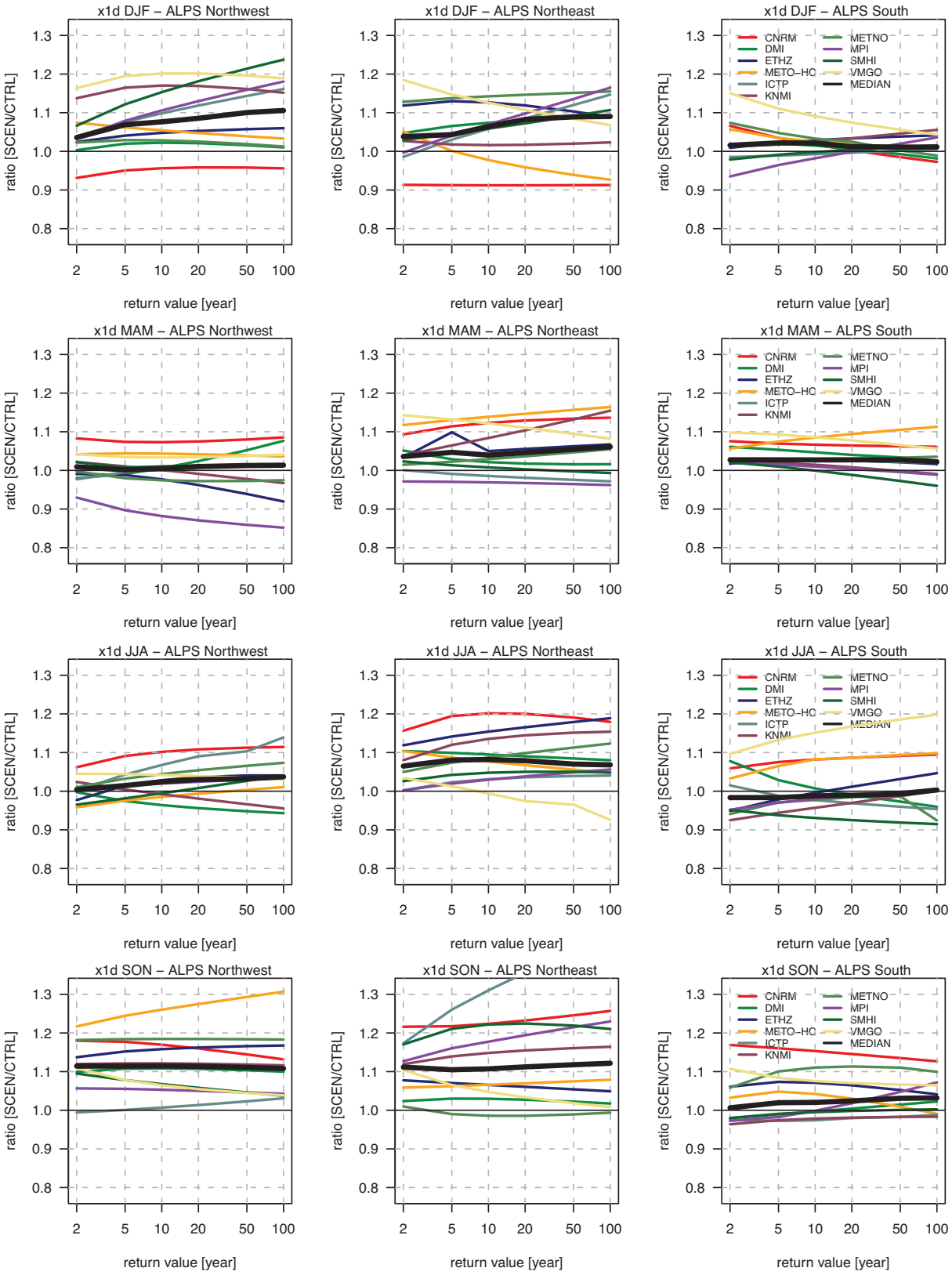

Figure A 18: Simulated change structure across increasing return periods (2 to 100 years) as simulated by 10 ENSEMBLES RCMs regarding 1-day precipitation extremes on sub-regional (columns) and seasonal level (ratios (SCEN/CTRL) depict domain-mean values, whereas SCEN: 2021-2050 & CTRL: 1961-1990).

Acknowledgements

First of all I would like to thank Prof. Dr. Christoph Schär for supervising this thesis and giving me the possibility to carry out the MSc thesis in his group at the Institute for Atmospheric and Climate Sciences at ETH Zürich. Secondly I am indebted to Dr. Pardeep Pall who has advised this thesis, helped me through difficult parts of the analyses and always took time to discuss findings and results. In this regard, I also thank Dr. Christoph Frei for providing extreme value analysis tools in R and answering methodological questions. Furthermore, I thank Julian Arnold for giving me good advice in R and for providing me climatological data and evaluation figures that have been used in this report. In regard of technical help, I also want to mention Dr. Urs Beyerle and Dr. Dani Lüthi for quickly solving computational problems when they came up.
I would also like to thank PD Dr. Christoph C. Raible from the Climate and Environmental Physics Department at the University of Bern for his effort. From the Oeschger Centre´s Graduate School of Climate Sciences (University of Bern), I want to thank Dr. Lorenz Martin for his advice concerning administrative issues and Prof. Dr. Martin Grosjean for supporting me in the opportunity to write my thesis externally at ETH Zürich.
Furthermore, I want to thank the Federal Office of Meteorology and Climatology (MeteoSwiss, Zürich) for giving me the possibility to carry out research and a part of my two-year Master´s project at their institution. Special thanks are thereby dedicated to the Climate Services team and especially Dr. Mark Liniger, Dr. Andreas Weigel and Dr. Andreas Fischer, who supervised me and largely enriched my statistical skills during my time at MeteoSwiss.
Last but not least I want to thank all the people that enrich my life outside of University.

Declaration

under Art. 28 Para. 2 RSL 05

Last, first name: **Rajczak, Jan**

Matriculation number: 09-130-113

Programme: MSc. in **Climate Sciences**

Bachelor ☐ Master X Dissertation ☐

Thesis title: Analysis of Extreme Precipitation Events in Regional Climate Simulations for the Alpine Region

Thesis supervisor: Prof. Dr. Christoph Schär, ETH Zürich

PD Dr. Christoph C. Raible

I hereby declare that this submission is my own work and that, to the best of my knowledge and belief, it contains no material previously published or written by another person, except where due acknowledgement has been made in the text. In accordance with academic rules and ethical conduct, I have fully cited and referenced all material and results that are not original to this work. I am well aware of the fact that, on the basis of Article 36 Paragraph 1 Letter o of the University Law of 5 September 1996, the Senate is entitled to deny the title awarded on the basis of this work if proven otherwise

.....

Place, date

.....

Signature